Technical Report Documentation Page

1. Report No. FHWA/TX-06/0-1401-2	2. Government Accession No.	3. Recipient's Catalog No.
4. Title and Subtitle Stay-Cable Vibration Monitoring of The Fred Hartman Bridge (Houston, Texas) and The Veterans Memorial Bridge (Port Arthur, Texas)		5. Report Date October 2005 6. Performing Organization Code
7. Author(s) Delong Zuo and Nicholas P. Jones		8. Performing Organization Report No. 0-1401-2
9. Performing Organization Name and Address Center for Transportation Research The University of Texas at Austin 3208 Red River, Suite 200 Austin, TX 78705-2650		10. Work Unit No. (TRAIS) 11. Contract or Grant No. 0-1401
12. Sponsoring Agency Name and Address Texas Department of Transportation Research and Technology Implementation Office P.O. Box 5080 Austin, TX 78763-5080		13. Type of Report and Period Covered Technical Report (04/2000 – 08/2005) 14. Sponsoring Agency Code
15. Supplementary Notes Project conducted in cooperation with the Federal Highway Administration and the Texas Department of Transportation.		

16. Abstract

This report summarizes the accomplishments of a field investigation project that was conducted in order to understand the mechanisms of wind- and rain-wind-induced stay cable vibrations and to assess the effectiveness of passive viscous dampers and cross-ties in mitigating such vibrations.

The field investigation project was based on two full-scale measurement systems installed on the Fred Hartman Bridge in Houston, Texas and the Veterans Memorial Bridge in Port Arthur, Texas. The systems systematically monitored the vibrations of selected stay cables on these two bridges, as well as the vibrations of the bridge decks and the corresponding meteorological conditions at the bridge sites. The system on the Fred Hartman Bridge started collecting data in October, 1997; the system on the Veterans Memorial Bridge became functioning in January, 1999. Both systems have remained in operation through the present time.

17. Key Words FSEL, dampers, cross-ties, cable, vibration, Fred Hartman Bridge, Veterans Memorial Bridge	18. Distribution Statement No restrictions. This document is available to the public through the National Technical Information Service, Springfield, Virginia 22161; www.ntis.gov.

19. Security Classif. (of report) Unclassified	20. Security Classif. (of this page) Unclassified	21. No. of pages 142	22. Price

Form DOT F 1700.7 (8-72) Reproduction of completed page authorized

FERGUSON STRUCTURAL ENGINEERING LAB
The University of Texas at Austin

Stay-Cable Vibration Monitoring of The Fred Hartman Bridge (Houston, Texas) and The Veterans Memorial Bridge (Port Arthur, Texas)

Delong Zuo
Nicholas P. Jones

CTR Research Report:	0-1401-2
Report Date:	October 2005
Research Project:	0-1401
Research Project Title	Determination of Fatigue Damage in Cable Stays

Center for Transportation Research
The University of Texas at Austin
3208 Red River
Austin, TX 78705

www.utexas.edu/research/ctr

Disclaimers

Author's Disclaimer: The contents of this report reflect the views of the authors, who are responsible for the facts and the accuracy of the data presented herein. The contents do not necessarily reflect the official view or policies of the Federal Highway Administration or the Texas Department of Transportation (TxDOT). This report does not constitute a standard, specification, or regulation.

Patent Disclaimer: There was no invention or discovery conceived or first actually reduced to practice in the course of or under this contract, including any art, method, process, machine manufacture, design or composition of matter, or any new useful improvement thereof, or any variety of plant, which is or may be patentable under the patent laws of the United States of America or any foreign country.

Notice: The United States Government and the State of Texas do not endorse products or manufacturers. If trade or manufacturers' names appear herein, it is solely because they are considered essential to the object of this report.

Engineering Disclaimer

NOT INTENDED FOR CONSTRUCTION, BIDDING, OR PERMIT PURPOSES.

Sharon L. Wood, The University of Texas at Austin, Texas P.E. #83804

Nicholas P. Jones, Johns Hopkins University

Research Supervisors

Acknowledgments

We greatly appreciate the financial support from the Texas Department of Transportation that made this project possible. The support of the project director, Keith Ramsey (BRG), and program coordinator, Randy Cox (BRG) is also very much appreciated. We extend our appreciation to the project monitoring committee, Mike Lynch (BRG), Elton Brown (BRG), Howard Caldwell (Beaumont), Quincy Allen (Houston) and Tom Rummell (BRG).

Special Acknowledgement

The authors would like to acknowledge the following individuals and agencies for their respective contributions.

Dr. Joseph Main, currently a research associate at the National Institute of Standards and Technology, was a key member of the research group at the Johns Hopkins University that was responsible for the design, installation and maintenance of the full-scale measurement systems. Dr. Main made significant contributions in developing the data processing procedures and in interpreting the full-scale measurement data, as well as understanding the mechanism of dampers in mitigating stay cable vibrations.

Dr. Luca Caracoglia, currently an assistant professor at Northeastern University, helped with the maintenance of the full-scale measurement systems and assisted in the analysis of full-scale measurement data, as well as understanding the dynamics of cable networks formed with cross-ties.

Dr. Ender Ozkan, currently an engineer with Arup Corporation, contributed to the maintenance of the full-scale measurement systems and participated as a significant member in analyzing the full-scale measurement data. Dr. Ozkan's contribution in understanding deck-stay interactions should be specifically acknowledged.

Mr. Mehedy Mashnad, currently a Ph.D. student at the University of Illinois, performed wind tunnel tests of the bridge decks of the Fred Hartman Bridge, the results of which have been used to assist the interpretation of deck-induced stay cable vibrations.

Mr. Jack Spangler, a senior mechanical engineer in the Department of Civil Engineering at the Johns Hopkins University, was the primary architect of the full-scale measurement systems. Mr. Spangler has also been one of the major reasons why the full-scale measurement systems stayed functional and effective through out the eight years of project.

Ms. Mitchell Porterfield, formerly a student at the Johns Hopkins University, was actively involved in the development, installation and maintenance of the full-scale measurement systems.

Mr. Elton Brown, a technological correspondent in the Bridge Division of Texas Department of Transportation, helped in every stage of the field investigation project. Mr. Brown provided all assistance required by the research group at Johns Hopkins University, especially the downloading and transportation of data from the bridges to the Johns Hopkins University. He has also provided personal insights into the dynamic behavior of the stay cables and the performance of the mitigation devices based on his field experience.

The National Science Foundation and the Federal Highway Administration funded research programs associated with the current project, for which the co-authors are grateful.

In addition, the various contribution of Mr. David Tayabji, an undergraduate student at the University of Illinois at Urbana-Champaign and Mr. Wei Li, formerly an undergraduate student at the Johns Hopkins University, are also acknowledged.

Executive Summary

This report summarizes the accomplishments of a field investigation project that was conducted in order to understand the mechanisms of wind- and rain-wind-induced stay cable vibrations and to assess the effectiveness of passive viscous dampers and cross-ties in mitigating such vibrations.

The field investigation project was based on two full-scale measurement systems installed on the Fred Hartman Bridge in Houston, Texas and the Veterans Memorial Bridge in Port Arthur, Texas. The systems systematically monitored the vibrations of selected stay cables on these two bridges, as well as the vibrations of the bridge decks and the corresponding meteorological conditions at the bridge sites. The system on the Fred Hartman Bridge started collecting data in October, 1997; the system on the Veterans Memorial Bridge became functioning in January, 1999. Both systems have remained in operation through the present time. Details of the measurement systems are presented in the third chapter of this report.

The full-scale measurement systems have collected large quantity of data, which can be divided into two baseline sets: One data set consists of data associate with the vibrations of unrestrained stay cables, and the other set consists of data associated with the vibrations of stay cables restrained by dampers or cross-ties, or both.

Analysis of the unrestrained stay cable vibrations has revealed important characteristics of such vibrations and their relationship with both wind and rain. Based on these characteristics and relationship, a number of types of stay cable vibration have been identified, which include the classical Kármán-vortex-induced vibrations, the so-called rain-wind-induced vibrations, a type of dry cable vibration and vibrations induced by deck oscillation. In particular, important similarities between the frequently occurring large-amplitude rain-wind-induced vibrations and a type of large-amplitude dry cable vibration are discovered, indicating a close connection between the mechanisms of these two types of vibration. Furthermore, it is revealed that the key characteristics shared by such large-amplitude vibrations with and without rainfall are also similar to the corresponding characteristics of the classical Kármán-vortex-induced vibrations, except that rain-wind-induced vibrations and the type of large-amplitude dry cable vibration both occur over a reduced velocity range that is much higher than the range over which Kármán-vortex-induced vibration occurs. This suggests that the large-amplitude vibrations occurring at high reduced velocity, regardless of rainfall, might be induced by a type of vortex-shedding that is different from the traditional Kármán-vortex shedding. The characteristics of the observed types of vibration, as well as the understanding about their respective mechanism, are presented in chapter 5 of the report.

Based on the data set associated with the restrained vibrations of stay cables, the performance of the mitigation devices installed on the two bridges under monitoring are evaluated.

All the dampers installed on the bridges, except the compact hydraulic damper attached to stay B13 on the Veterans Memorial Bridge, have generally been effective in suppressing wind- and rain-wind-induced vibrations. The only exception is that under certain wind conditions, when the direction of the vibration is in the out-of-plane direction of the cables, the dampers installed in the vertical cable plane were not able to suppress such vibrations. In addition to confirming the overall effectiveness of most dampers, analysis of the restrained vibrations also revealed that the static friction in the dampers, which was

ignored in the initial design, significantly affected the performance of the dampers and that this effect should be considered in future damper design.

Full scale measurement data also suggest that the cross-ties installed on the Fred Hartman Bridge have mostly been effective in mitigating stay cable vibrations. As in the case of the dampers, however, the effectiveness of cross-ties was limited when the vibration was primarily in the out-of-plane direction. In addition, it is also discovered that the performance of cross-ties can be significantly affected by imperfect design. This has manifested in the fact that the cross-ties were unable to suppress certain local modes of vibration of some stay cables because they are tied with the cables at locations close to the nodal points of these local modes.

These results of the assessment based on the full-scale measurement data suggest that thorough understanding of both the mitigation devices and the vibrations, such as the static friction in the dampers and the possible direction and the prevalent modes of vibration, is essential for effective and rational design of mitigation devices. Details of the assessment of mitigation devices are presented in chapter 6 of the report.

Table of Contents

List of Figures

1 Overview

Under certain wind conditions, stay cables of cable-stayed bridges have frequently exhibited large-amplitude vibrations. A prevalent type of vibration is associated with the simultaneous occurrence of wind and rain, and has been consequently referred to as rain-wind-induced vibrations. This type of vibration, as well as other types of vibrations occurring without rainfall, has been a concern for researchers and engineers because they potentially induce undue stresses and fatigue in the cables themselves and in the connections at the bridge deck and tower, and therefore threatens the safety and serviceability of cable-stayed bridges.

Both the Fred Hartman Bridge in Houston, Texas and the Veterans Memorial Bridge in Port Arthur, Texas have experienced such large-amplitude vibrations induced by wind or the combination of wind and rain since the completion of their construction. Concerned by these problematic vibrations, the Texas Department of Transportation (TxDOT) initiated a comprehensive research program aiming at studying the mechanisms of wind- and rain-wind-induced vibrations and developing rational and effective mitigation strategies.

The research program began in April 1997 and has been performed by a team initially coordinated by Whitlock Dalrymple Poston & Associates, Inc. (WDP). As part of the team, the group at the Johns Hopkins University (JHU), headed by Professor Nicholas P. Jones, was primarily responsible for the field investigation of the characteristics of stay cable vibrations and the evaluation of the performance of mitigation countermeasures devised to address the problematic vibrations. This report summarizes the work performed by the group at JHU during the period between October, 1997 and August 2005. It complements the report compiled by a research group at Texas Tech University, which describes an independent full-scale measurement project on the Veterans Memorial Bridge and wind tunnel tests conducted to study the aerodynamics of stay cables.

1.1 Objectives

The goals of the field investigation project are achieved through the following objectives:

- Development of a robust full-scale measurement system;
- Installation of full-scale measurement systems on the Fred Hartman Bridge and the Veterans Memorial Bridge;
- Establishment of a baseline set of data taken under varying atmospheric conditions with the stays unrestrained;
- Characterization and interpretation of observed stay cable vibrations;
- Assessment of the nature of wind- and rain-wind-induced stay cable vibrations;
- Establishment of a baseline set of data taken under varying atmospheric conditions with the stays restrained; and
- Evaluation of the performance of the mitigation devices installed by comparing restrained and unrestrained stay cable vibrations.

1.2 Accomplishments

The field investigation project has continued for the past eight years. During this period of time, the objectives of the project have been successfully fulfilled. Major accomplishments of the project include:

- Comprehensive, computer-based full-scale measurement systems have been built and installed on both the Fred Hartman Bridge and the Veterans Memorial Bridge.
- Based on an automatic triggering mechanism and a remote access scheme, the full-scale systems have continuously monitored the vibrations of the stay cables and the bridge decks, as well as the corresponding meteorological conditions at the bridge sites with relatively little interruption.
- Characteristics of observed vibrations have been thoroughly investigated. Interpretation of these characteristics and their relationship with wind and rain has resulted in effective categorization of the vibrations. Investigation of individual types of vibration has led to significant understanding of the mechanisms of wind- and rain-wind-induced stay cable vibrations, including previously unanticipated types. For example, the investigation has revealed important connections between rain-wind-induced vibrations and a type of large-amplitude dry cable vibration.
- Comparison between the vibrations with and without restrainers has enabled the evaluation of the effectiveness of the dampers and cross-ties installed on the bridges. In particular, analysis of the observed performance of these two types of mitigation devices has revealed specific factors that have to be considered in their future design.
- The field investigation project has resulted in a number of publications in the form of Ph.D. dissertations, journal papers and conference proceedings. The present report will be primarily derived from these publications. A list of the publications is provided in Appendix A. Full text of these publications is included in the literature package that accompanies this report.
- Data recorded through the full-scale measurement systems, in the form of both raw data and computed statistics, have been provided to other groups in the team for other research topics, such as the evaluation of lifetime fatigue cycles of stay cables (University of Texas at Austin).

1.3 Structure of Report

The report begins with a comprehensive literature review of the problem of wind- and rain-wind-induced stay cable vibrations and the state-of-the-art mitigation countermeasures. In Chapter 3, the full-scale measurement systems on the Fred Hartman Bridge and the Veterans Memorial Bridge are described in detail. Chapter 4 summarizes the data that accompanies the present report. This Chapter also gives a brief description of the data processing and presentation techniques used to analyze the raw data. In Chapter 5, the observed characteristics of individual types of vibration are presented. Special attention is directed to rain-wind-induced vibrations, Kármán-vortex-induced vibrations, a type of large-amplitude dry cable vibration and stay cable vibrations induced by the oscillation of bridge decks. The connection among the first three types of vibrations is also explored. Chapter 6 is devoted to the evaluation of the mitigation devices installed on the stay cables of the Fred Hartman Bridge and the Veterans Memorial Bridge. Concluding comments are presented in Chapter 7.

2 Background and Context

2.1 The Problem of Wind- and Rain-Wind-Induced Vibrations

The phenomenon of wind-induced cable vibration in the stays of cable-stayed bridges was first observed several decades ago (e.g., Wianecki 1979). It caught the attention of investigators when Hikami and Shiraishi (1988) observed that, during the construction of the Meikonishi Bridge in Japan, under the excitation from wind during rain, the stay cables often exhibited large-amplitude vibrations. This type of stay cable vibration, characterized by a large amplitude and an oscillation frequency that is much lower than the corresponding Strouhal frequency for classical Kármán-vortex-induced vibrations, has since been frequently observed on many cable-stayed bridges around the world (e.g., Matsumoto et al. 1995) and termed rain-wind-induced vibrations. In the last two decades, rain-wind-induced vibrations have been subjected to extensive study for two reasons: First, this type of vibration occurs often at large amplitude and potentially threatens the safety and serviceability of cable-stayed bridges (Raoof 1992). In fact, there have been reports in the literature of both cable failure (Virlogeux 1998) and damage to the cable-deck connection (Gu et al. 1998) due to rain-wind-induced vibrations. Second, the mechanism of rain-wind-induced vibrations, as will be discussed in detail in the following sections of this report, is complicated and does not fall simply into the categories of classical, relatively better understood, aeroelastic phenomena.

In addition to rain-wind-induced vibrations, other types of wind-induced stay cable vibrations have also been observed. These include the classical Kármán-vortex- induced vibrations and the so-called "deck-induced" vibrations, wherein the vibration of the stay cables is initiated by wind-induced bridge deck oscillation (e.g., Warnitchai et al. 1995). These vibrations, as well as vibrations that have been observed but not effectively categorized, are also of significant concern to bridge engineers as they can reach moderate or even large amplitude and cause unexpected stresses both in stay cables and in the connections between the cables and the bridge deck, which potentially lead to fatigue failure of structural members.

2.2 Current Understanding

Observed large-amplitude stay cable vibrations are often associated with rainfall, therefore the current study has been primarily focused on the problem of rain-wind-induced vibrations. The investigation was initiated with full-scale measurements on several bridges around the world (e.g., Hikami and Shiraishi 1988; Wianecki 1979), from which some characteristics of the vibrations, such as the vibration amplitude and the frequency, as well as their dependence on wind and rain have been reported. Observations from these full-scale measurements, however, are not comprehensive and do not necessarily reveal the complete picture of wind- and rain-wind-induced stay cable vibrations. In fact, many observations reported in the literature are contradictory. While early reports suggested that only the stays declining in the direction of wind were susceptible to rain-wind excitation (Hikami and Shiraishi 1988), subsequent observations (Matsumoto et al. 1990) indicated that stays with opposite inclination can be excited simultaneously. Early reports also indicated that rain-wind-induced vibrations were restricted to a wind speed range of 6 to 17 m/s, which is in the sub-critical range of the corresponding Reynolds number (Matsumoto et al. 1995). Later observations, however, have reported vibrations occurring at a wind speed as high as 40 m/s (Matsumoto et al. 1998). Further, the role of rainfall in the excitation mechanism has also been debated. While most observations suggested that large amplitude vibrations occur only

with rainfall and that it is the water rivulet forming on the cable surface that renders the cable cross-section aerodynamically unstable (e.g., Hikami and Shiraishi 1988), other observations (Matsumoto et al. 1998) however, have reported stay cables vibrating at large amplitude without precipitation.

To study the problem in a controlled manner, wind tunnel tests have been conducted in an attempt to replicate the vibrations observed in the field. Many tests were designed expressly to study the perceived important role of rain. Very different observations and, consequently, different hypotheses on the mechanism of the vibrations, however, have resulted from these tests depending on the manner in which rainfall was simulated. Some tests (e.g., Cosentino et al. 2003; Hikami and Shiraishi 1988; Ruscheweyh 1999) used shower heads to spray water onto cable models and water rivulets were observed to form and move at the same frequency as the cable vibration. Interpretation of these tests claimed that large-amplitude stay cable vibrations are the result of a two-degree-of-freedom aerodynamic instability formed by the coupled oscillations of the stay cable and the water rivulet. In some other tests, rigid bars were attached on the surface of cable models to simulate water rivulets, and large-amplitude vibrations of the cable were also successfully reproduced in the wind tunnel (e.g., Bosdogianni and Olivari 1996; Matsumoto et al. 1992). It was subsequently proposed based on these wind tunnel tests that the actual motion of the water rivulets plays a negligible role in the excitation mechanism, and that it is the average position of the water rivulet that is important in changing the cross-section of the cable and rendering it susceptible to wind excitation.

In addition to the wind tunnel tests designed to study rain-wind-induced vibrations, some tests were also performed without the simulation of rainfall to investigate the inherent aerodynamic instability of dry stay cables (e.g., Matsumoto et al. 1992; Matsumoto et al. 2001). In particular, Matsumoto et al. (1992) observed vortex-shedding from dry cable models at a frequency that is much lower than the frequency of Kármán vortex shedding and concluded that the vibration of dry cables is due to the interaction between the Kármán vortices and axial vortices that travel along the axis of the cable. In another wind tunnel test, Cheng et al. (2003b) also observed a type of "limit-amplitude" dry cable vibration as well as a galloping type of divergent vibration at very high wind speed. It was subsequently suggested that dry stay cables are inherently susceptible to galloping excitation when wind speed is in the critical Reynolds number range.

While most of these wind tunnel tests have been successful in reproducing large-amplitude vibrations and illustrating specific aspects of stay cable vibrations, such as the sensitivity of the cables to the excitation of wind or wind and rain and the dependence of the vibrations on wind speed and direction, they all have their respective drawbacks or limitations, both in the setup of the tests and the interpretation of the results, and may not adequately or faithfully reveal the true mechanisms of the phenomena of interest.

Based on observations from both the field and the wind tunnel tests, analytical formulations have also been pursued in attempt to explain and predict the problematic vibrations under specific wind and rain conditions. Yamaguchi (1990) proposed a two-degree-of-freedom galloping model involving the coupling of the cable vibration and the circumferential oscillation of the water rivulet. This approach has generally been followed by subsequent analytical studies, with different treatment of the forces acting on the water rivulet and the cable-rivulet interface (e.g., Cosentino et al. 2003; Peil and Nahrath 2003; Wang and Xu 2003). All these models, however, are based on a simplified quasi-steady

assumption of the wind force, which may not faithfully represent the true aeroelastic nature of rain-wind-induced vibrations. In addition, these models are also essentially two-dimensional and, as will be discussed in detail in the subsequent chapters, cannot represent the inherent three-dimensional nature of the vibrations. A robust and successful model can be developed only if the mechanism of the prototype problem is fully understood.

2.3 Mitigation Countermeasures

Although the mechanism of wind- and rain-wind induced vibrations is still not fully understood, mitigating countermeasures have been developed to suppress the excessive vibrations. Current countermeasures can be put into three categories according to the principles on which they are based. One type of countermeasure attempts to change the aerodynamic properties of the cable so that it remains stable under wind or rain-wind excitations. Commonly used countermeasures in this category include intentionally modifying the configuration of the cable surface with ducts or dimples (Fujino 2002; Virlogeux 1998) or by winding a wire helically around the cable to prevent the formation of water rivulets. While some wind tunnel tests (e.g., Flamand 1995) have demonstrated the effectiveness of surface treatment in suppressing rain-wind-induced vibration, practice on some cable-stayed bridges in Japan has indicated that it may not be effective in counteracting vortex-induced vibrations (Fujino 2002). In addition, due to the limitation in its working mechanism, this type of countermeasure is ineffective in suppressing the vibrations of stay cables induced by deck or tower motion. The second type of countermeasure attempts to suppress the vibrations by tying multiple cables together with secondary cables called cross-ties to form cable networks so that the energy in individual cables can be redistributed either to the higher modes of vibration or to adjacent cables in the network (Ehsan and Scanlan 1989). However, the cross-ties between the stays are considered a distraction to the aesthetic beauty of cable-stayed bridges (Pacheco et al. 1993) and, due to the large stresses to which they are subjected, there have been incidents of cross-tie failures, such as that reported on the Erasmus Bridge in the Netherlands (Virlogeux 1999). The third type of countermeasure uses external devices, such as high-damping rubbers (Yamaguchi and Fujino 1998) and dampers attached at the vicinity of the cable anchorages (e.g., Virlogeux 1998), to supplement the inherent mechanical damping in the cables. This inherent structural damping is believed to be at an extremely low level and a critical contributory factor to the susceptibility of stay cables to aerodynamic excitations (Yamaguchi and Fujino 1998). Among these damping supplementing devices, passive viscous dampers have been extensively studied (e.g., Krenk 2000; Main and Jones 2002a; Pacheco et al. 1993) and their effectiveness in suppressing stay cable vibrations has been widely accepted (Yamaguchi and Fujino 1998). In recent years, the potential application of active and semi-active dampers has also been investigated in attempt to achieve improved damping performance over other damping supplementing devices (e.g., Johnson et al. 2003). Although the effectiveness of such active and semi-active dampers has been confirmed by experimental tests, there still remain many theoretical as well as practical issues to be resolved (Yamaguchi and Fujino 1998). In most cases, these three types of countermeasures have been applied separately. On some bridges, however, more than one of them has been employed. For example, all three types of countermeasures were applied on the Normandie Bridge (Fuzier and Stubler 1994). Whether or not these countermeasures can work together effectively is also a subject of further study.

Although the above-discussed types of countermeasures have been demonstrated to be effective in suppressing some or all types of wind- and rain-wind-induced vibrations, the

design still remains semi-empirical. For example, in the design of dampers, an efficient and reliable means to estimate the inherent damping in the cables is still not available, and it is still not fully clear how much supplemental damping is needed to suppress the vibrations. To enable more rational and efficient design of countermeasures, a better understanding of the mechanisms of wind- and rain-wind-induced stay cable vibrations, as well as the key parameters involved, is needed.

3 Full-Scale Measurement Systems

3.1 Monitoring System on the Fred Hartman Bridge

The Fred Hartman Bridge is a twin-deck cable-stayed bridge with a main span of 381 m. Each of the decks is 24 m wide and consists of precast concrete slabs on steel girders and floor beams. The decks are supported by a total of 192 cables, arranged in four inclined planes (designated A, B, C and D, respectively) originated at each of the two double-diamond shaped towers. The stays range from 59 to 198 m in length, with varying diameters. They are connected with the decks at 15.2m intervals and are labeled according to their locations. Figure 3.1 shows an elevation and plan view of the bridge, together with the labeling scheme for the stay cables.

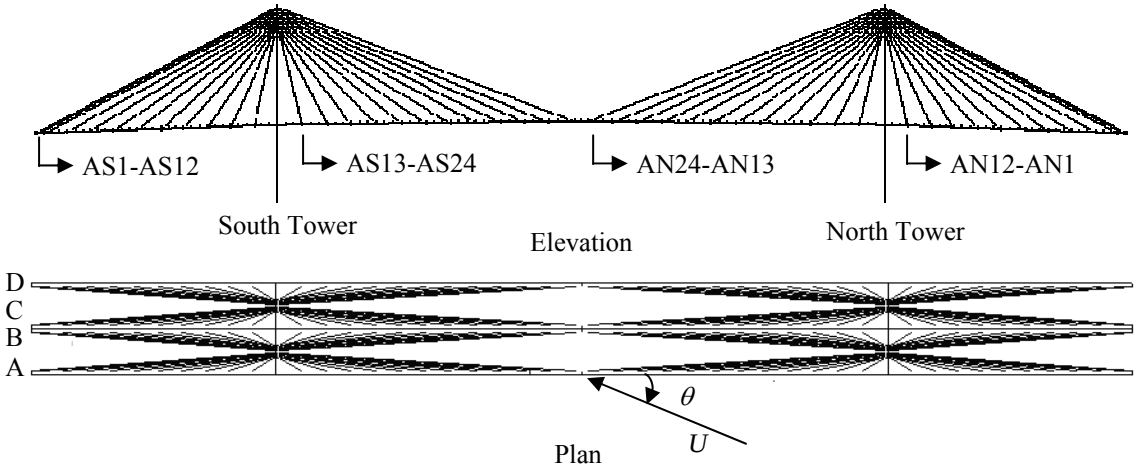

Figure 3.1 Elevation and plan view of the Fred Hartman Bridge showing stay lines A-D

The instrumentation system on the Fred Hartman Bridge was installed on the bridge and began collecting data in October 1997. Measurements taken include:

- in-plane and lateral acceleration of selected stays and the deck at several locations;
- in-plane and lateral displacement of selected stays at specific locations;
- damper forces at two stays with dampers installed, and
- meteorological conditions at the bridge site, which include, primarily, wind and rain, and some contextual measurement, such as the temperature and barometric pressure of the air.

As many as 83 channels have been simultaneously instrumented on the bridge, although this number has changed considerably during the full-scale measurement program. A complete list of the instrumented channels can be found in Appendix B.1. The detailed status of these channels during the duration of the full-scale measurement project can be found in a MS Excel file in the data package that accompanies the present report (File "Hartman_Transducer_Timeline.xls"). All channels are continuously monitored by an onsite computer and, once predetermined thresholds in wind speed or cable acceleration are exceeded, the system triggers and samples all channels for 5 minutes at a frequency of 40 Hz. The data acquisition system on the computer is managed by the Labtech software. To exclude high frequency noise, the signals were filtered by a low-pass analog filter with a cut-off frequency of 10 Hz. The five-minute records are numbered according to the time at which they are recorded. For example, record "199710031" is the first record collected on October

3, 1997. The controlling computer can be remotely accessed through the internet, but recorded data were downloaded onsite to high capacity Jazz disks and shipped to the Johns Hopkins for analysis.

3.1.1 Wind Measurement

The speed and direction of wind at the bridge site are monitored at three locations by two types of anemometers. At the deck level, two sets of Gill UVW anemometers (Young Instruments, model 27005) are installed on steel poles that extend 4.57 m from the edge of the east deck at mid-span and at the anchorage of stay AS18, respectively. The UVW anemometers have a threshold of 0.4 m/s and can measure wind speed of up to 35 m/s. At the top of the southeast tower, a propeller-vane anemometer (Young Instruments, model 05305) is installed on a steel pole at a height of about 134 m above the water surface. This propeller-vane anemometer has a threshold of 0.4 m/s and can measure wind speed up to 50 m/s. The resolution of this anemometer is 0.2 m/s for speed measurement, and 3° for direction measurement. Figure 3.2 shows the pictures of the UVW anemometer and propeller-vane anemometer. Figure 3.3 shows the locations of the three anemometers installed on the Fred Hartman Bridge. Both types of anemometers are oriented so that wind approaching from the north towers towards the south towers, along the bridge axis, is designated zero degrees. The coordinate system for wind speed and direction is shown in Figure 3.1 (with U as wind speed and θ as wind direction).

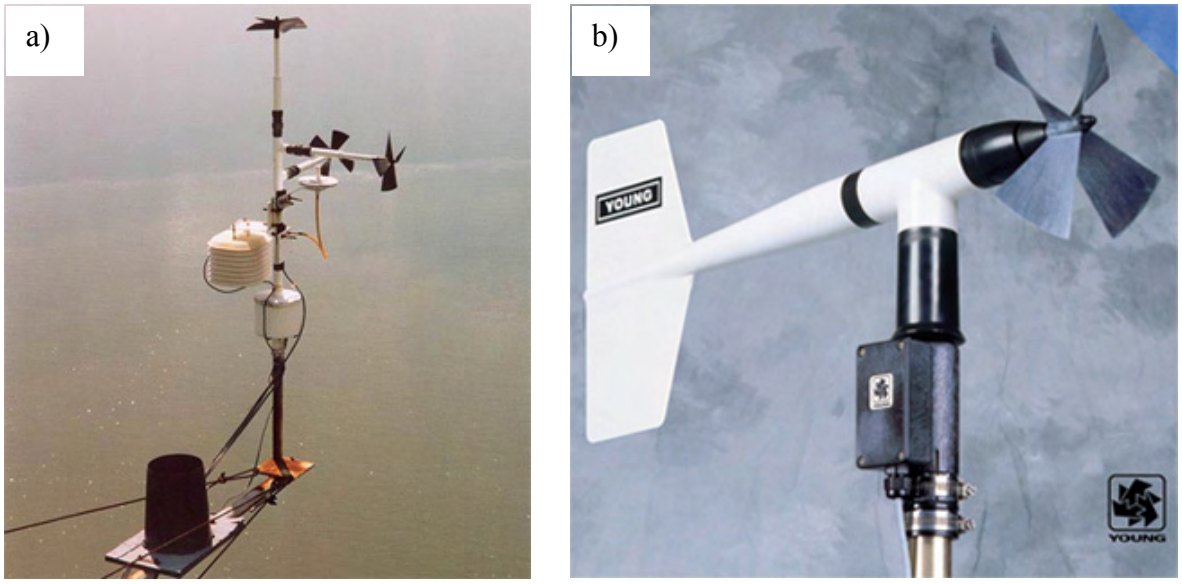

Figure 3.2 a) UVW and b) propeller-vane anemometer

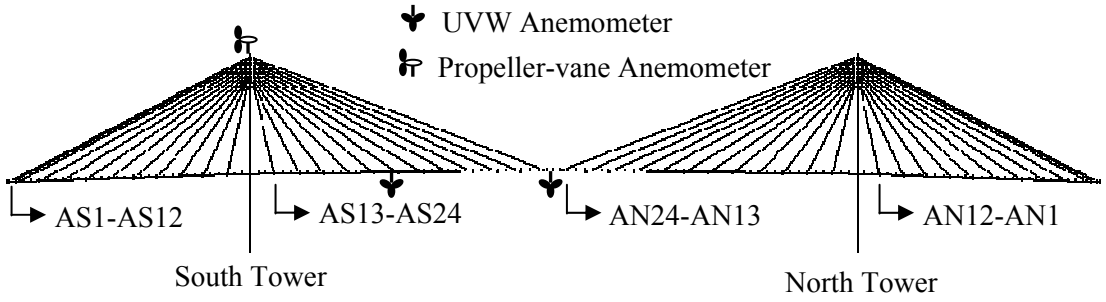

Figure 3.3 Location of anemometers on the Fred Hartman Bridge

In general, these two types of anemometers have been consistent in providing wind measurements at the bridge site. Due to the physical limitations of the anemometers and the manner in which the measurement system was originally configured, however, specific corrections have to be made to the wind data collected and, in some situations, discretion has to be exercised in order to interpret the measurements appropriately.

The first physical limitation of the anemometers that needs to be considered is the response characteristics of the anemometers to wind approaching from different directions (Kristensen 1993). This is particularly true for the Gill UVW anemometers installed at the deck level. Each set of UVW anemometer consists of three propellers (designated U, V and W, respectively) mounted on three fixed shafts. Each propeller is designed and calibrated in such a manner that it accurately measures the speed of the wind approaching along the axis of its shaft. When wind approaches from a direction other than the axis of the shaft, however, the propeller may overestimate or underestimate the true wind speed, depending on the relative angle between the direction of the wind and the axis of the propeller shaft. To account for this factor, wind tunnel tests are usually performed to provide correction factors for the measurement of wind approaching from different directions. Figure 3.4 shows the correction factors supplied by the manufacturer of the Gill UVW anemometers. These correction factors have been applied to the wind measurements taken at the deck level of the Fred Hartman Bridge by both sets of UVW anemometers. For the propeller-vane anemometer installed at the top of the southeast tower, such corrections are not necessary since the vane of this type of anemometer adjusts automatically to the approaching direction of the wind (Kristensen 1993).

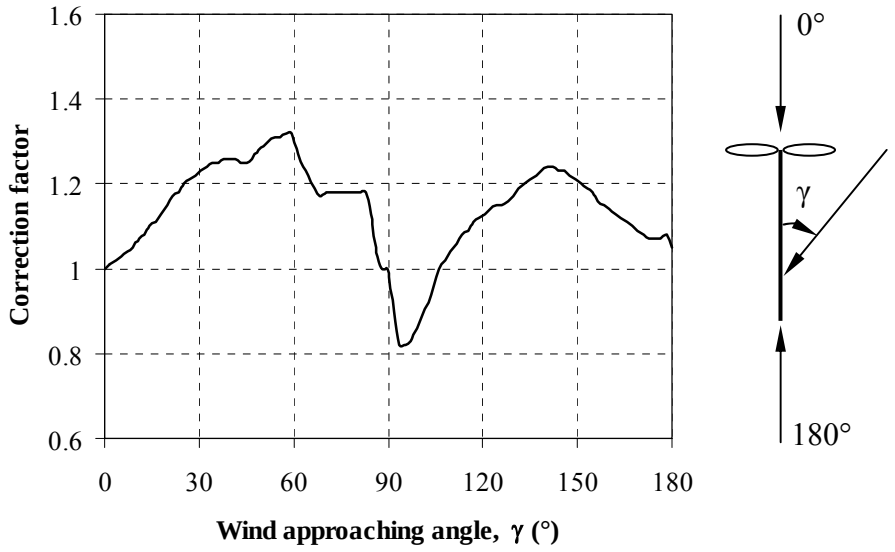

Figure 3.4 Correction factors for Gill UVW anemometers

The second physical limitation of the anemometers that requires consideration is the different frequency response range of different anemometers. For the wind measurement system on the Fred Hartman Bridge, the UVW anemometers and the propeller-vane anemometer have different frequency response ranges, which can potentially result in different measurement of the wind by these two devices. In particular, the propeller-vane anemometer at the tower top has a relatively narrow frequency response range and can potentially provide erroneous measurements when the turbulence in the wind is very high. Corrections to this possible problem with wind measurement at the Fred Hartman Bridge, however, were not performed since no reliable reference measurement is available.

Another factor that requires consideration in wind measurement is the potential distortion of the flow by the structure. This is particularly important in the case of wind measurement at the Fred Hartman Bridge. At the deck level, since the Gill UVW anemometers are installed at locations that are only 4.57 m away horizontally from the east edge of the 2.87 m tall east deck, when wind approaches from the west side of the decks, they will be directly in the wake of the decks so that the measurements taken by these anemometers cannot represent the free-stream wind. When wind approaches from the east side of the twin decks, on the other hand, the flow at the location of the anemometers will likely be either accelerated or retarded due to the presence of the decks and, as a result, the measurements taken at this points will either overestimate or underestimate the velocity of the free-stream wind. Similarly, the wind measurement by the propeller-vane anemometer can also be affected by the disturbance from the massive tower structure. When wind approaches from certain directions, the presence of the upper part of the diamond-shaped tower can potentially result in complex three-dimensional flow in the vicinity of the anemometer. In such conditions, the measurement taken by the propeller-vane anemometer will not be able to faithfully represent the free stream wind at this altitude either.

Statistical analysis of the wind measurement data suggests that the wind measurements at the deck level by the two sets of UVW anemometers are very consistent with each other when wind approaches from the east side of the bridge. The data also suggest, however, that wind measurement at the tower-top by the propeller-vane anemometer appears

to have a significantly non-linear relationship to the measurement at the deck level. Details of the statistical analysis can be found in Appendix C. These characteristics of the wind measurement are suspected to be due to the fact that the flow profile in the vicinity of the propeller-vane anemometer can be rendered significantly three-dimensional by the complex shape of the tower top, and that as a result, the measurement by the anemometer represents the distorted flow instead of the free stream wind.

Due to these characteristics of the wind measurement and the fact that the wind profile is inherently sheared in the atmospheric boundary layer, it is impossible to designate a specific measurement as the representative wind at the bridge site. The wind measurement by an individual anemometer can only represent the wind profile at its vicinity and does not necessarily correspond to the exact wind responsible for the vibration of a specific structural member of the bridge. The wind measurements, therefore, can only be used as an imperfect reference in interpreting the vibration of the stay cables. In the subsequent parts of the present report, the reference wind speed and direction are primarily chosen to be those measured near the anchorage of stay AS18. When the measurement at this location is not available due to problems such as malfunctioning propeller(s), the measurement at mid-span is used because the wind measurements at the deck level by the two sets of UVW anemometers are statistically consistent. In the relatively unusual cases when both sets of anemometers at the deck level are unavailable, the wind measurement at the tower top by the propeller-vane anemometer is used and will be explicitly specified.

3.1.2 Measurement of Rainfall

The rainfall at the bridge site is monitored by two rain gauges (Davis Instruments): one located at the top of the southeast tower and the other at the deck level near the anchorage of stay AS18. The rain gauges are so configured that the rain bucket tips each time 0.0254 cm of rain is collected. In the recorded signal, each bucket-tip is represented by a change of voltage from 5 v to 0 v. With these rain gauges, however, the measurement system is not able to provide the instantaneous rate of rainfall. In the present study, the following schemes are utilized to compute the rate of rainfall according to the bucket tips recorded:

For isolated records (i.e., no other records were recorded immediately before or after these records):

- If only one bucket tip is recorded, it is assumed that the rain falls uniformly throughout the duration of the record. The rate of rainfall during this period of time therefore is computed as 0.0254 cm per five minutes.
- If multiple tips were recorded, the rate of rainfall is computed based on the assumption that the rain falls at a constant rate between adjacent tips. At the two ends of the five-minute record, however, special assumptions have to be applied, since no information about the starting and ending time of the rain was recorded. In the present study, it is assumed that the rate of rainfall is the same right before and after the first bucket tip was recorded during the five minutes and that the same is true right before and after the last tip. Based on this assumption, the onset and ending time of the rainfall can be artificially determined and the rate of rainfall for the whole record can be computed accordingly.

For successive records (i.e., the records are recorded immediately before or after one and another), the five-minute records are first connected back to back according to the time sequence to form a long record and the rate of rainfall is computed according to a scheme similar to that for the isolated records:

- If only one bucket tip is recorded during the duration of a long record, since no information about the starting and ending time of the rainfall is available, the duration of the rainfall is assumed to be 5 minutes and centered at the time of the bucket tip. The rate of rainfall during this five-minute of time is computed accordingly and assumed to be zero for the rest of the long record.
- If multiple bucket tips were recorded, the rate of rainfall is again assumed to be constant between adjacent tips except in the cases that the time between two adjacent tips are longer than 20 minutes. In this special case, it is assumed that, during this time of more than 20 minutes, the rain has stopped after the first of the two adjacent tips and restarted before the second of the adjacent tips. This assumption is the same as assuming that multiple rain events have occurred during this long record and that the rate of rainfall has to be computed separately for each event. The rate of rainfall at the beginning and end of these separate rain events are computed based on the same assumption applied to the case of isolated records.

Figure 3.5 shows the time history of bucket-tips recorded at the deck level for an example five-minute record (1998062817), together with the corresponding rate of rainfall computed according to the schemes described herein. The abrupt changes in the computed rainfall rate at the time of the bucket tips are obviously not realistic. But this rainfall rate so computed can still provide a reasonable assessment of the intensity of rainfall during the time the bucket tips were recorded. In the study herein, the representative rate of rainfall at the bridge site is taken as the maximum value of the rainfall rate computed based on the measurement at the tower top and that computed based on the measurement at the deck level.

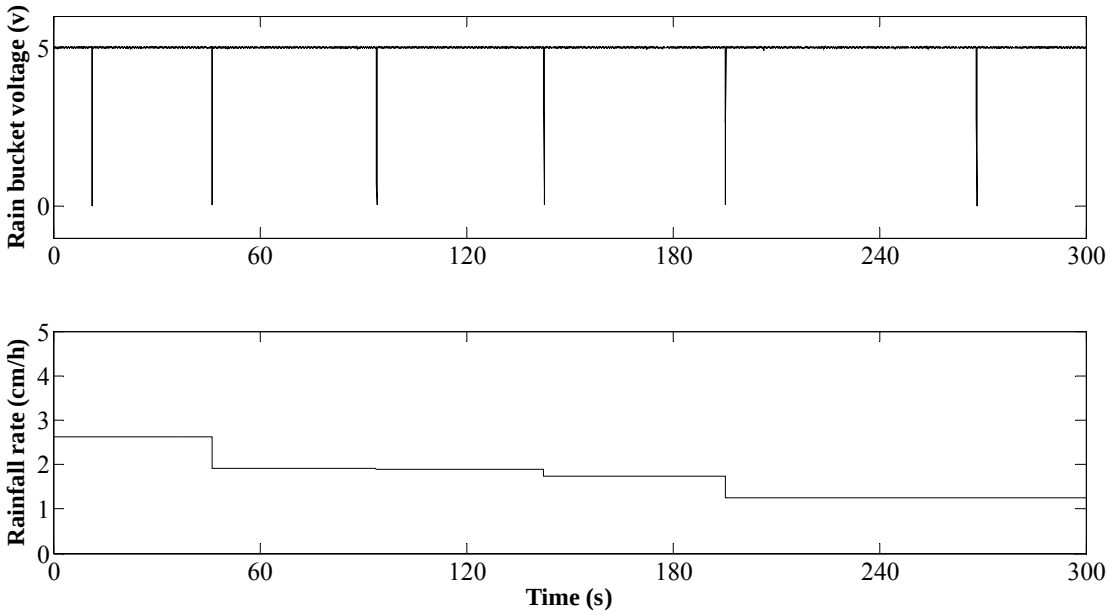

Figure 3.5 Example record showing bucket tips and corresponding rainfall rate computed

It should be pointed out that these schemes adopted to compute the rate of rainfall can be very imperfect in some cases due to the limitations of the rain gauges. It is therefore important to interpret the measurement of rainfall in the context of other measurements.

3.1.3 Measurement of Stay Cable Vibrations

The vibrations of selected stay cables of the Fred Hartman Bridge are primarily monitored by bi-axial accelerometers (Crossbow Technology, model CXL04LP3). The accelerometers have a threshold of 4 g and a noise level of 10 mg. They are installed on the stay cables at locations about 6 meters above the deck surface, and are oriented so that their two axes record the components of the vibrations in the in-plane and out-of-plane (referred to as "lateral" hereafter) directions simultaneously. To supplement the acceleration measurements, string-pot LVDTs (Unimeasure, HX-PB series) are also installed on selected stays at the deck rail level to monitor the in-plane and lateral displacements of these stays. The string-pot LVDTs can measure displacement of up to 5 cm and their listed resolution is essentially infinity.

A total of 20 stays have been instrumented on the Fred Hartman Bridge, although this number has varied from time to time during the measurement program. The major physical properties of the instrumented stays are listed in Table 3.1. The values listed in the table are "as built" values provided by TXDot. The plane angles are measured between the projections of the stays in the horizontal plane and the deck axis. All the stays listed have been instrumented with accelerometers, but only stays AS16, AS23, AS24, BS16 and BS24 are regularly monitored by string pot transducers.

Table 3.1 Properties of the instrumented stays of The Fred Hartman Bridge

Stay Name	Length (m)	Diameter (m)	Density (kg/m)	Tension (kN)	Inclination Angle (°)	Plane Angle (°)
AS1	172.35	0.310*	95.36*	5102.11	27.11	175.70
AS3	167.32	0.310	80.97	4457.12	27.06	175.72
AS5	136.96	0.168	70.12	3683.13	32.21	174.90
AS9	87.28	0.141	47.98	2028.39	48.95	170.80
AS16	87.33	0.141	47.93	2157.39	45.92	8.70
AS18	106.18	0.141	52.87	2393.14	35.30	6.09
AS20	139.70	0.168	70.12	3349.51	28.56	4.82
AS22	168.40	0.168	70.12	3545.23	24.13	4.08
AS23	183.06	0.194	76.03	4283.64	22.52	3.76
AS24	197.85	0.194	76.03	4528.29	21.11	3.52
AN24	197.85	0.194	76.03	4528.29	21.11	176.48
BS1	172.35	0.310*	95.36*	5102.11	27.11	175.70
BS8	98.73	0.141	52.87	2602.20	43.25	172.45
BS16	87.33	0.141	47.93	2157.39	45.92	351.31
BS18	106.18	0.141	52.87	2393.14	28.56	353.91
BS24	197.85	0.194	76.03	4528.29	21.11	356.48
CS1	172.35	0.310*	95.36*	5102.11	27.11	175.70
CS24	197.85	0.194	76.03	4528.29	21.11	3.52
DS1	172.35	0.310*	95.36*	5102.11	27.11	175.70
DS24	197.85	0.194	76.03	4528.29	21.11	3.52

*Represent the lower segments of the cables up to a distance 30 m from the anchorage at deck level, upper portion of the cables have the same diameter and density as stay AS24.

3.1.4 Measurement of Deck Vibration

The vibration of the bridge decks is also monitored by accelerometers at several locations. Initially, the same accelerometers used to monitor the stay cable vibrations were installed at the east edge of the decks near the anchorages of stays AS9, AS16, AS19, CS19, and at the mid-span of the east deck, respectively. In November 1999, the accelerometers installed on the east deck were replaced by more sensitive uni-axial accelerometers (Sunstrand Data Controls, Model QA-700). The uni-axial accelerometers have a range of 30 g and a bias level of 8 mg. During the later stages of the full-scale measurement program, the accelerometer at CS19 was moved to a location near the anchorage of stay BS19 to enable a more thorough assessment of the torsional vibration of the east deck.

3.1.5 Measurement of Damper Force

To monitor the performance of the dampers, load cells (Cooper Instruments and Systems, LGP 310) were installed in line with the dampers on stays AS16 and AS23. The load cells have a range of 0.02 to 2224.11 kN.

3.2 Monitoring System on the Veterans Memorial Bridge

Compared to the Fred Hartman Bridge, the Veterans Memorial Bridge is a structure much smaller in scale. It has a main span of 195 m. The 2.44 m high, 17 m wide box-girder deck is supported by a total of 112 cables, arranged in two parallel vertical planes originated from each of the two H shaped towers. The stays range from 11 m to 96 m in length, with varying diameters, and are connected to the bridge deck at a horizontal interval of 6 m.

The instrumentation system on the Veterans Memorial Bridge is similar in concept and design to the one on the Fred Hartman Bridge, but smaller in scale. It was installed on the bridge and began collecting data in February 1999. As many as 33 channels have been instrumented on the Veterans Memorial Bridge, although this number has changed considerably during the measurement program. A complete list of the instrumented channels can be found in Appendix B.2. The detailed status of these channels during the duration of the full-scale measurement project can be found in a MS Excel file in the data package that accompanies the present report (File "Veterans_Transducer_Timeline.xls"). The major physical properties of the instrumented stays are listed in Table 3.2. Again, the values listed in the table are "as built" values provided by TXDot. An important aspect of the full-scale measurement system is that unlike in the case of the wind measurements at the Fred Hartman Bridge, the wind measurements at the tower top and at the deck level of the Veterans Memorial Bridge are quite consistent. Statistical analysis of the wind measurements at the Veterans Memorial Bridge can be found in Appendix D. For brevity, the details of the monitoring system on the Veterans Memorial Bridge will not be described herein.

Table 3.2 Properties of the instrumented stays of the Veterans Memorial Bridge

Stay Name	Length (m)	Diameter (m)	Density (kg/m)	Tension (kN)	Inclination Angle (°)
A14	96.13	0.107	28.49	1490.15	21.58
A12	82.96	0.107	28.49	1556.88	21.58
A10	69.78	0.107	29.31	1690.32	21.58
B13	89.54	0.107	28.49	1512.40	21.58
B11	76.37	0.107	28.49	1623.60	21.58
B9	63.20	0.107	30.14	1768.17	21.58
C13	89.54	0.107	28.49	1512.40	21.58
C11	76.37	0.107	28.49	1623.60	21.58
D12	82.96	0.107	28.49	1556.88	21.58
D14	96.13	0.107	28.49	1490.15	21.58

4 Data Summary

A large quantity of data has been collected since the installation of the full-scale measurement systems. To date, the monitoring system on the Fred Hartman Bridge has recorded about 64000 five-minute records, and the system on the Veterans Memorial Bridge has recorded about 14000 records. To analyze and present this large amount of data, data processing techniques are applied to rationally interpret the raw measurements. This chapter outlines the data processing procedures used in the present study and summarizes the data packages that accompany this report.

4.1 Data Processing

4.1.1 Numerical Integration and Differentiation

The vibrations of the stay cables are mainly monitored by accelerometers that provide acceleration time histories. The acceleration measurement, however, inherently exaggerates the high-frequency components in the signal, which can represent either the higher modes in the vibrations that are not the primary modes of interest, or simply undesirable noise. In the present study, the acceleration time histories are numerically integrated twice to obtain the corresponding displacement time histories at the locations of the accelerometers. By numerically integrating the acceleration time histories, however, the low frequency noise in the signal will be exaggerated, which can produce a false drift in the generated displacement signal. This effect of numerical integration is eliminated by applying a sixth-order high-pass Butterworth filter (Mitra 2001) to the signal after each step of integration. The cut-off frequency for the high-pass filter is usually set to be half of the estimated fundamental frequency of the stays (assuming that the stays are taut strings with clamped ends), unless the acceleration shows significant vibration components at frequencies significantly lower than the fundamental frequency of the stay cables, such as in the case of stay cable vibration induced by low-frequency deck oscillation. In the latter case, the cut-off frequency is set to be 0.1 Hz lower than the frequency of the lowest frequency component of the vibration.

Figure 4.1 shows the in-plane acceleration time history of stay AS1 on the Fred Hartman Bridge for an example five-minute record (1997120737) and the corresponding displacement time history generated through numerical integration. To illustrate the effectiveness of the Butterworth filter in eliminating the false drift produced by the numerical integration process, the displacement time histories before and after filtering are both included in the graph. Figure 4.1 also shows the irregularities generated by the spurious end effects of the filter at both ends of the displacement time histories. In the subsequent discussions, the beginning and ending ten-second segments of the five-minute records will be discarded since they are numerically contaminated.

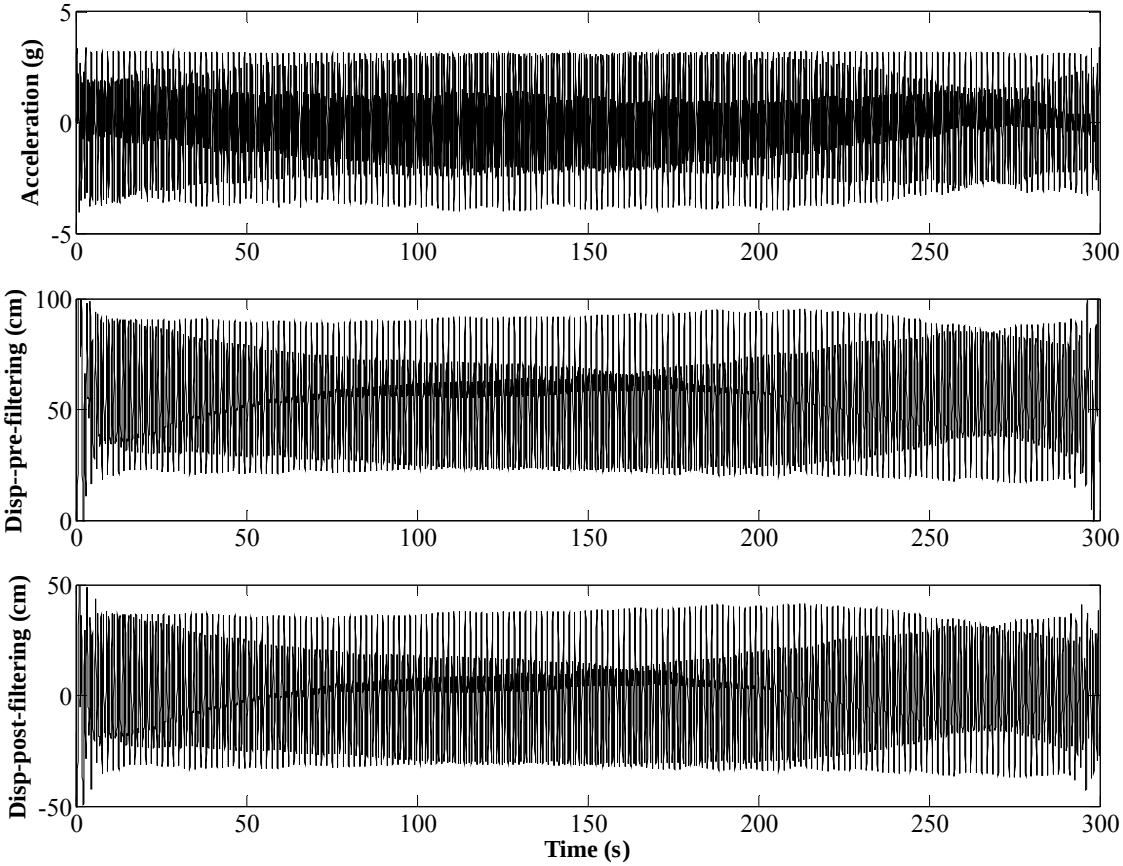

Figure 4.1 Example record showing generation of displacement by numerically integrating acceleration measured by accelerometers

4.1.2 Band-Pass Filtering

Analysis of the full-scale measurement data suggests that wind- and rain-wind-induced stay cable vibrations are usually composed of one to several significant modes and some relatively insignificant ones. Figure 4.2 shows the Spectrogram of the displacement time histories displayed in Figure 4.1. The spectrogram function of the displacement is estimated by computing the windowed discrete-time Fourier transform of the data using a sliding Hanning window of 256 points (6.04 seconds) in length, with each window overlapping adjacent ones by half the length. The magnitude of the spectrogram function at a specific time-frequency point is represented by its color depth: the darker the color, the greater the magnitude. The spectrogram is chosen herein as the primary approach to qualitatively represent the vibrations in the frequency domain because the vibrations recorded are not usually stationary. Figure 4.2 suggests that for this particular example record, the in-plane displacement of stay AS1 is dominated by the second and third modes.

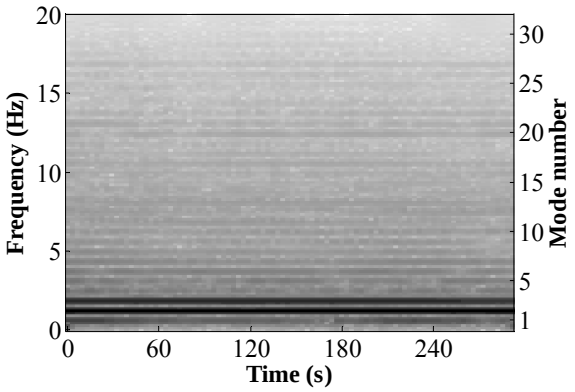

Figure 4.2 Spectrogram of an example displacement time history

Figure 4.1 and Figure 4.2 have only shown the in-plane response of stay AS1 for the example record. Full-scale measurement data suggest that wind- and rain-wind-induced vibrations can be highly two dimensional. In particular, if the vibration consists of multiple significant modal components, different amplitude, direction and phase combinations of the significant modes can result in very complex patterns of vibration. This can be illustrated in Figure 4.3, which depicts the vibration locus of stay AS1 at the accelerometer location for a fourteen-second segment of an example record, of which the in-plane component has already been shown in Figure 4.1. For complex patterns such as this, it is often difficult to effectively and efficiently characterize the overall vibrations. It is therefore desirable to characterize the vibrations at the modal level.

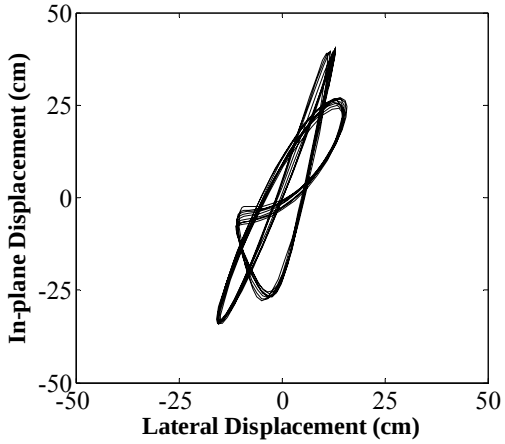

Figure 4.3 Complex vibration locus of an example record segment

To investigate the modal characteristics of the vibrations and study the excitation mechanisms that are responsible for each mode of vibration, the sixth-order band-pass Butterworth filter (Mitra 2001) is used to decompose the overall displacement response into modal components. For each cable of interest, the pair of cut-off frequencies for the Butterworth filter are chosen to be a quarter of the theoretical fundamental frequency of the cable below and above the frequency of the mode of interest. The theoretical frequencies were computed based on the assumption that the cables can be treated as linear strings clamped at both ends. To illustrate the effectiveness of the band-pass filtering process, the fourteen-second segment of vibration shown in Figure 4.3 is decomposed into the first

several modes of the stay (AS1). Figure 4.4 shows the vibration locus of the second and third modes, which are the most significant modes of vibration for this specific segment. It is evident that although the overall pattern of the vibration (Figure 4.3) is complex, the vibration loci of the individual modes are rather simple and appear to be near-elliptical. Figure 4.5 shows the original vibration locus (a)) alongside with the locus reconstructed by adding the modal components in the second and third modes together (b)). It can be seen that the primary characteristics of the original vibration have been quite faithfully preserved by the reconstructed vibration. The difference between the two can be attributed to the fact that some less-significant modal components are present in the original record but not in the reconstructed record.

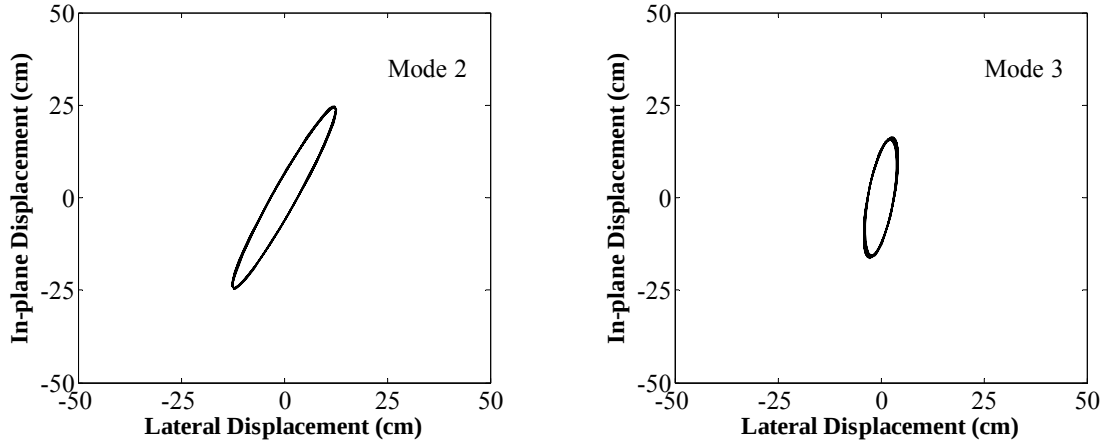

Figure 4.4 Vibration locus of significant modes decomposed from an example record

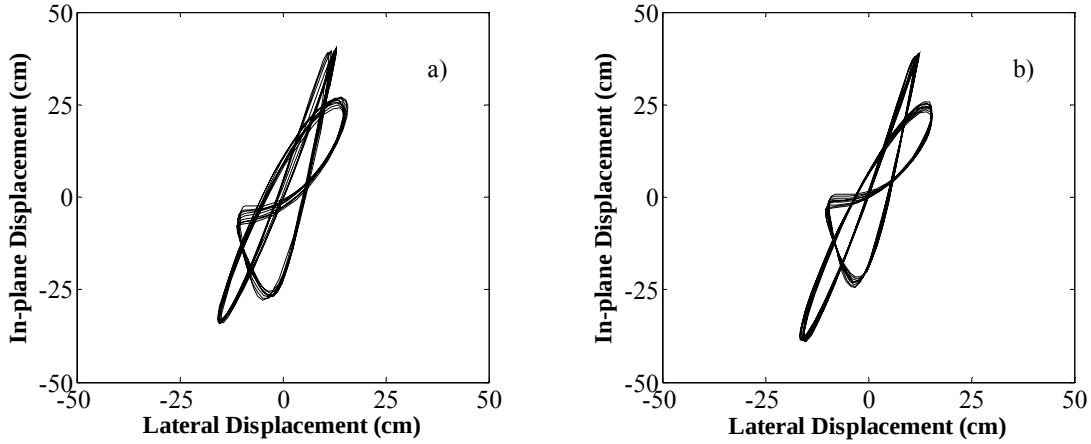

Figure 4.5 a) Original and b) reconstructed vibration locus of an example record

4.1.3 Spatial Characterization of Vibrations

It has to be pointed out that the modal vibration loci of the stay cables are near-elliptical only when the vibrations in these modes are close to stationary. This is not usually true for the five-minute records recorded by the full-scale measurement system. In the

present study, to enable better resolution for analysis, the five-minute displacement time histories are broken into 20 fourteen-second segments after the beginning and ending ten-second segments are discarded. If a fourteen-second segment is close to stationary, a least-squares method (Fitzgibbon et al. 1999) is used to fit the near-elliptical vibration locus with an ellipse. Figure 4.6 shows the result of the ellipse-fitting procedure for the vibration locus of an example fourteen-second segment. To investigate the vibration in the context of the three-dimensional wind-cable environment, a spatial coordinate system is also defined and shown in Figure 4.6. In this coordinate system, the modal vibration is characterized in the directions of the major and minor axes of the ellipse. The amplitudes of the vibration in these two directions are taken as the length of the major axis (OA) and minor axis (OB) of the ellipse, respectively, and the major direction of the modal vibration is approximated as the angle between the major axis of the ellipse and the vertical cable plane (φ). Because the accelerometers are not necessarily located at the anti-nodal points of the individual modes of the stay cables, the major-axis amplitude and minor-axis amplitude of the stay cables are scaled to the anti-nodal points, based on the assumption of sinusoidal mode shapes, to estimate the anti-nodal modal amplitudes of the vibration. To assist the interpretation of the vibrations, the inclination angle of the stay cable is designated α in the coordinate system, and the angle between the direction of the wind and the projection of the cable axis in the horizontal plane is defined as the attack angle of wind (β). The attack angle ranges from 0° to 180°.

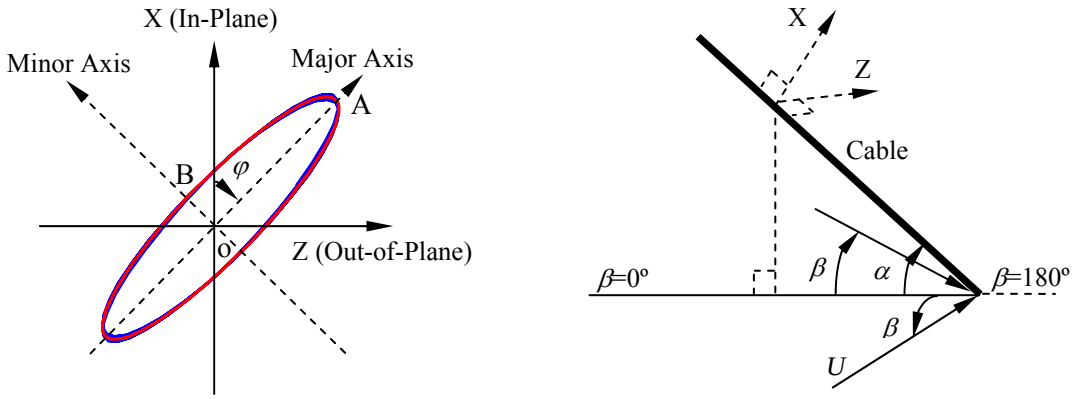

Figure 4.6 Coordinate system for characterization of stay cable vibrations

4.1.4 Frequency Estimation Using the Hilbert Transform

While better resolution can be achieved for the analysis in the time domain by breaking the five-minute records into 20 fourteen-second segments, the length of these short segments is not sufficiently long to provide adequate resolution for frequency estimation using spectral analysis techniques . In the study herein, the Hilbert Transform (Bendat and Piersol 1986), through which the amplitude and frequency of a process can be simultaneously identified, is used to estimate the instantaneous frequency of the modal vibration. Figure 4.7 shows the frequency estimation results for the third-mode component of the in-plane displacement time history shown in Figure 4.1. For illustration purposes, the instantaneous vibration amplitude identified through the Hilbert Transform is also included. It can be seen

that both the amplitude and the frequency of the vibration have been consistently identified through the Hilbert Transform. The irregularities at both ends of the record are again induced by the spurious filter effects created during the high-pass and band-pass procedures. In the study herein, the representative frequency of the modal vibration in the individual fourteen-second segments is taken as the average value of the estimated instantaneous frequency during these periods of time.

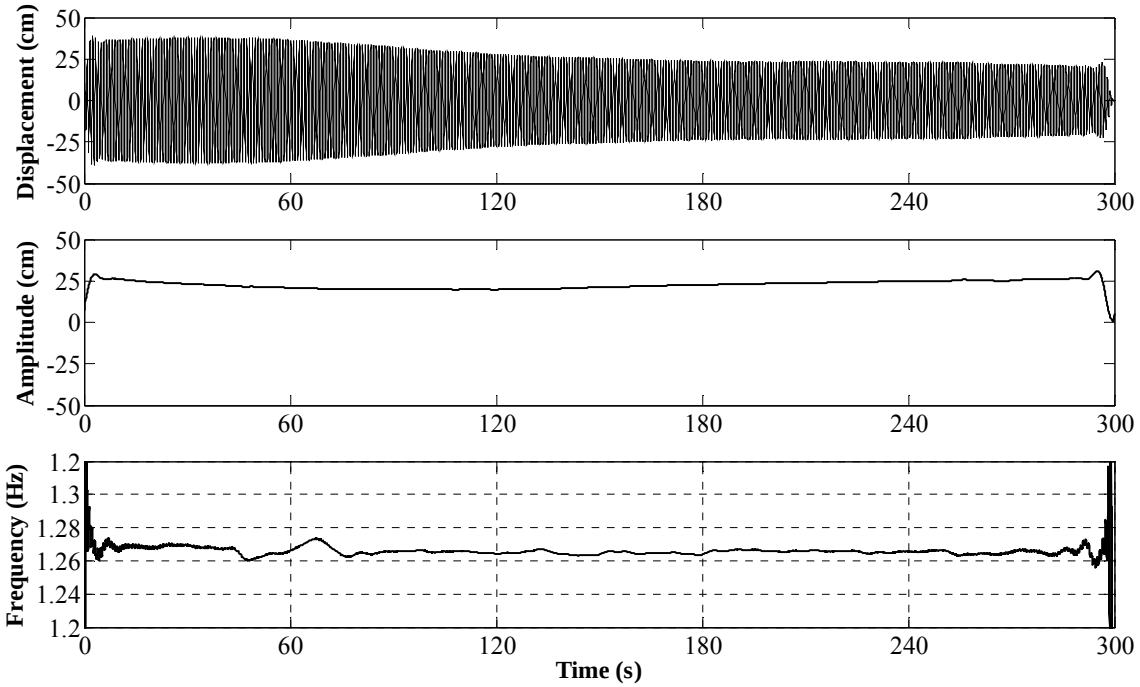

Figure 4.7 Frequency estimation using the Hilbert Transform

4.2 Data packages

The full-scale measurement system on the Fred Hartman Bridge and that on the Veterans Memorial Bridge have each generated a data set of five-minute records. With the data processing procedures described herein, the fourteen-second-average modal amplitude, frequency and direction of the recorded vibrations can be estimated for the stay cables under monitoring. Because the vibrations usually occur in the lower modes of the stay cables, in the study herein, these average characteristics of the vibrations are computed only for those of the first ten modes of the stay cables, of which the displacement amplitude is greater than two percent of the cable diameter. These modal characteristics of the vibrations, as well as the corresponding fourteen-second mean meteorological conditions (i.e., wind and rain) are stored in relational databases, within which queries can be issued and specific data of interest can be retrieved. Two such databases have been compiled from the full-scale measurement data, one for each bridge. These two databases, which represent the core results of the field investigation project, are included in one of the data packages accompanying the present report. Other data packages that accompany the report include all the five-minute records collected by the full-scale measurement systems and two complimentary databases, in which some statistics of the raw measurement, such as the one-minute root-mean-square (RMS) value of the recorded acceleration of the stay cables, are stored. A complete list, as well as detailed descriptions of the data packages, can be found in Appendix E.

5 Observed Vibrations

Analysis of the characteristics of recorded vibrations and their relationship with wind and rain has led to the identification of several distinct types of wind- and rain-wind-induced stay cable vibrations. These include Kármán-vortex-induced vibrations, rain-wind-induced vibrations, a particular type of large-amplitude dry cable vibration, vibrations induced by the oscillation of the bridge deck and some large-amplitude vibrations that are yet to be categorized. This chapter presents the observed characteristics of these individual types of vibrations. Special attention is directed to Kármán-vortex-induced vibrations, rain-wind-induced vibrations and a type of large-amplitude dry cable vibration. The possible connection among these three types of vibrations is also explored. Although many cables have been observed to exhibit multiple types of vibrations, the discussion herein will primarily be based on the vibrations of several of the stay cables instrumented, because only these cables have been instrumented for sufficiently long periods of time while unrestrained that the characteristics of the vibrations observed can be considered adequately exhaustive and representative.

5.1 Kármán-Vortex-Induced Vibrations

Kármán-vortex-induced vibrations are characterized by the classical Strouhal relationship between the mean wind velocity and the shedding frequency of the von Kármán vortices, as well as the ability of the shedding frequency of the vortices to lock in with the mechanical frequency of the structure when the two are close, and to create vibration of significant amplitude. Kármán-vortex-induced vibration is one of the most frequently observed types of stay cable vibrations on both the Fred Hartman Bridge and the Veterans Memorial Bridge. Although the typical displacement amplitude of this type of vibration is small compared to that of vibrations induced by many other mechanisms, the observations on the bridges suggest that Kármán-vortex-induced vibrations of inclined stay cables have unique characteristics and that understanding of these characteristics may shed light onto the understanding of some other types of vibrations that share similar characteristics with Kármán-vortex-induced vibrations, but whose amplitude is much higher.

Figure 5.1 shows the displacement time histories and the corresponding spectrograms of a typical Kármán-vortex-induced vibration record (200109236, stay AS22, Fred Hartman Bridge), and Figure 5.2 shows the associated wind speed and direction. It can be seen in these two figures that, under the excitation from the relatively smooth, low-speed wind, stay AS22 has exhibited relatively high-frequency, low-amplitude vibration. The spectrograms of the displacements in both directions, however, also suggest that for this particular record, the vibration has significant components in both the seventh and the eighth modes of the cable. This fact that multiple modes are present in the locked in Kármán-vortex-induced vibration is not typical for a short circular cylinder subjected to Kármán vortex excitation from uniform wind perpendicular to its axis, wherein the response is dominated by only one primary frequency component, which is the Strouhal frequency of the cylinder at this particular wind speed.

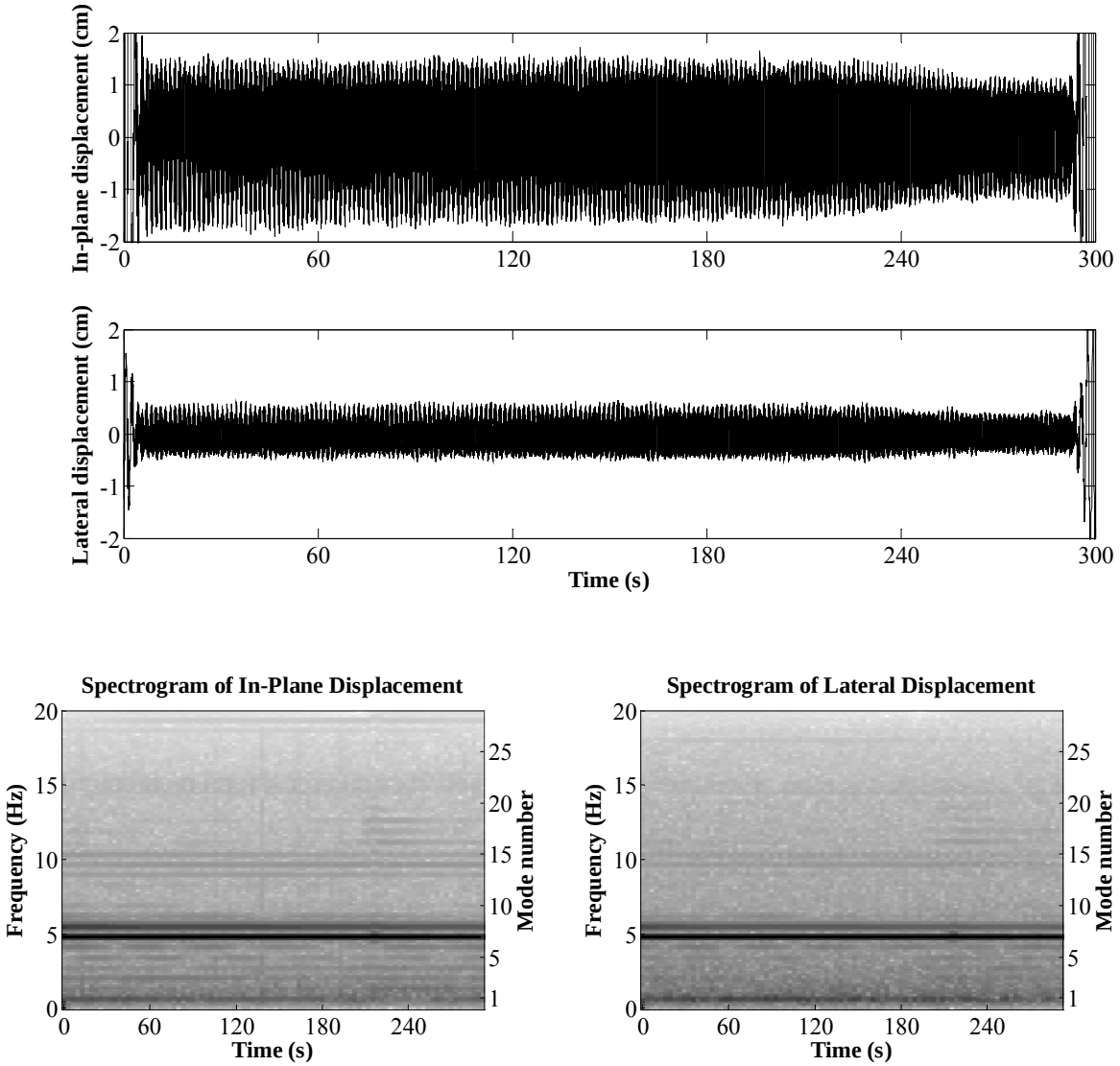

Figure 5.1 Time histories and spectrograms of an example Kármán-vortex-induced vibration record

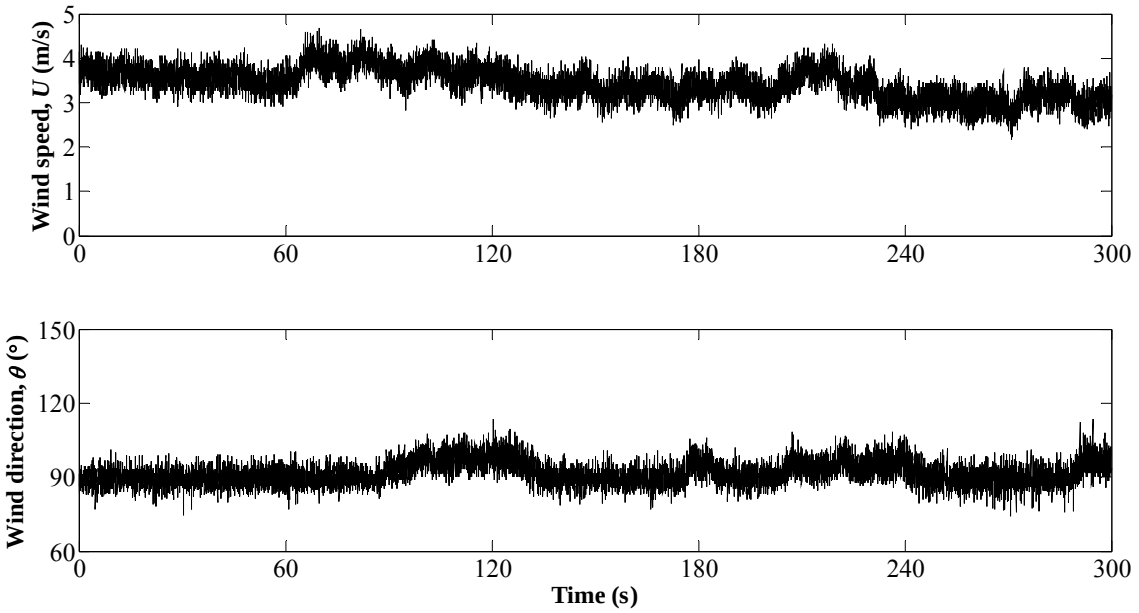

Figure 5.2 Wind speed and direction associated with a Kármán-vortex-induced vibration record

The presence of the two significant modes in this record can be explained by the fact that the mean wind speed increases with height due to the profile of the boundary layer. Because the Strouhal frequency depends linearly on mean wind speed, the frequency of Kármán vortex shedding also increases with height. Consequently, for an inclined cable, Kármán vortex shedding can be locked in with different modal frequencies over different regions along the cable axis. The "lock-in region" for a specific mode is that portion of the cable over which the shedding frequency of Kármán vortices is sufficiently close to the modal cable frequency for lock-in to occur. Further, for a specific mode, the generalized force is integrated with the mode shape along the axis of the cable. The energy input in a specific mode therefore depends on the fraction of the cable over which the lock-in region for that mode extends. As a result, the same excitation force acting over different lock-in regions will produce different generalized forces and therefore different amplitudes of the vibration. In the sheared profile of the boundary layer, when the wind speed changes, the "lock-in region" for each mode moves along the axis of the cable and the generalized force and consequently the amplitude of the cable response also change correspondingly. This sheared profile of the boundary layer therefore inhibits a simple relationship between the amplitude of Kármán-vortex-induced vibrations and the speed and direction of wind.

In addition to the significant components in the seventh and the eighth modes, the spectrograms also revealed noticeable modal components at the frequency of about 10 Hz, which is about twice the Strouhal frequencies. These modal components are suspected to be due to the super-harmonics associated with the potentially non-harmonic Kármán vortex excitation, although it also can be due to unidentified nonlinearities in the system.

The displacement time histories in Figure 5.1 also suggest that, for this specific record, the vibration induced by Kármán vortex shedding is highly two-dimensional. Figure 5.3 shows the vibration loci of the two significant modal components at the location of the accelerometer for a fourteen-second segment of the record. For both modes, the vibration

locus is near-elliptical. The major characteristics of such near-elliptical vibrations can be represented in the coordinate system shown in Figure 4.6.

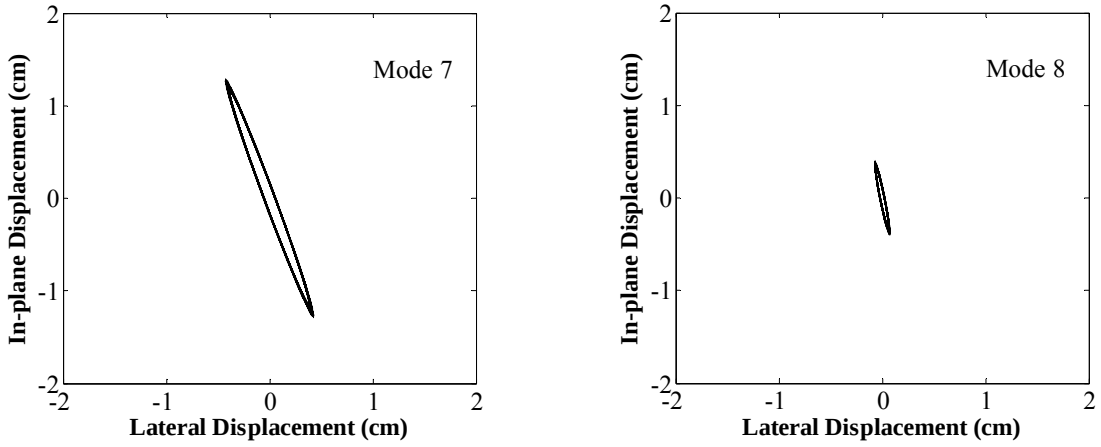

Figure 5.3 Modal vibration loci of an example Kármán-vortex-induced vibration record

Figure 5.4 shows the fourteen-second mean anti-nodal amplitude of recorded steady-state Kármán-vortex-induced vibrations of stay AS23 versus the corresponding mean wind speed and attack angle at the deck level. Only data points with displacement amplitude larger than three percent of the cable diameter have been included. In the graph, the amplitude of the vibration is represented by the diameter of the circles. For reference purposes, the diameter of the cable (1D) is also shown. Although there is no clear relationship between the amplitude of the vibrations and the mean wind speed and direction, Figure 5.4 does suggest that Kármán-vortex-induced vibration occurs at relatively low wind speed over a broad range of wind directions, and that the modal amplitudes of the vibrations are obviously self-limiting and are small compared to the diameter of the stay cable. The figure also reveals that different modes of vibration cluster in different regions of wind speed and direction. In particular, for the same attack angle, the higher modes of Kármán-vortex-induced vibration occur at higher wind speeds, and for each mode, there is a trend of increasing lock-in wind speed when the attack angle deviates from 90°. This suggests that the cable might have been excited only by a component of the wind, for example, the component normal to the cable axis.

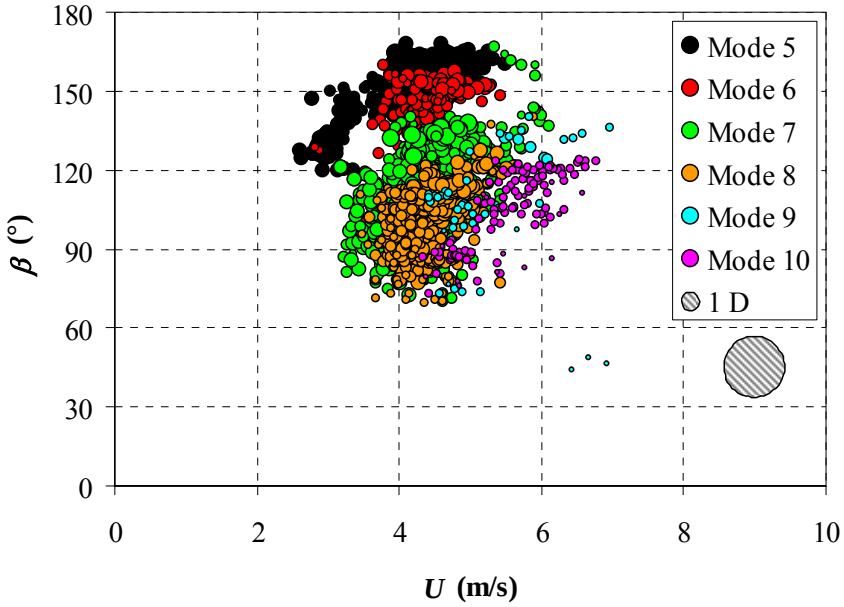

Figure 5.4 Amplitude vs. wind speed and attack angle for Kármán-vortex-induced vibration of stay AS23

To investigate the Strouhal relationship between recorded Kármán-vortex-induced vibration and wind, Figure 5.5 displays the steady-state vibration amplitudes against the reduced velocity V_r and the attack angle β; $V_r = U/(fD)$, where f is the frequency of the vibration. For locked-in Kármán-vortex-induced vibration, the reduced velocity is the reciprocal of the Strouhal number. For a circular cylinder subjected to the excitation of uniform wind normal to its axis, the value of reduced velocity at which Kármán-vortex-induced vibration occur is about 5. Figure 5.5 suggests that when the attack angle is about 90°, the Strouhal relationship for stay AS23 is the same as, or close to, that of a circular cylinder subjected to perpendicular uniform wind. The fact that the data points are centered at a value less than 5 is believed to be due to the fact that the reduced velocity is computed based on the wind speed measured at the deck level, which is less than the actual wind speed that is responsible for the excitation. This fact can also be used to interpret the considerable spread of the data in the graph. Figure 5.5 also suggests, however, that when the attack angle increases beyond about 120°, the required reduced velocity for the vibrations to occur becomes much higher than 5.

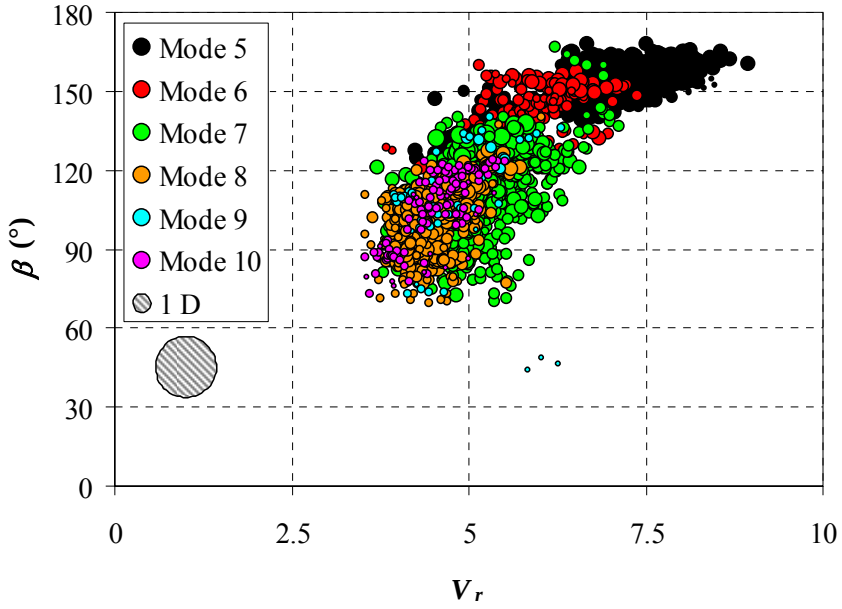

Figure 5.5 Amplitude vs. reduced velocity and attack angle for Kármán-vortex-induced vibration of stay AS23

Figure 5.6 shows the steady-state vibration amplitude of Kármán-vortex-induced vibrations against the reduced velocity computed based on the component of wind that is normal to the vertical cable plane, which is designated $V_{n,r}$; $V_{n,r} = U \sin\beta / (fD)$. It is evident that the reduced velocity associated with Kármán-vortex-induced vibrations is significantly different from the theoretical value of 5 when the attack angle is beyond about 120°. This

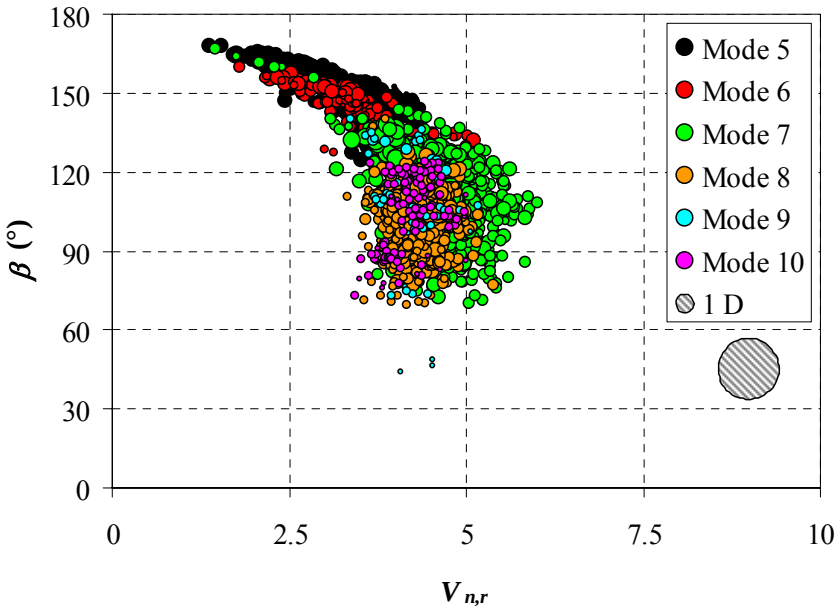

Figure 5.6 Amplitude vs. reduced velocity of wind component normal to vertical cable

suggests that the Kármán-vortex-induced vibrations of inclined and yawed stay cables cannot be simply treated as the result of the excitation from the wind component normal to the vertical cable plane.

To spatially characterize wind- and rain-wind-induced vibrations of inclined stay cables, Matsumoto et al. 1999) introduced the so-called relative yaw angle, which is shown as β' in Figure 5.7 and defined as

$$\beta' = \arcsin(\cos\alpha \cdot \cos\beta) \tag{5.1}$$

Accordingly, the plane in which the relative yaw angle is in is also defined (Plane OAB) and termed the "π plane". To more intuitively and directly characterize the angle between the wind and the cable axis in the cable-wind plane, the study herein uses the angle β^* shown in Figure 5.7, which is designated the effective attack angle of wind and has the value of

$$\beta^* = \arccos(\cos\alpha \cdot \cos\beta) \tag{5.2}$$

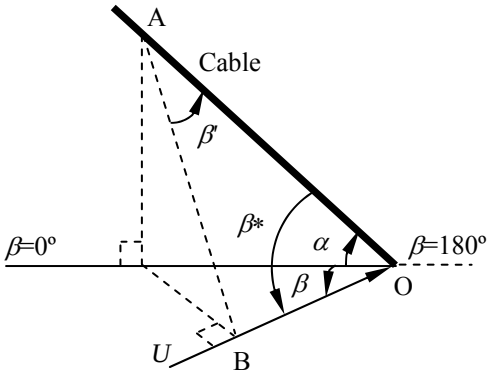

Figure 5.7 Relative wind attack angle

Figure 5.8 shows the relationship between steady-state Kármán-vortex-induced vibrations and the reduced velocity computed based on the component of wind that is in the π plane and normal to the cable axis, which is designated $V^*_{n,r}$; $V^*_{n,r} = U\sin\beta^*/(fD)$. It is evident that this relationship is also complex when the effective wind attack angle deviates considerably from 90°, although this relationship appears to be more consistent over the entire range of attack angles than the corresponding relationships shown in Figure 5.5 and Figure 5.6 . This suggests that for yawed and inclined cables, the component of wind in the π plane and normal to the cable axis cannot be treated as the "effective wind component" responsible for the Kármán-vortex-induced vibrations either.

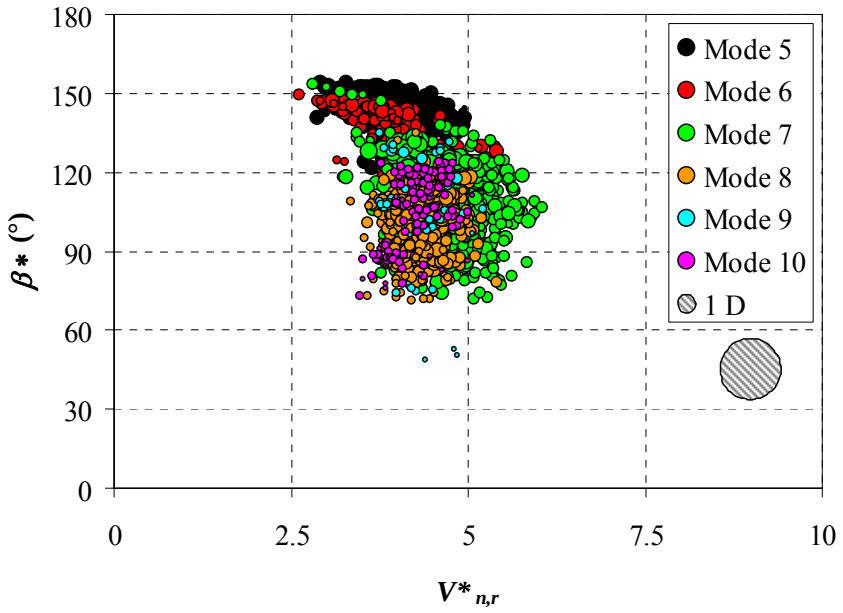

Figure 5.8 Amplitude vs. reduced velocity of wind component normal to cable axis in the π plane and effective attack angle for Kármán-vortex-induced vibration of stay AS23

The complex relationship between Kármán-vortex-induced vibrations and the wind excitation also manifests in the nonlinear relationship between the major direction of the vibration and the direction of the approaching wind, as shown in Figure 5.9. For comparison purposes, Figure 5.9 also includes the angle between the vertical cable plane and the plane normal to the π plane, which is designated φ^*, for stay AS23 for different attack angles. For a given pair of inclination angle α and attack angle β, it can be seen in Figure 5.9 that the observed major direction of the Kármán-vortex-induced vibrations is usually not in the plane perpendicular to the π plane. In particular, Figure 5.9 also indicates that the vibration is not exactly in the vertical cable plane even when the approaching direction of wind is perpendicular to this plane. This figure does suggest, however, that there is a clear, consistent, relationship between the direction of the Kármán-vortex-induced vibrations and the direction of the approaching wind.

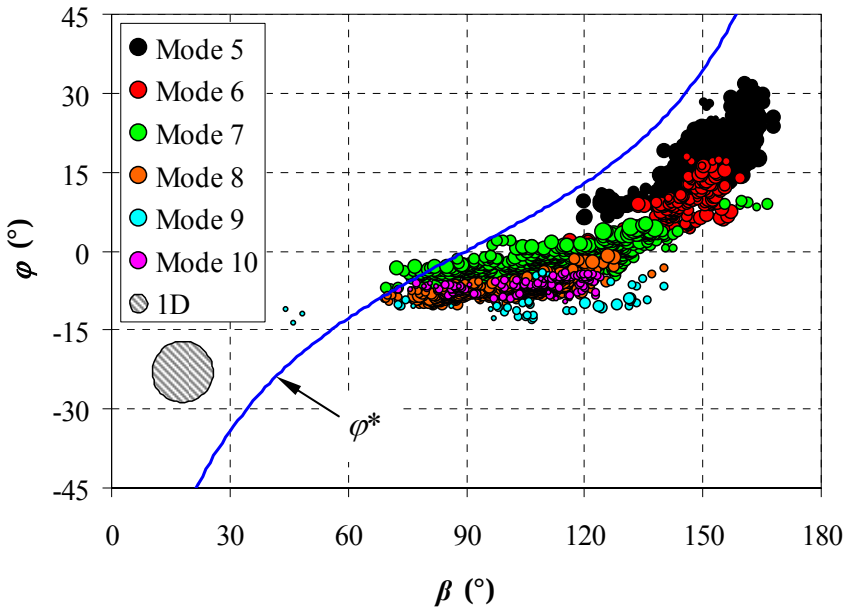

Figure 5.9 Major axis angle vs. attack angle for Kármán-vortex-induced vibration of stay AS23

All this evidence suggests that when the attacking wind is not perpendicular to the axis of the stay cable, Kármán-vortex-induced vibration cannot be simply treated as the response of the stay cable to the normal component of wind. This is in agreement with the observations from wind tunnel tests by Shirakashi et al. (1986). Observations from the same wind tunnel tests also suggest that, when wind is not perpendicular to the axis of the circular cylinder, the trace of the Kármán vortices is also not normal to the axis of the cylinder. The cross-section between the cable and the trace of the flow around it, therefore, is not necessarily circular. It is then suspected that, due to the complex structure of the vortices, when wind is not perpendicular to the cylinder, the Strouhal number corresponding to Kármán-vortex-induced vibrations can be significantly different from 0.2, which is approximately the value for a circular subjected to uniform perpendicular wind. For Kármán-vortex-induced vibration of inclined stay cables, the problem is potentially much more complicated since the structure of the vortices will likely be more complex due to the sheared nature of wind in the boundary layer. This has in fact been indicated in Figure 5.9 that even when the direction of the wind is normal to the vertical cable plane, the vibration of the cable still has a lateral component (i.e., $\varphi \neq 0°$). Also due to the sheared nature of the flow in the atmospheric boundary layer, the effective wind attack angle β^* is in fact not necessarily a good parameter for characterizing the relationship between Kármán-vortex-induced stay cable vibrations and the approaching direction of wind. For example, for a stay cable of any inclination, the effective wind attack angle would be 90° if the direction of the approaching wind is perpendicular to the vertical cable plane. But the aeroelastic behavior of a horizontal or vertical cable subjected to wind perpendicular to the cable plane is obviously different from that of a significantly inclined cable subjected to the same wind.

It is important to point out that, according to Figure 5.5, for Stay AS23, Kármán-vortex-induced vibration appears to occur only when the attack angle is greater than about 70°. This, however, is a false impression due to the fact that these Kármán-vortex-induced

vibrations were recorded during a relatively short period of time (from October 3, 1997 to December 10, 1997), and that during this time, low speed wind seldom approached from the directions that correspond to attack angles in the range of 0° to 70° for stay AS23. This fact can be observed in Figure 5.10, which shows the histogram of the attack angles for stay AS23, for recorded wind speeds in the range of 2 m/s to 7 m/s, which is the range over which Kármán-vortex-induced vibrations of significant amplitude were recorded for stay AS23.

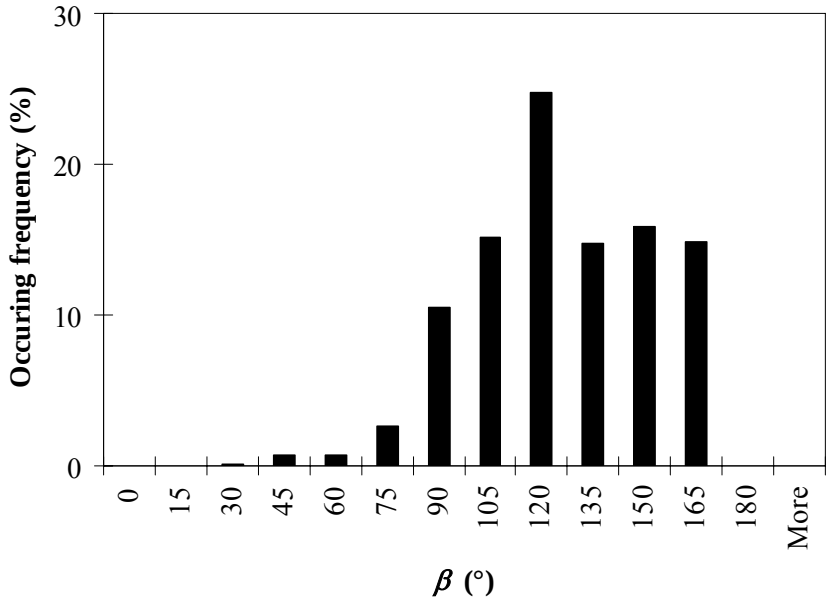

Figure 5.10 Histogram of attack angle relative to stay AS23 for wind speed in the range of 2 m/s to 7 m/s

In fact, Kármán-vortex-induced vibrations can occur over a broad range of attack angles for inclined stay cables. Figure 5.11 shows the fourteen-second mean displacement amplitude of steady-state Kármán-vortex-induced vibrations of stay A14 on the Veterans Memorial Bridge versus the corresponding mean wind speed and attack angle, and Figure 5.12 shows the correlation between the major direction of the vibrations and the attack angle. As can be seen in these two figures, for this particular stay, Kármán-vortex-induced vibrations occurred over almost the whole range of wind directions, but the correlation between the vibrations and the speed and direction of the wind are similar to those of the Kármán-vortex-induced vibrations of stay AS23 on the Fred Hartman Bridge.

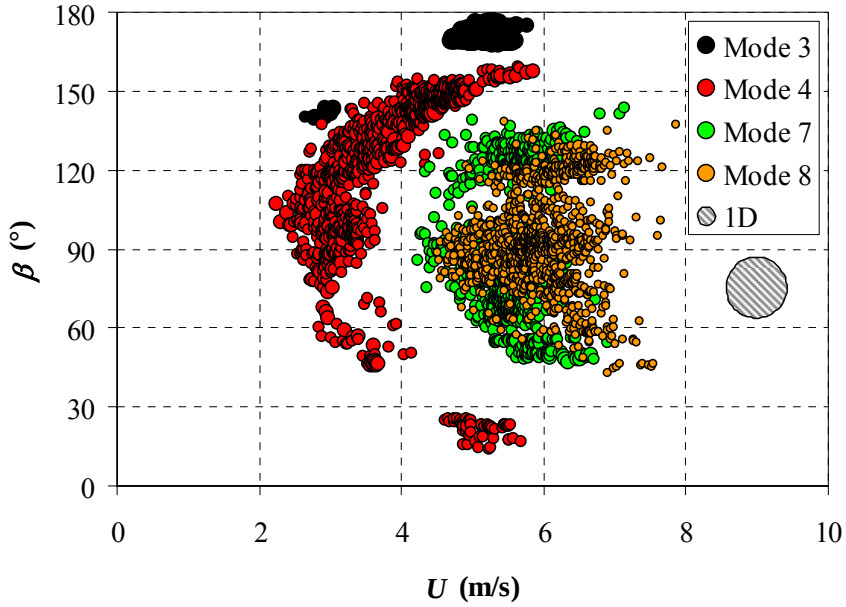

Figure 5.11 Amplitude vs. wind speed and attack angle for Karman-vortex-induced vibration of stay A14

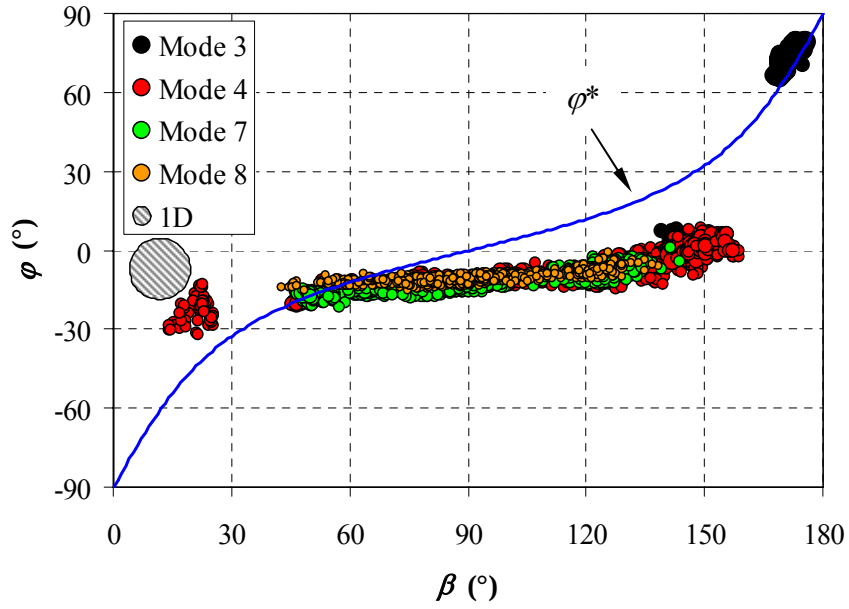

Figure 5.12 Major Axis angle vs. attack angle for Kármán-vortex-induced vibrations of stay A14

It has to be noted, however, that for some stays, Kármán-vortex-induced vibrations did not reach significant amplitude. In particular, the longer stays on both bridges have more frequently exhibited locked-in Kármán-vortex-induced vibrations than have the shorter ones. This different susceptibility of different stays to Kármán-vortex-induced vibrations is suspected to be due to the different level of damping and stiffness in different stays. If a stay did exhibit significant-amplitude Kármán-vortex-induced vibrations, however, the data

suggest that the characteristics of the vibrations and their correlation with wind are similar to those for stays AS23 and A14.

5.2 Rain-Wind-Induced Vibration

Rain-wind-induced vibrations are the most frequently observed large-amplitude vibrations on cable-stayed bridges around the world. The name "rain-wind-induced vibrations" is coined because these vibrations are usually associated with the simultaneous occurrence of wind and rain. Other important known characteristics of rain-wind-induced vibrations include that they usually occur at frequencies that are much lower than the nominal Strouhal frequency at the corresponding wind speed, and that they can reach very large amplitude. Rain-wind-induced vibrations have been observed to occur over a broad range of wind speed, but the onset of the vibrations appears to be closely related to the direction of the approaching wind.

Rain-wind-induced stay cable vibrations have been frequently observed on both the Fred Hartman Bridge and the Veterans Memorial Bridge. Figure 5.13 a) and Figure 5.13 b) indicate the ranges of wind speed and attack angle over which stays AS16 and AS24 on the Fred Hartman Bridge have exhibited large-amplitude rain-wind-induced vibrations. The black open circles in the graphs represent the speed and attack angle of the wind during the events when rainfall was simultaneously recorded, and the solid red circles represent the portions of events of simultaneous occurrence of wind and rain wherein the stay cables have exhibited vibration amplitude of more than 5 percent of the their respective diameters at frequencies much lower than the nominal Strouhal Frequencies. These graphs suggest that for both stays, the vibrations occurred over broad ranges of wind speed, but the ranges of attack angle over which the vibrations occurred are very different for these two stays. Specifically, stay AS16 exhibited large-amplitude vibrations only when the attack angle was around or less than 90°, while for stay AS24, the vibrations occurred over a much broader attack angle range of approximately 40° to 160°, although it does appear that for stay AS24, rain-wind-induced vibrations occurred more frequently when the attack angle was around or less than 90°. This difference between the attack angle ranges over which large-amplitude rain-wind-induced vibrations occur is believed to be primarily due to the different inclination angles of stay AS16 ($\alpha = 46.02°$) and stay AS24 ($\alpha = 21.94°$). It is particularly important to note that for stay AS24, rain-wind-induced vibrations occurred when the attack angle was much greater than 90°, which is contrary to previous reports that only stay cables declining in the direction of wind are susceptible to rain-wind excitations (Hikami and Shiraishi 1988). This fact also has significant implication on the role of rainfall in the excitation mechanism of rain-wind-induced vibrations: When the wind approaches from an attack angle significantly greater than 90°, the mean drag force will push the water on the cable surface downward, which will prevent a sustained, well-organized water rivulet from being formed on the upper surface of the cable. The hypothesis that rain-wind-induced vibrations are initiated by the movement or the position of the water rivulet on the windward side upper surface of cable (e.g., Hikami and Shiraishi 1988; Bosdogianni and Olivari 1996), therefore, still needs to be subjected to further investigation.

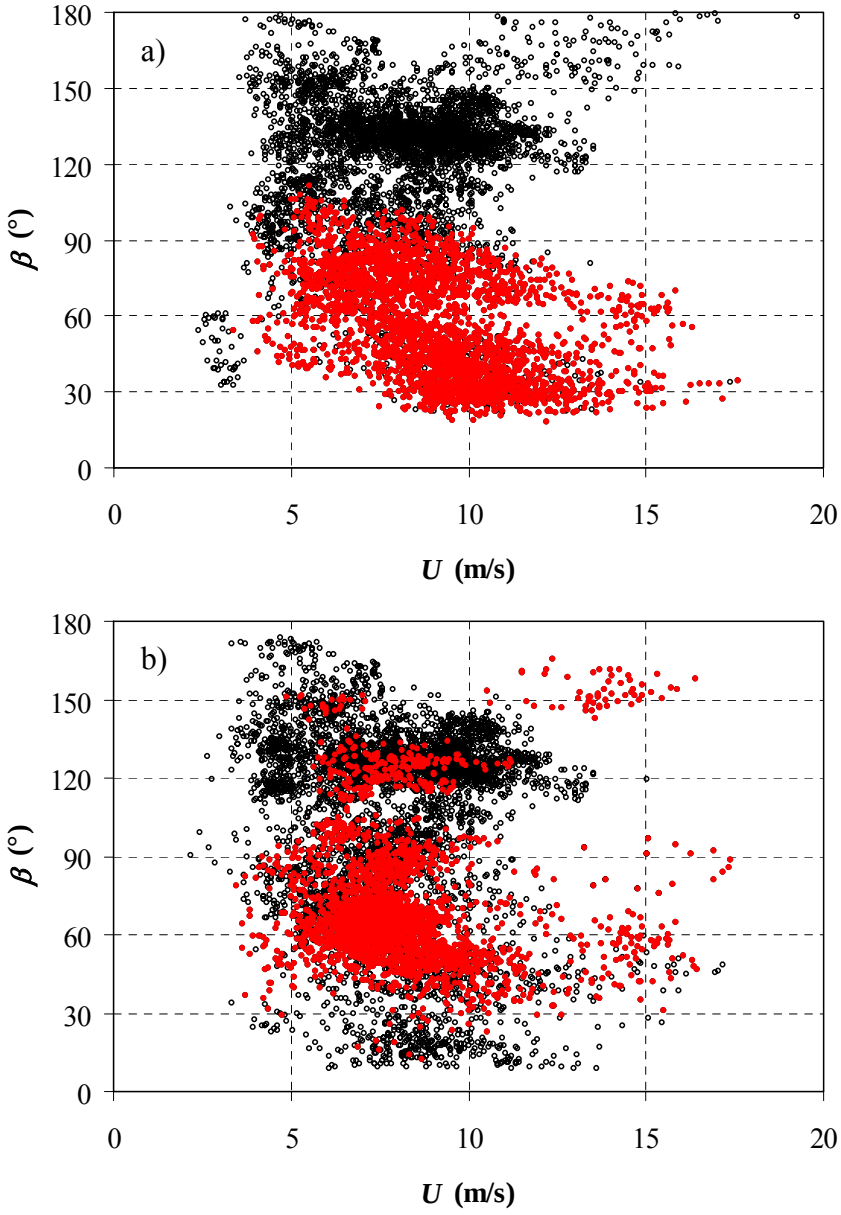

Figure 5.13 Ranges of wind speed and attack angle for rain-wind-induced vibrations: a) stay AS16 and b) stay AS24

While field observations have indicated that the effective attack angle β^* cannot completely characterize the directional effects of wind excitation on Kármán-vortex-induced vibrations. It is of interest to explore whether this parameter can be used to reasonably characterize rain-wind-induced vibrations. Figure 5.14 a) and Figure 5.14 b) show the ranges of wind speed and effective attack angle over which rain- wind-induced vibrations occurred for stays AS16 and AS24, respectively. It can be seen that these two stays have exhibited rain-wind-induced vibrations over two very different ranges of effective wind attack angle.

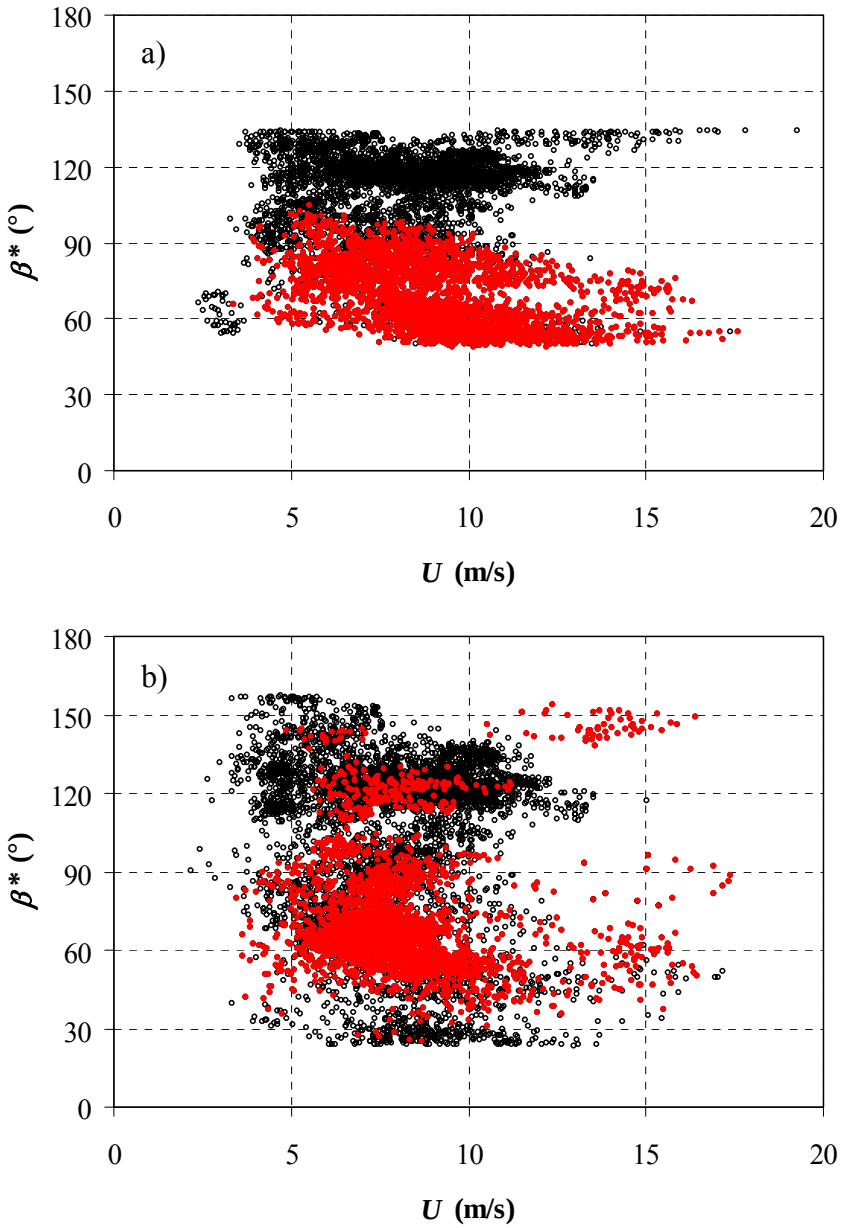

Figure 5.14 Ranges of wind speed and effective attack angle for Rain-wind-induced vibrations: a) stay AS16 and b) stay AS24

This observation suggests that, as in the case of Kármán-vortex-induced vibrations, although the effective attack angle incorporates both the inclination angle of the cable and the attack angle of the wind, it does not necessarily fully represent the directional effect of wind in the excitation mechanism. In particular, due to the sheared profile of wind in the atmospheric boundary layer, the inclination of the stay cable and the direction of wind in the horizontal plane will have different effects on the structure of the flow around the cable surface. It therefore appears inappropriate to use an angle that simply combines the inclination angle and the attack angle geometrically to characterize the angle of the attacking wind.

While the direction of wind appears to be an important parameter for rain-wind-induced vibrations, full-scale measurement data suggest that the onset of such vibrations is relatively insensitive to either the turbulence in the wind or the rate of rainfall. Figure 5.15 a) and Figure 5.15 b) shows the ranges of turbulence intensity (I_U) and rainfall rate (R_r) over which rain-wind-induced vibrations have occurred for stay AS16. Again, the open circles represent the simultaneous occurrences of wind and rain, and the solid circles represent the portion of rain-wind occurrences when large-amplitude vibrations were recorded. For this stay, when the direction of wind is favorable for rain-wind-induced vibrations, the vibrations occurred almost over the entire range of turbulence intensity and rainfall rate recorded. In particular, these two figures suggest that rain-wind-induced vibrations can occur in very turbulent wind and under very heavy rainfall, which is contrary to previous belief that rain-wind-induced vibrations occur only under light to moderate rain and only in smooth wind (Larose and Smitt 1999).

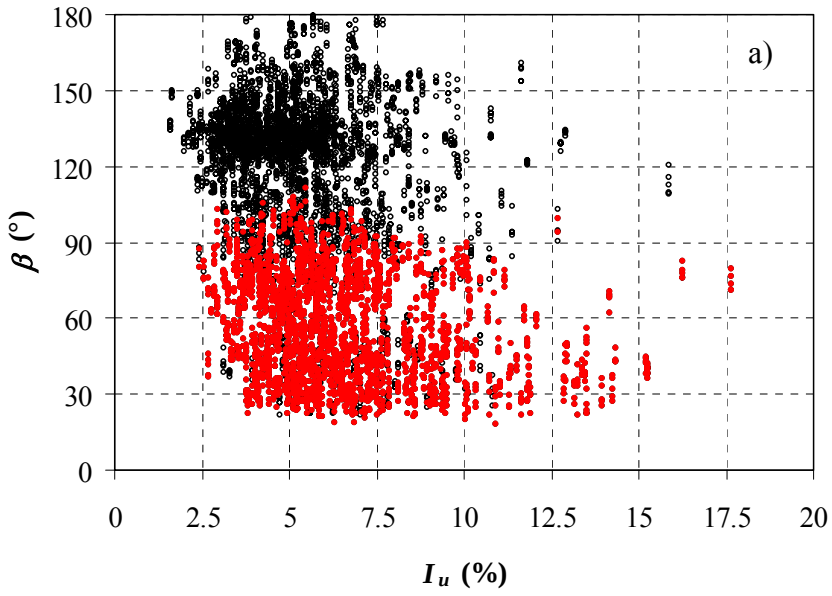

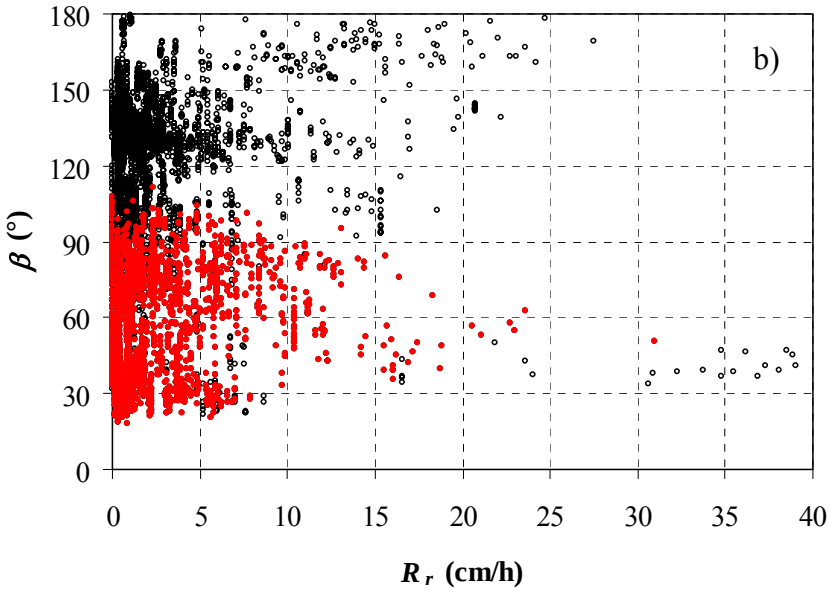

Figure 5.15 Effects of a) turbulence and b) rainfall rate on the onset of rain-wind-induced vibrations

It has to be pointed out, however, that although Figure 5.13 to Figure 5.15 give indications of the ranges of wind speed, attack angle, turbulence intensity and rainfall rate over which rain-wind-induced vibrations have been observed for stays AS16 and AS24, it does not necessarily mean that one can judge precisely whether or not rain-wind-induced vibrations would occur for a specific stay under specific wind and rain conditions based on graphs like these. The frequency and amplitude of the vibration at a specific time are the cumulative response of the stay to the rain and wind excitation prior to this time. Although the solid red circles in the graphs all represent vibration segments of significant amplitude, these significant-amplitude vibrations, however, are not necessarily the direct result of the rain-wind excitation during the same period of time. The vibrations can be associated with the wind and rain during the same period of time only if the records are stationary. Therefore, to understand the mechanism of rain-wind-induced vibrations, it is important to investigate the characteristics of stationary vibrations and their dependence on wind and rain.

Figure 5.16 shows the fourteen-second mean anti-nodal displacement amplitude of recorded steady-state rain-wind-induced vibrations of stay AS24 versus the corresponding mean wind speed and attack angle at the deck level. Only data points with amplitude larger than five percent of the cable diameter are included. Again, the amplitude of the vibrations is represented by the diameter of the circles, and the dimension of the cable diameter (1D=19.38 cm) is included for reference purposes. This figure suggests that under the excitation from wind and rain, stay AS24 can vibrate in a number of its lower modes, and that different modes of vibration cluster in different regions of wind speed and direction. In particular, the vibrations in the higher modes usually occur at higher wind speed for the same attack angle. In addition, for the second and third modes of vibration, which occurred over broad ranges of attack angles, the required wind speed for the vibrations to occur seems to increase when the attack angle deviates from 90°. These characteristics of rain-wind-induced vibrations are very similar to those of Kármán-vortex-induced vibrations, as suggested in the last section. The difference between these two types of vibrations is that rain-wind-induced

vibrations occur at much larger amplitude and at much higher wind speed than do locked-in Kármán-vortex-induced vibrations, although the amplitude of the vibrations does appear to be self-limiting.

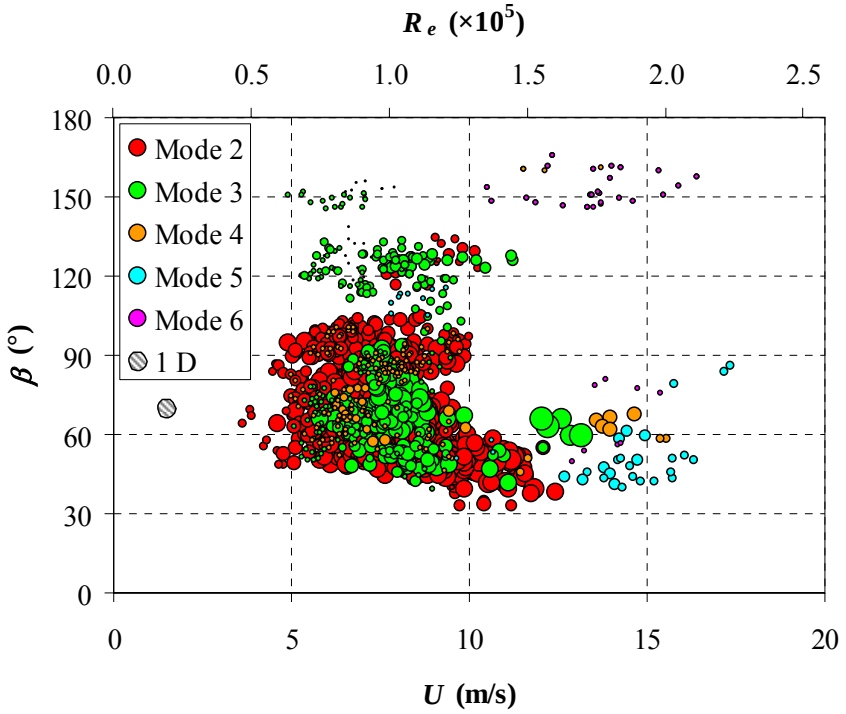

Figure 5.16 Amplitude vs. wind speed and attack angle for Rain-wind-induced vibrations of stay AS23

The fact that some circles representing different modes overlap in Figure 5.16 is due to the fact that some rain-wind-induced vibration records have significant components from multiple modes. One reason for this multi-modal participation of rain-wind induced vibrations is believed to be the same as why Kármán-vortex-induced vibrations of long stay cables usually have multiple modal components: That is, due to the profile of the atmospheric boundary layer, yawed and inclined stay cables are subjected to sheared flow and different sections of the cables can be exposed to different wind speeds, and therefore different vibration frequencies if the frequency of the excitation is wind speed dependent. Another factor that can potentially cause the overlapping of different modes in Figure 5.16 is the fact that the periodic excitation from wind and rain can be non-harmonic, which introduces super-harmonics in the responses of stay cables. Figure 5.17 shows the displacement spectrograms of an example rain-wind-induced vibration record of stay AS24 (2001030831). In this record, the displacements in both directions are dominated by the second mode of the cable. In addition to the vibration in the second mode, the figure also reveals very noticeable displacement components in the fourth, sixth and eighth modes, and so on, in both directions; the mode numbers of these noticeable higher-mode components are integer multiples of that of the second mode. At the same time, the vibration does not have significant participations from the odd-numbered modes. It is then suspected that in this case, the frequency of the rain-wind excitation is the same or very close to the natural frequency of the second mode of stay AS24, but because the excitation is not perfectly harmonic, the stay responded to the super-harmonics of the base frequency of the excitation

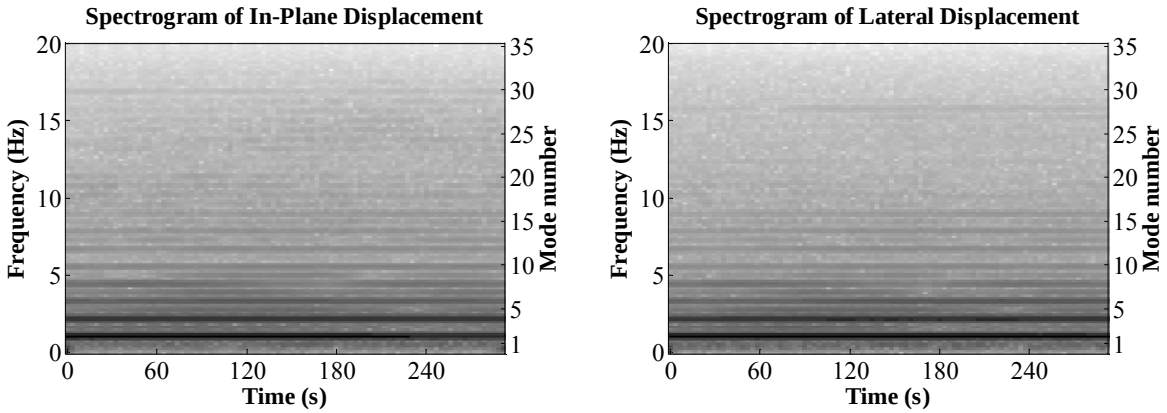

Figure 5.17 Spectrogram of example rain-wind-induced vibration record showing super-harmonics

To investigate the Reynolds number effects on rain-wind-induced vibrations, Figure 5.16 also includes a secondary axis in terms of the Reynolds number (R_e). It is apparent that the majority of rain-wind-induced vibrations of stay AS24 occurred in the sub-critical Reynolds number range. This statement will remain true even if the wind speeds measured at the tower top, instead of those measured at the deck level, are used to compute the Reynolds numbers. It has to be noted, however, that the Reynolds numbers shown in Figure 5.16 are computed based on the assumption that the cross-section between the cable and the flow around it is approximately circular, which is not necessarily true for an inclined cable subjected to wind approaching from specific directions. At this stage of the study, however, it is believed that the Reynolds number so computed suffices for the purpose of approximately assessing the Reynolds number range over which rain-wind-induced vibrations occur. Also, the exact range of the sub-critical region can potentially be affected by the roughness of the cable surface and the turbulence in the wind. However, the surface of the stays on the Fred Hartman Bridge and the Veterans Memorial Bridge is very smooth, and according to Ohya (2004) the effect of turbulence on the drag coefficient for circular cylinders is not significant. This means that it is still valid to state that the majority of rain-wind-induced vibrations occurred in the sub-critical Reynolds number range even though the cable surface is not perfectly smooth and the wind can be turbulent in some cases.

Figure 5.18 plots the mean amplitude of rain-wind-induced vibrations against the reduced velocity and the attack angle. By comparing Figure 5.18 to Figure 5.5, it is evident that rain-wind-induced vibrations occur at much higher reduced velocities than those of Kármán-vortex-induced vibrations. Figure 5.18 also suggest that for each mode, Rain-wind-induced vibrations occur over a broad range of reduced velocities. This broad spread of the data points for each mode can be partially attributed to the fact that the wind speed presented is that measured at the deck level, which does not necessarily represent the wind speed "responsible" for the excitation. Whether or not individual modes of rain-wind-induced vibrations do occur over a wide range of reduced velocity, however, cannot be judged with full-scale measurement data such as these. Furthermore, the actual wind speed at which rain-wind-induced vibrations occur should always be higher than the wind speed at the deck level, since the portion of the cable subjected to rain-wind excitation is always located above the surface of the deck. This also means that the actual reduced velocity range over which rain-

wind-induced vibrations occurred for stay AS24 should be higher than that suggested by Figure 5.18.

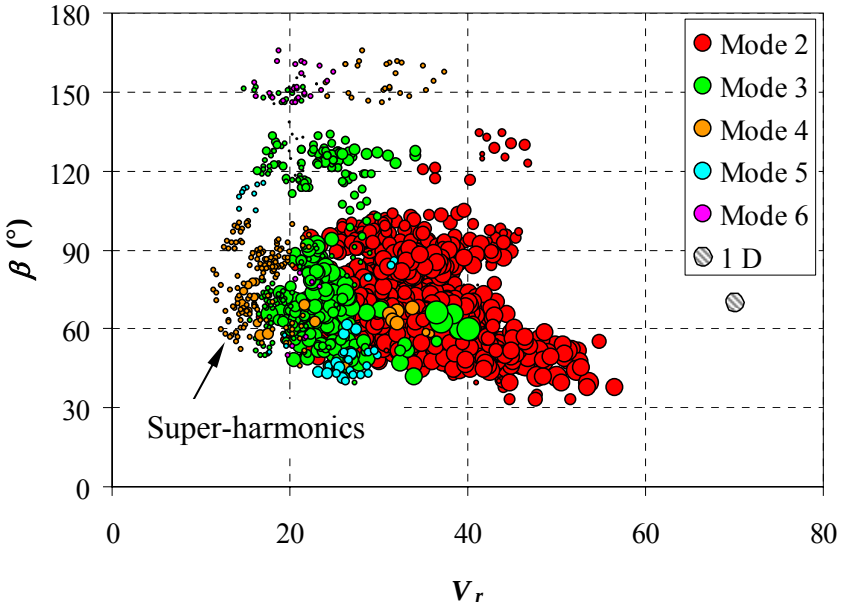

Figure 5.18 Amplitude vs. reduced velocity and attack angle for rain-wind-induced vibrations of stay AS24

Figure 5.18 also reveals a cluster of fourth mode vibrations that occur at lower reduced velocities than the reduced velocities at which other modes of vibration occur in the same attack angle range. This cluster of fourth mode vibrations, however, is the result of the super-harmonics of the corresponding second mode vibrations and does not represent the primary frequency component of the excitation.

As in the case of Kármán-vortex-induced vibrations, due to the three-dimensional nature of the cable-wind system, rain-wind-induced stay cable vibrations can be highly two-dimensional. Figure 5.19 shows the relationship between the major direction of the vibrations in individual modes and the attack angle of the approaching wind for rain-wind-induced vibrations of stay AS24. For reference purposes, the angle between the vertical cable plane and the plane normal to the π plane, φ^*, is also presented for different attack angles. According to this figure, there exists a clear (non-linear) relationship between the direction of the rain-wind-induced vibrations and the direction of the attacking wind. It is also apparent in this figure that the major direction of the modal vibrations is usually not exactly in the plane perpendicular to the π plane. These characteristics of rain-wind-induced vibrations are also similar to those observed in Kármán-vortex-induced vibrations, as shown in Figure 5.9 and Figure 5.12.

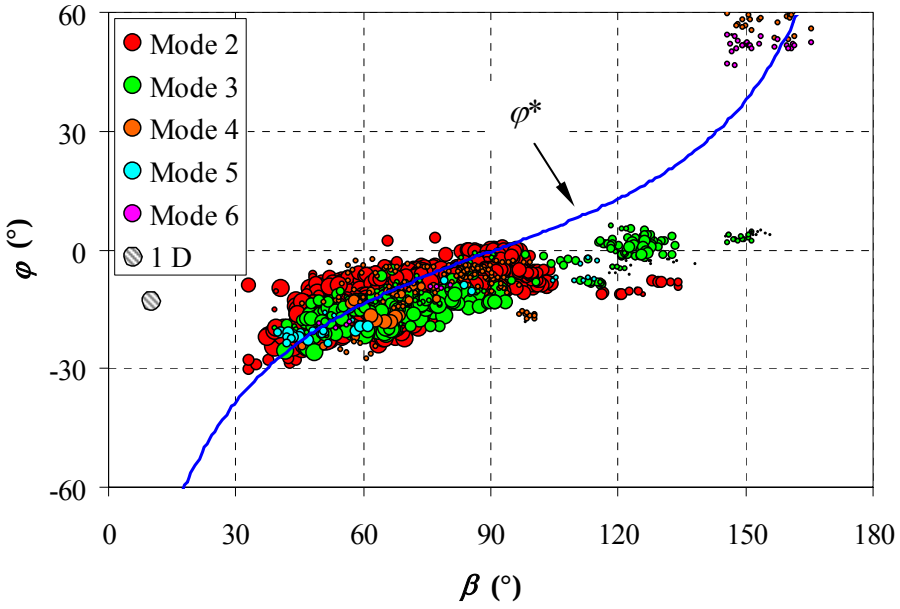

Figure 5.19 Major axis angle vs. attack angle for rain-wind-induced vibrations of stay AS24

To compare the dependence of rain-wind-induced vibrations on wind for different stays with different physical properties, Figure 5.20 displays the modal amplitude of observed rain-wind-induced vibrations of individual modes of several stays (Locations of these stays are shown in Figure 5.21) on the Fred Hartman Bridge against the reduced velocity and attack angle. To exclude the possibility of complex mechanisms such as potential interactions between different frequency components in the excitation, this figure includes data from those records dominated by only a single mode. According to the figure, for all the stays presented, rain-wind-induced vibrations occurred over reduced velocities that are at a much higher level than the reduced velocity range over which Kármán-vortex-induced vibrations occur. For different stays, however, rain-wind-induced vibrations do not necessarily occur over the same reduced velocity range. Due to the complexity of the three-dimensional wind-cable system and the limitations of full-scale measurements, the exact reasons for this difference between rain-wind-induced vibrations of different stays have not been precisely identified. But the inclination angle of the stay cables is believed to be a critical factor that affects the structure of the flow around the cable, which can potentially affect the reduced velocity range over which rain-wind-induced vibrations of a specific mode of a specific cable occur.

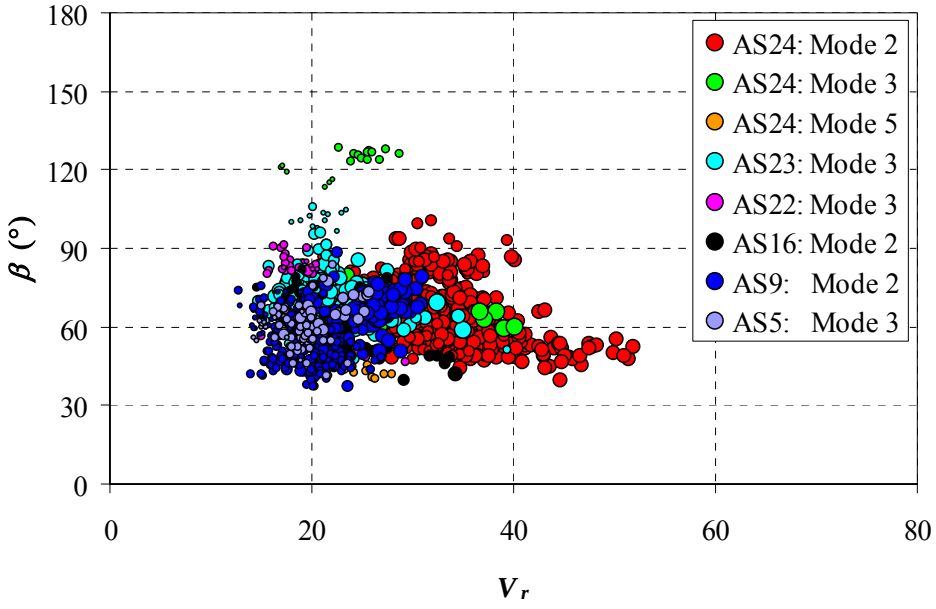

Figure 5.20 Amplitude vs. reduced velocity and attack angle for rain-wind-induced vibrations of different stays on the Fred Hartman Bridge

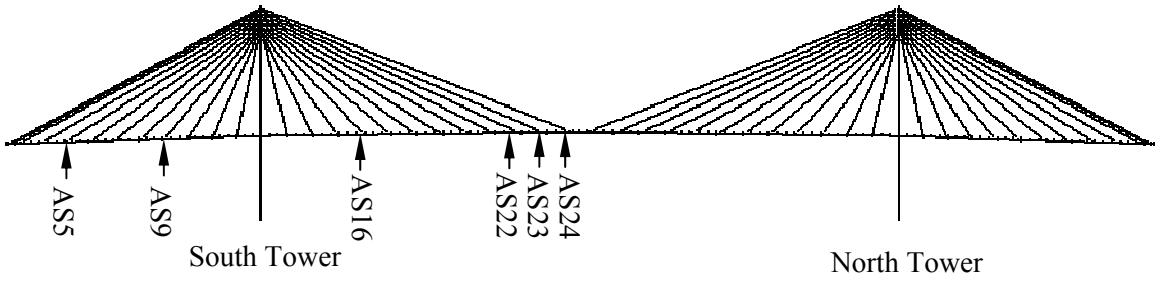

Figure 5.21 Stays of the Fred Hartman Bridge used for comparison

Figure 5.22 shows the correlation between the major direction of the modal vibrations and the attack angle for several stays on the Fred Hartman Bridge. It is evident that for each stay, there is a clear relationship between the direction of the modal vibration and the direction of the approaching wind. Figure 5.22 also suggests that for the same attack angle, the stays with smaller inclination angle, such as stays AS24 and AS23, usually vibrate with a smaller major axis angle than do stays with larger inclination angle. This is strong evidence that the structure of the flow around the cable can be greatly affected by the inclination of the stay cable.

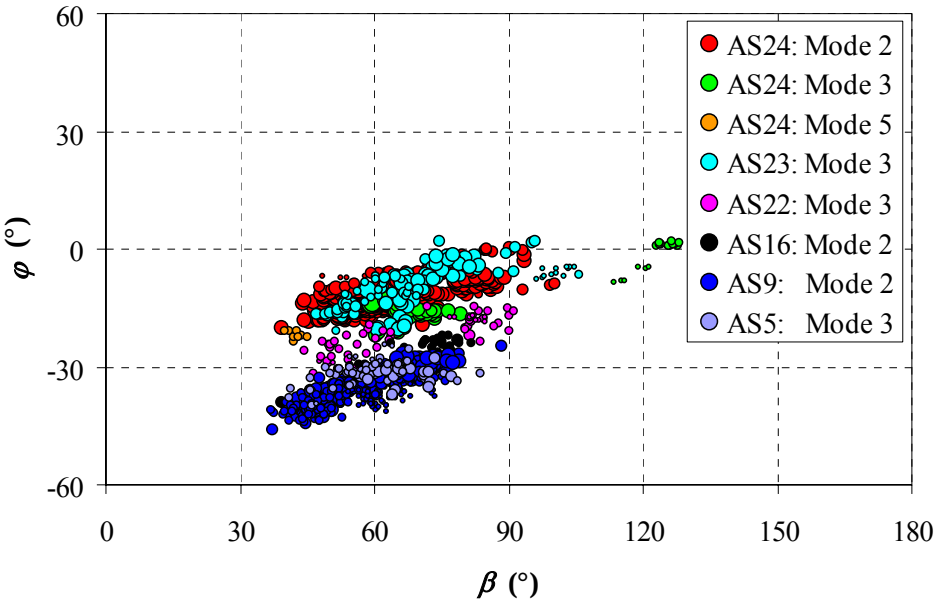

Figure 5.22 Major axis angle vs. attack angle for Kármán-vortex-induced vibration of different stays on the Fred Hartman Bridge

Discussion so far has revealed some general, but important, characteristics of rain-wind-induced stay cable vibrations and their correlation with wind and rain in an average sense. Although some specific details of these characteristics and their precise relationship with wind and rain are still unclear due to the complexity of the problem and the limitations of the full-scale measurement systems, the data do suggest a strong resemblance between rain-wind-induced vibrations and Kármán-vortex-induced vibrations, except that rain-wind-induced vibrations occur at much higher reduced velocity with much larger amplitude than do Kármán-vortex-induced vibrations. This resemblance further indicates that rain-wind-induced vibrations might be due to an excitation mechanism induced by a vortex structure that is different from the classical von Kármán type. This indication, however, cannot be completely verified by the full-scale measurement data, it has to be subjected to further investigation through controlled wind tunnel tests.

While the general characteristics can provide significant implication to the mechanism of rain-wind-induced vibrations, due to the complexity of this type of vibration, some particular aspects of the problem can only be revealed by examining individual records in detail. The remaining portion of this section will be dedicated to the examination of some important example records.

Figure 5.23 displays the displacement spectrograms of stay AS22 under the excitation of wind and rain shown in Figure 5.24 (record 2001100520). For this particular record, since the wind is approaching from the west side of the bridge and cannot be faithfully measured by the anemometers at the deck level, the wind speed and direction measured by the propeller-vane anemometer on the tower top is used. These two graphs suggest that under the excitation from high-speed, highly turbulent wind and heavy rainfall, the vibration of stay AS22 has significant components in the fifth and sixth modes, of which the corresponding frequencies are about 3.46 Hz and 4.16 Hz, respectively. These vibration frequencies of stay AS22 in this case are well beyond the frequency range of 1 to 3 Hz over which rain-wind-induced vibrations are previously believed to occur (Hikami and Shiraishi 1988). In addition

to the vibration components at high frequencies, the vibration also has a strong lateral component in the first mode.

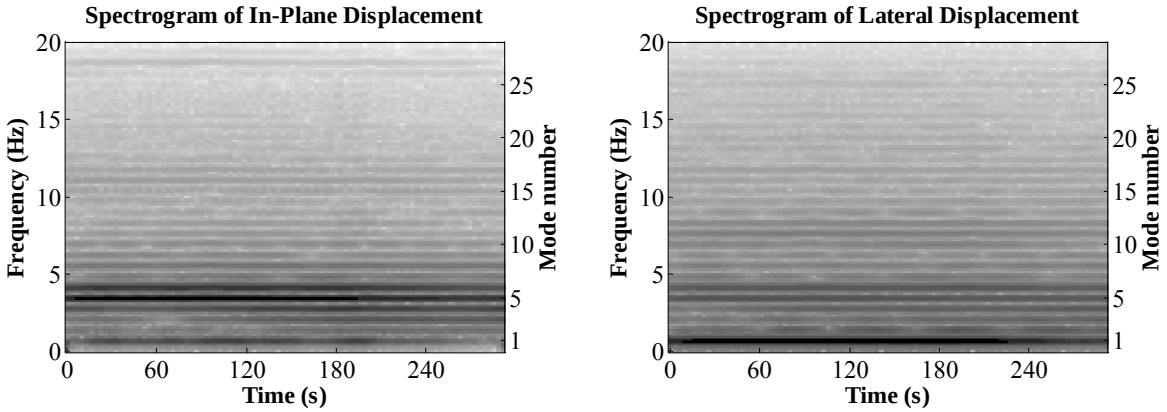

Figure 5.23 Response spectrograms of stay AS22 in an event of high wind speed and heavy rainfall

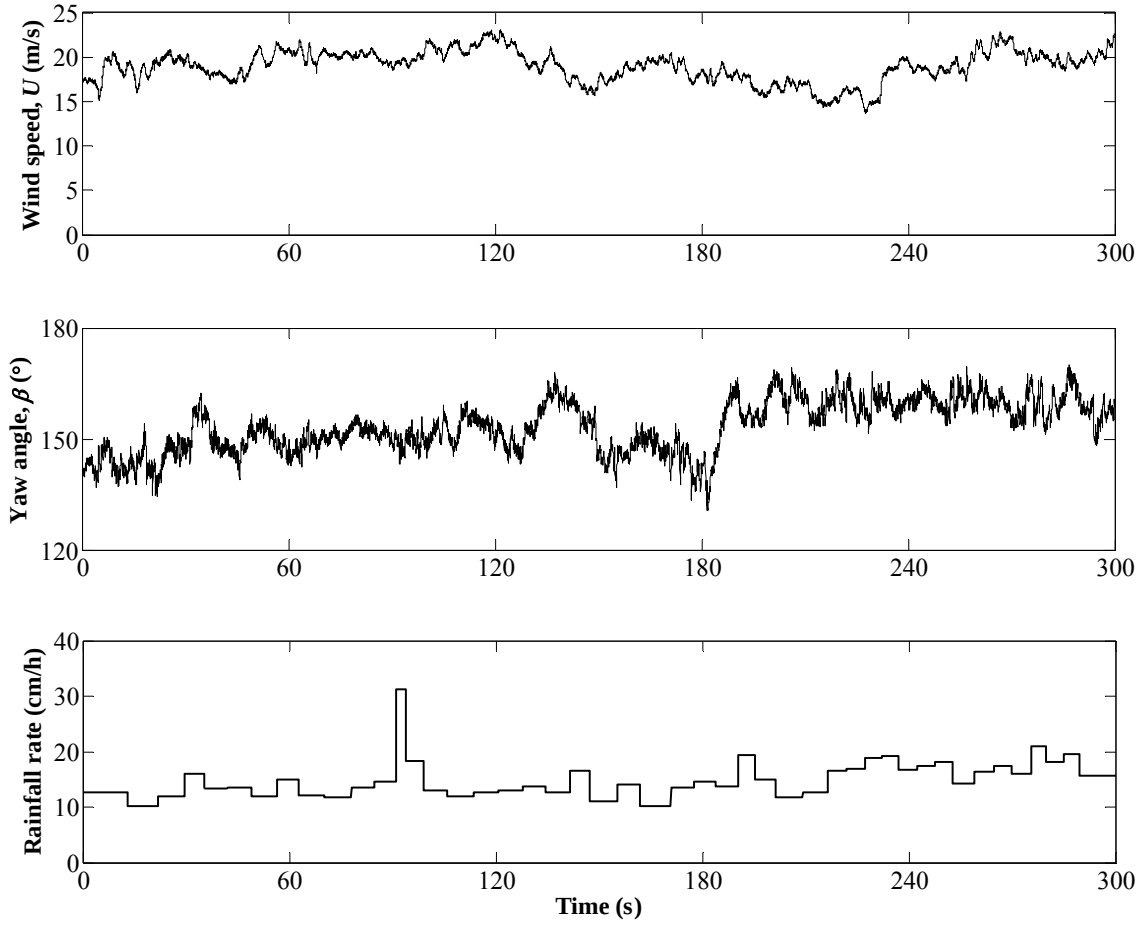

Figure 5.24 Meteorological conditions during a rain-wind-induced vibration event

Figure 5.25 shows the reduced velocities corresponding to these three significant modes of vibration. To be consistent with the manner in which wind is presented with the general characteristics of the vibrations (Figure 5.18 and Figure 5.20), in computing the reduced velocities, the wind speed shown in Figure 5.23 is divided by a factor of 1.38 to approximately obtain the corresponding wind speed at the deck level. According to this figure, the reduced velocities at which the vibration components in the fifth and the sixth modes occur are in the range over which rain-wind-induced vibrations usually occur, as suggested by Figure 5.20. For the vibration in the first mode, however, the corresponding reduced velocity is much higher and well beyond this range.

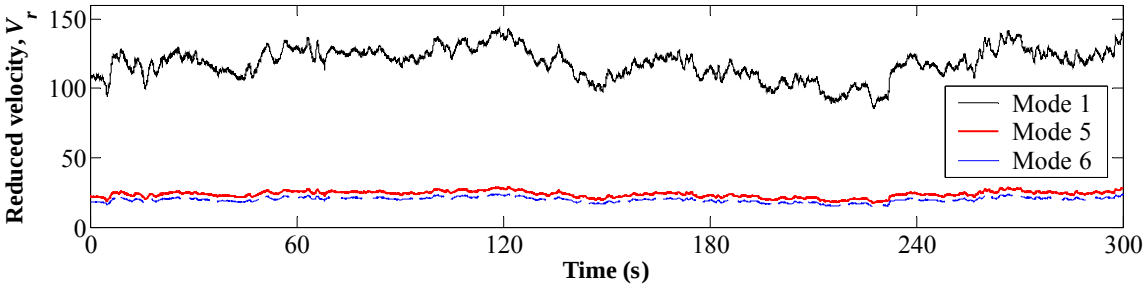

Figure 5.25 Reduced velocities corresponding to three significant modes of vibration

Furthermore, the vibrations in the different modes also differ with each other in that they occur in different planes. Figure 5.26 shows the vibration loci of the first, fifth and sixth mode, respectively, for a fourteen-second segment of the record. While the components in the fifth and the sixth modes both vibrate at noticeable inclinations that are very close to each other, for the component in the first mode, however, the vibration takes place primarily in the lateral direction.

These differences between the characteristics of the first mode vibration and those of the vibration components in the fifth and sixth modes suggest that they might have been induced by two different mechanisms. Specifically, judged by the characteristics of the individual modal components, the vibration components in the fifth and the sixth modes are likely to be similar to those shown in Figure 5.20 and Figure 5.22, which are dependent on the mean wind speed and direction. The mechanism that induced the vibration in the first mode, on the other hand, is less clear due to the limited number of occurrences of this pattern of vibration. It is observed, however, that this type of low frequency vibration is always associated with high level of turbulence in the wind and high rate of rainfall. The exact mechanism of this type of vibration is subjected to further investigation.

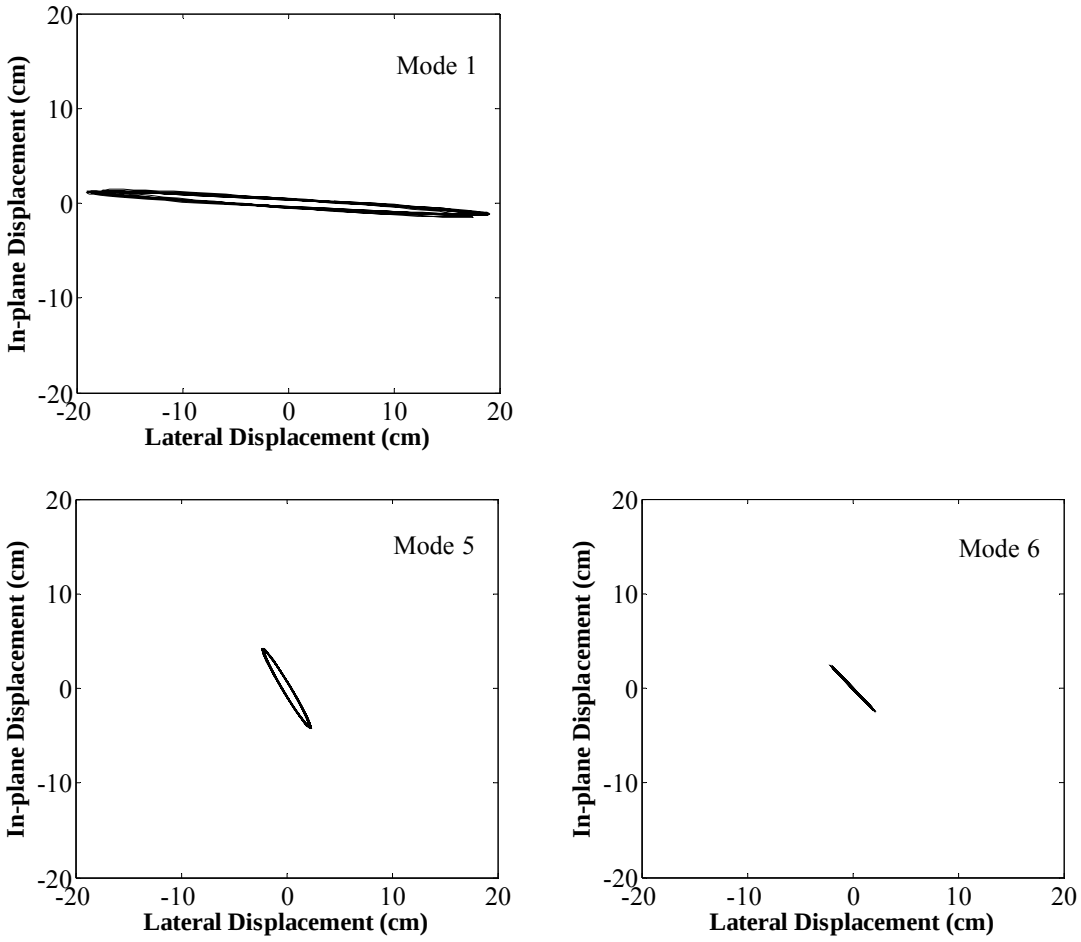

Figure 5.26 Different vibration directions of different modal components

An important implication of the record shown in Figure 5.23 to Figure 5.26 is that a stay cable can be subjected to simultaneous excitations of different mechanisms. Full-scale measurement data suggest that rain-wind-induced vibrations can also occur simultaneously with classical Kármán vortex shedding. Figure 5.27 shows the acceleration spectrograms of stay AS22 on the Fred Hartman Bridge under the excitation from the wind and rain shown in Figure 5.28 (record 200110137). In this example record, the acceleration spectrograms instead of the displacement spectrograms are used to show the high frequency components of interest. These spectrograms revealed two distinct groups of frequency components: The first group consists of vibration in the third, sixth, and ninth modes, which are the major components of the response, and the second group consists of weak but obviously visible components at frequencies around 13 Hz. In fact, the actual vibration components in the second group should be more significant than they appear to be in the spectrograms, because the spectrograms shown are computed based on the signal that has been low-pass-filtered at the frequency of 10 Hz by an analog filter. The focus herein, however, is the existence of this second group of high frequency, so the exact effects of the analog filter will not be analyzed. As discussed earlier in this chapter, for the components in the first group, the vibrations in the sixth and ninth modes are believed to be super-harmonics of the vibration in the third

mode. This group of frequency components therefore can be represented by the vibration in the third mode.

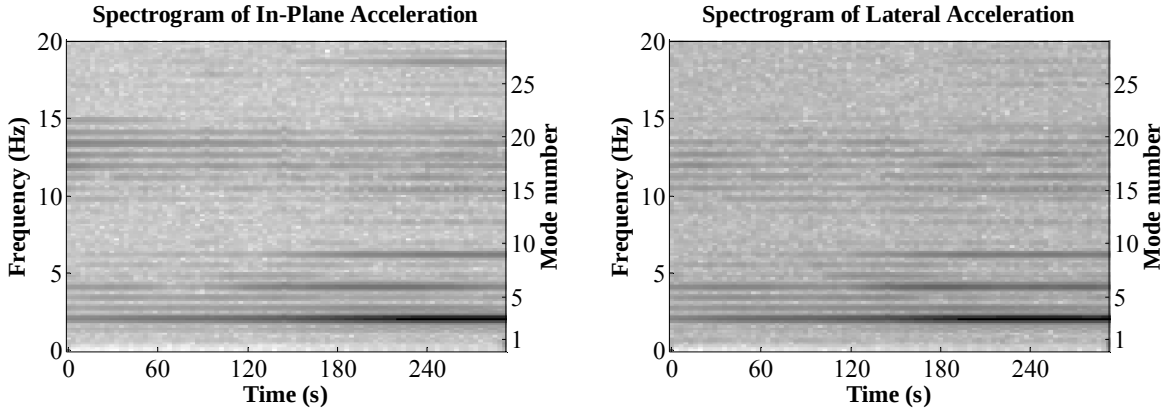

Figure 5.27 Acceleration spectrograms of stay AS22 showing simultaneous occurrence of rain-wind-induced vibration and Kármán vortex shedding

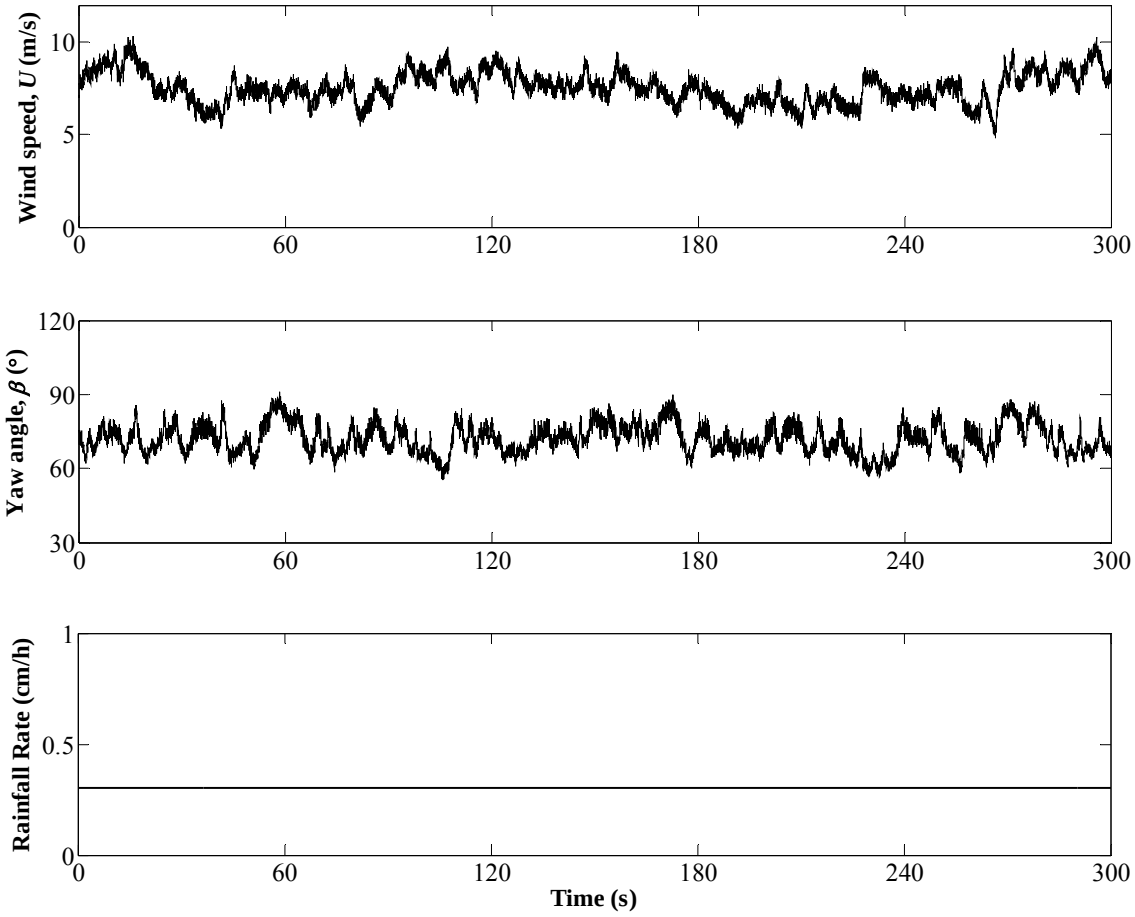

Figure 5.28 Time histories of wind and rain during a rain-wind-induced vibration event

Figure 5.29 shows the evolution of the reduced velocity for the vibration component in the third mode of the first group and that of the nineteenth mode (about 13.3 Hz), which is selected to be a representative of the second group. According to this figure, the component in the nineteenth mode occurred at a reduced velocity close to 5. This suggests that the second group of frequency components shown in Figure 5.27 is likely induced by Kármán vortex shedding. On the other hand, Figure 5.29 also reveals that the vibration component in the third mode occurred over a reduced velocity range of about 20 to 30. This observation suggests that this modal component of the vibration corresponds to large-amplitude rain-wind-induced vibration at high reduced velocity.

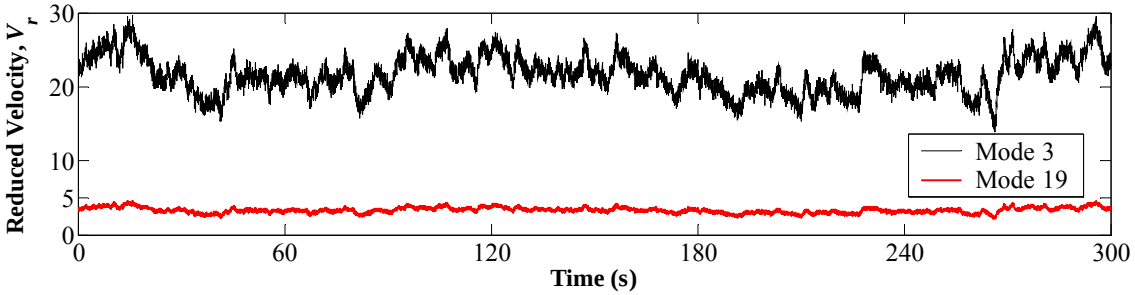

Figure 5.29 Reduced Velocity corresponding to two modal vibration components

The fact that large-amplitude rain-wind-induced vibrations and regular Kármán vortex shedding can occur simultaneously for stay cables, however, does not necessarily mean that these two types of vibrations are related mechanisms. Rather, full-scale measurement data suggest that depending on the condition of wind, both Kármán-vortex-induced vibrations and rain-wind-induced vibrations can occur during rain, and can occur independently.

For example, Figure 5.30 shows the spectrograms of the in-plane and lateral acceleration responses of stay AN24 on the Fred Hartman Bridge to the excitation of wind and rain shown in Figure 5.31 (record 1997120756). In this particular record, under the excitation from the smooth, relatively low speed wind, the stay clearly exhibited locked-in Kármán-vortex-induced vibrations in its seventh and eighth modes, although the rate of rainfall is high. At the same time, no evidence of rain-wind-induced vibration is present in the spectrograms.

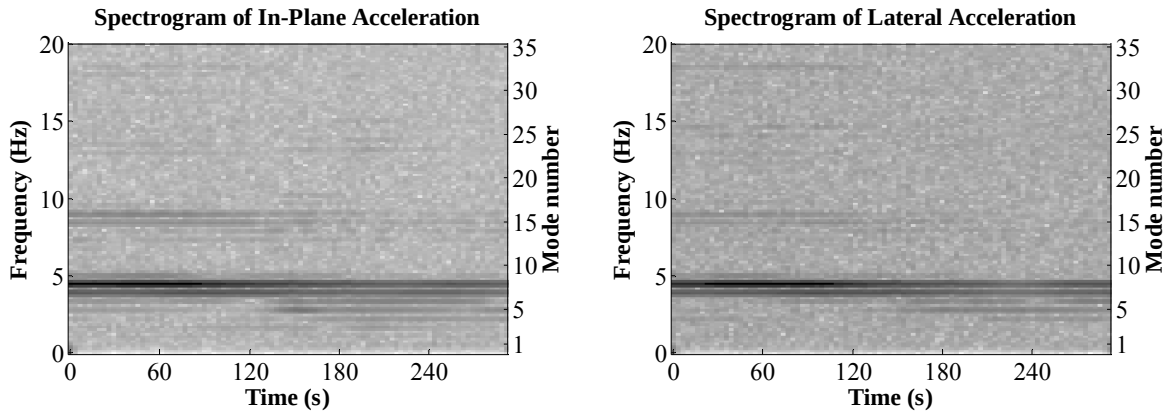

Figure 5.30 Spectrograms of acceleration response of stay AN24 showing Kármán-vortex-induced vibration under simultaneous excitation of wind and rain

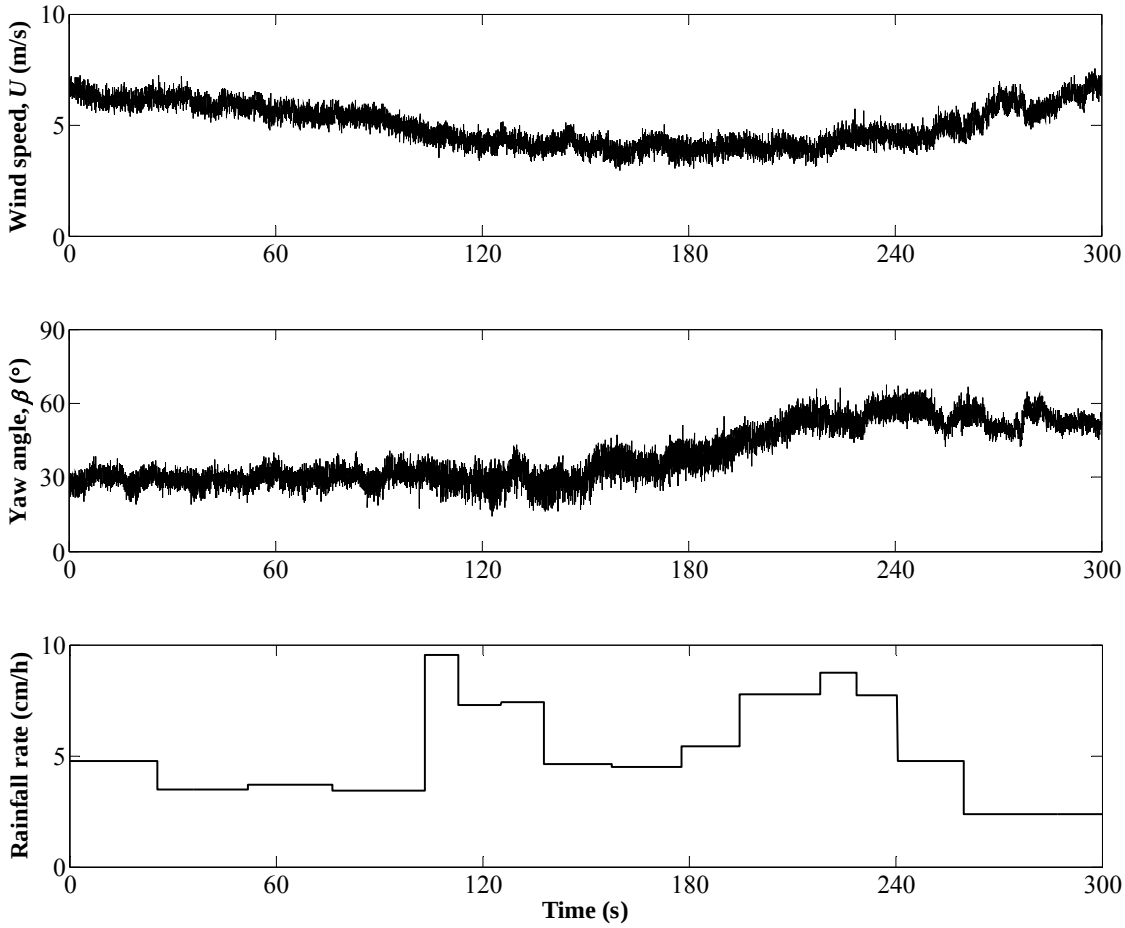

Figure 5.31 Time histories of wind and rain during a Kármán-vortex-induced vibration

Conversely, in some other events of simultaneous occurrence of wind and rain, the stay cables have exhibited only rain-wind-induced vibrations. Figure 5.32 displays the spectrograms of the acceleration response of stay B11 on the Veterans Memorial Bridge during such an event (record 200009211). The rain-wind-induced vibration in the second mode and its super-harmonics in the higher modes are clearly present in these spectrograms,

but there is no evidence of oscillation induced by Kármán vortex shedding. Because of the existence of such example records showing independent occurrence of rain-wind-induced vibrations and Kármán-vortex-induced vibrations during rain, it is suspected that, although rain-wind-induced vibrations and Kármán vortex shedding can occur simultaneously under specific conditions of wind and rain, the occurrence of one type of vibration, however, is not the result of the other.

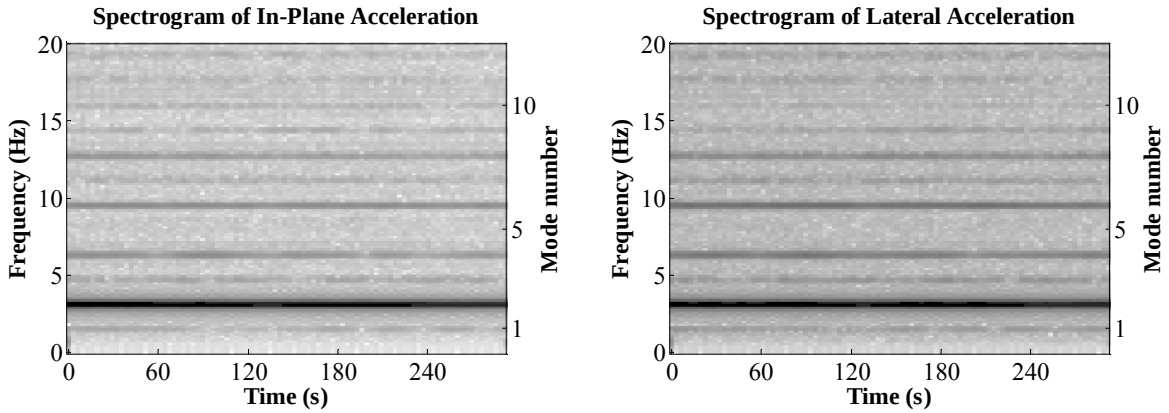

Figure 5.32 Acceleration spectrogram of stay B11 under the simultaneous excitation of wind and rain

Example records such as the ones shown herein are important. They illustrate that, although stay cables can be simultaneously susceptible to multiple types of excitation mechanisms and exhibit complex vibration characteristics, these multiple types of excitation mechanisms, however, are independent and are associated with independent characteristics in the vibration. The reason why multiple types of vibrations can occur simultaneously is suspected to be due to that the stay cables are in a sheared three-dimensional boundary layer and different portions of a stay cable can be subject to excitation of different mechanisms. This fact enables one to investigate the mechanism of a specific type of excitation mechanism based on the corresponding vibration characteristics. More importantly, investigation of such records can help identify the mechanisms that occur only under particular conditions, such as exceptionally high wind turbulence or very heavy rainfall and focus on the predominant mechanism that frequently induced the large-amplitude vibrations at high reduced velocity.

5.3 Large-Amplitude Dry Cable Vibration

While rain-wind-induced vibrations are the most frequently observed large-amplitude stay cable vibrations on the Fred Hartman Bridge and the Veterans Memorial Bridge, relatively infrequent, but large-amplitude vibrations have also been observed without precipitation. Among the dry cable vibrations recorded, a special type is of particular interest. This type of dry-cable vibration is not believed to be induced by either Kármán vortex shedding or the oscillation of the bridge decks, since the frequencies of such vibrations are not consistent with the Strouhal relationship associated with Kármán-vortex-induced vibrations, and very little deck oscillation has been simultaneously recorded. More importantly, such vibrations appear to occur over the same ranges of wind speed and direction as do rain-wind-induced vibrations. The possibility of rain gauge failure can also be

ruled out since the transducer did register rainfall in the days close to the ones during which the large-amplitude dry cable vibrations were recorded.

Figure 5.33 shows the displacement time histories of an example large-amplitude dry-cable vibration record (1997112810) for stay AS24, together with the corresponding

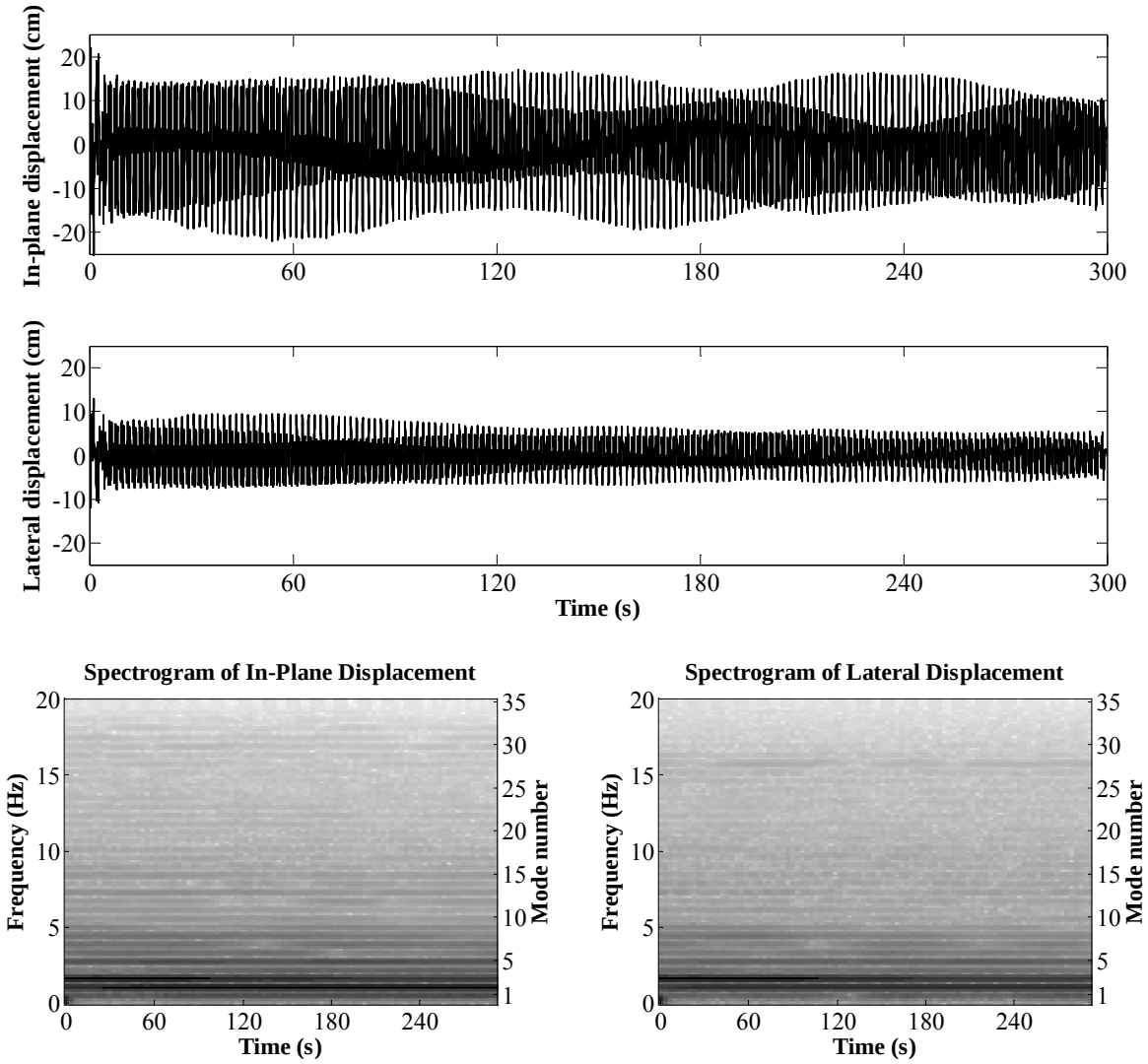

Figure 5.33 Time histories and spectrograms of example dry cable vibration record

spectrograms. It is evident that for this specific record, the large-amplitude response of the stay is highly two dimensional and that it is simultaneously dominated by the second and the third modes. The fact that the vibration has significant components from multiple modes is again believed to be due to the three-dimensional nature of the cable-wind system, as in the case of Kármán-vortex-induced vibrations and rain-wind-induced vibrations.

Figure 5.34 displays the vibration loci of the two significant modal components at the location of the accelerometer for a fourteen-second segment of the record. For both modes, the vibration locus is near-elliptical. This suggests that the coordinate system shown in Figure 4.6 can also be used to characterize the modal components of dry-cable vibrations.

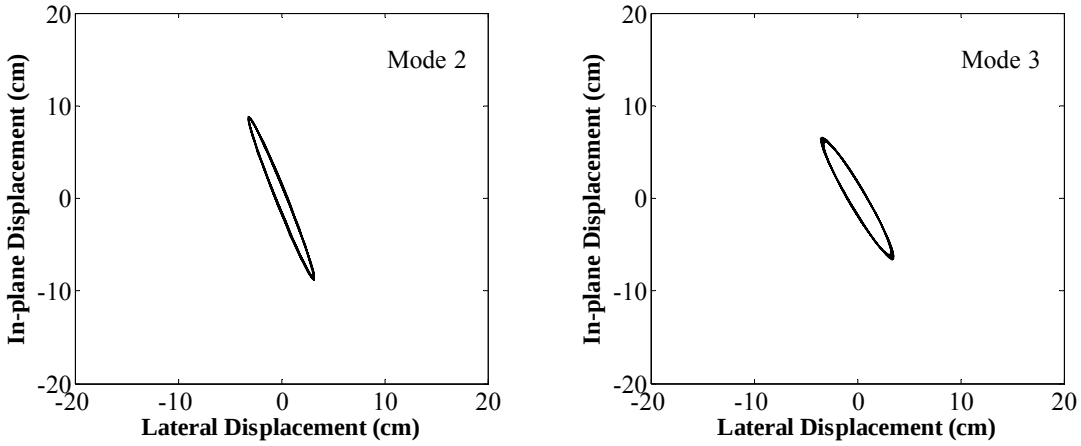

Figure 5.34 Modal vibration loci of an example dry cable vibration record

Figure 5.35 shows the fourteen-second mean anti-nodal displacement amplitude of steady-state large-amplitude vibrations of stay AS24 without rainfall versus the corresponding mean wind speed and attack angle at the deck level. Again, only segments with amplitude larger than five percent of the cable diameter (0.194 m) have been included, and the diameter of the cable (1D) is shown in the figure for reference purposes. This graph reveals that, for this particular stay, the amplitude of dry cable vibrations is comparable to that of rain-wind-induced vibrations, as shown in Figure 5.16. It can also be seen that for stay AS24, large-amplitude dry-cable vibrations occur when the attack angle is around or less than 90°, and that the required wind speed for the vibrations to occur seem to increase when the attack angle deviates from 90°. These characteristics of dry cable vibrations are similar to the corresponding characteristics of rain-wind-induced vibrations, as shown in Figure 5.16. The overlapping of the circles representing different modes is again due to the fact that some records have components from multiple modes. Furthermore, the secondary axis in terms of the Reynolds number indicates that all these dry cable vibrations occurred in the sub-critical Reynolds number range and that this remains true even if the wind speed at the tower top is used. These large-amplitude vibrations therefore are evidently different from the divergent type of dry cylinder vibration observed in the wind tunnel (Cheng et al. 2003a).

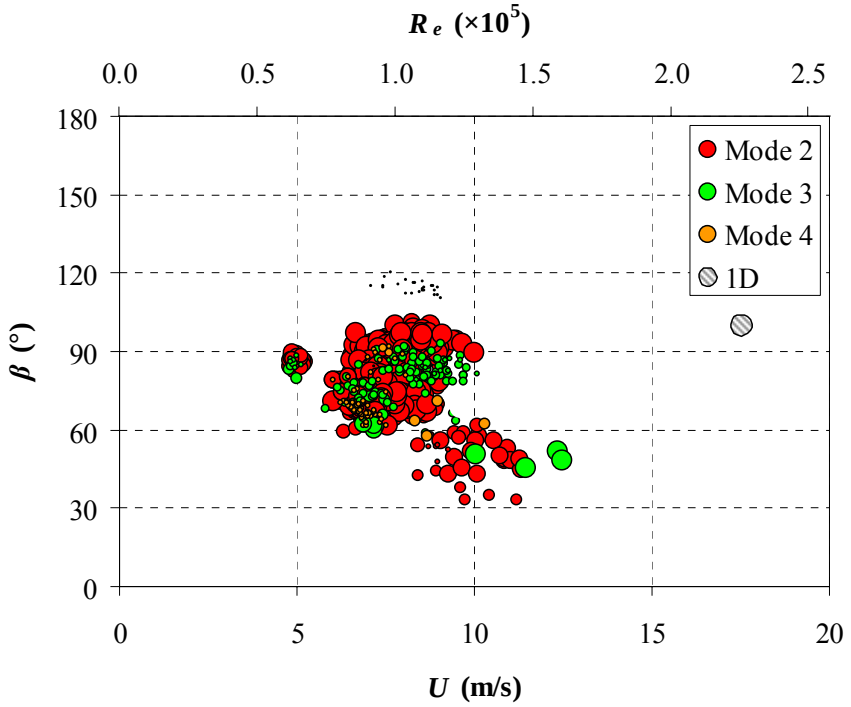

Figure 5.35 Amplitude vs. wind speed and attack angle for a type of vibration of stay AS24 without rainfall

Figure 5.36 displays the amplitude of observed large-amplitude dry-cable vibrations against the reduced velocity and attack angle for stay AS24. Comparison of this graph with Figure 5.18 indicates that these dry-cable vibrations occurred over a similar reduced velocity range as do rain-wind-induced vibrations for stay AS24.

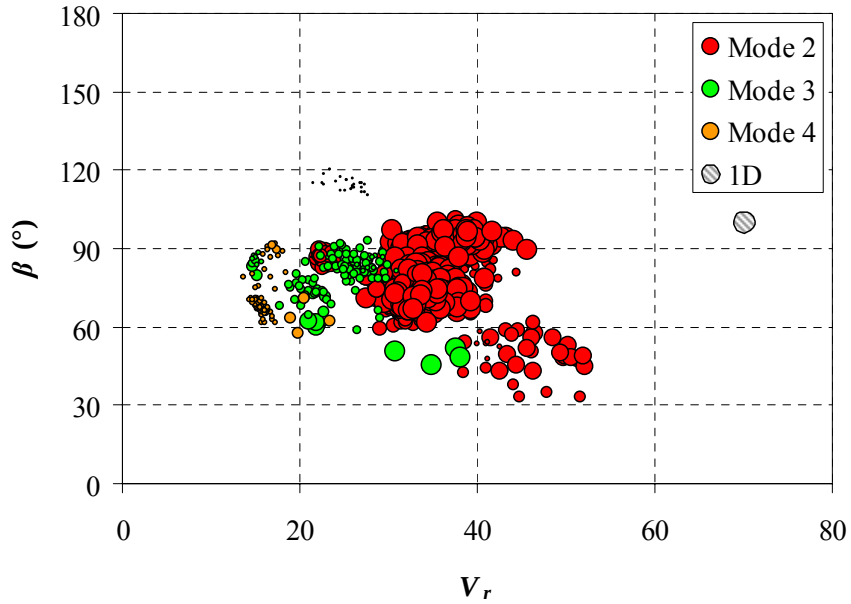

Figure 5.36 Amplitude vs. reduced velocity and attack angle for vibrations of stay AS24 without rainfall

Figure 5.37 shows the major axis angle of the large-amplitude dry-cable vibrations versus the attack angle for stay AS24. A reasonably clear (nonlinear) relationship between these two angles is present in this figure and the characteristics of this relationship is again similar to the corresponding relationship for rain-wind induced vibrations, as shown in Figure 5.19.

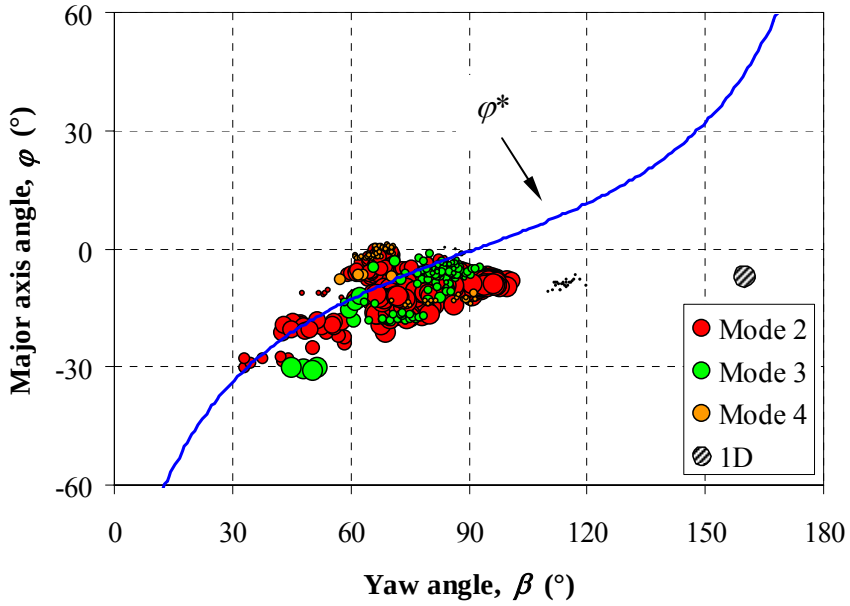

Figure 5.37 Correlation between major axis angle and attack angle for vibrations of stay AS24 without rainfall

These similar characteristics shared by large-amplitude vibrations with and without rainfall, as well as their similar dependence on wind strongly suggest the potential of a close connection between rain-wind-induced vibrations and this class of large-amplitude dry-cable vibrations. Specifically, it is suspected that the so-called rain-wind-induced vibrations may in fact be a mechanism that inherently exists for inclined and/or yawed cables regardless of the presence of rainfall, and that the role of the rainfall is to promote or stabilize this mechanism (or both). In addition, as indicated in Section 5.2, large-amplitude rain-wind-induced vibrations and dry-cable vibrations also share some similar characteristics with Kármán-vortex-induced vibrations, such as the reduced-velocity-dependent nature of the modal vibrations, and the fact that for each type of vibration there is a reasonably clear relationship between the major direction of the vibration and the direction of the approaching wind. The only major differences between these large-amplitude vibrations and Kármán-vortex-induced vibrations are the specific ranges of reduced velocity over which they occur and the attainable amplitude for each type of vibration. These observations indicate that the large-amplitude vibrations presented in Sections 5.2 and 5.3, occurring either with or without rainfall, are likely a vortex-induced type of oscillation that is different from the classical Kármán-vortex-induced vibrations. These hypotheses derived from field observations again have to be subjected to the validation of wind tunnel tests.

5.4 Deck-Induced Vibration

As long, line-like structural components, decks of cable-stayed bridges are often susceptible to wind excitation mechanisms such as vortex shedding, flutter and buffeting

(Simiu and Scanlan 1996). During the course of the field investigation project, multiple types of wind-induced deck vibrations have been observed on the Fred Hartman Bridge. The characteristics of these deck vibrations have been reported in detail in Ozkan (2003), which is included in the literature package that accompanies the present report.

While excessive deck vibrations themselves have long been a concern, It has also been theoretically predicted that these oscillations of the bridge deck can potentially induce large-amplitude vibrations of the stay cables (e.g., Perkins 1992; Pinto da Costa et al. 1996). This has been proven true for the Fred Hartman Bridge, as many stay cable vibrations recorded can be attributed to the wind-induced oscillations of the bridge decks.

Analysis of the full-scale measurement data suggests that the characteristics of deck-induced vibrations are closely associated with the ratio between the oscillation frequency of the bridge deck and the natural frequencies of the stay cables. Table 5.1 lists the estimated natural frequencies of the first sixteen modes of the decks of the Fred Hartman Bridge based on recorded deck vibrations (Ozkan 2003). Since the twin decks can oscillate either in-phase (denoted "I" in Table 5.1) or out-of-phase (denoted "O") with each other, the natural modes appear as pairs in Table 5.1. The table suggests that the frequencies of some deck modes are very close to some natural frequencies of a number of stay cables. For example, the frequencies of the third vertical deck modes are close to the fundamental frequencies of stays AS24 and AN24 and the other equivalent stays. The frequencies of the majority of these deck modes of interest, however, are different from the natural frequencies of the stay cables.

Table 5.1 Modal frequencies of Fred Hartman Bridge decks

Mode	Frequency (Hz)	Phasing	Description of Mode
1	0.287	I	1st Vertical
2	0.301	O	1st Vertical
3	0.372	I	2nd Vertical
4	0.385	O	2nd Vertical
5	0.413	I	1st Lateral
6	0.432	O	1st Lateral
7	0.570	I	3rd Vertical
8	0.588	O	3rd Vertical
9	0.686	I	1st Torsional
Mode	Frequency (Hz)	Phasing	Description of Mode
10	0.688	O	1st Torsional
11	0.665	I	4th Vertical
12	0.668	O	4th Vertical
13	0.715	I	5th Vertical
14	0.720	O	5th Vertical
15	0.786	I	6th Vertical
16	0.790	O	6th Vertical

Figure 5.38 shows the components of wind along (U) and normal (V) to the axes of the bridge decks during a thirty-minute event (records 200002230-5). The long time histories are formed by connecting successive five-minute records together while ignoring the ten-second gap in between (used by the data acquisition system to compute statistics of the measurement for triggering decisions). For unidentified reasons, the full-scale measurement system failed to record the information between the tenth and the fifteenth minutes.

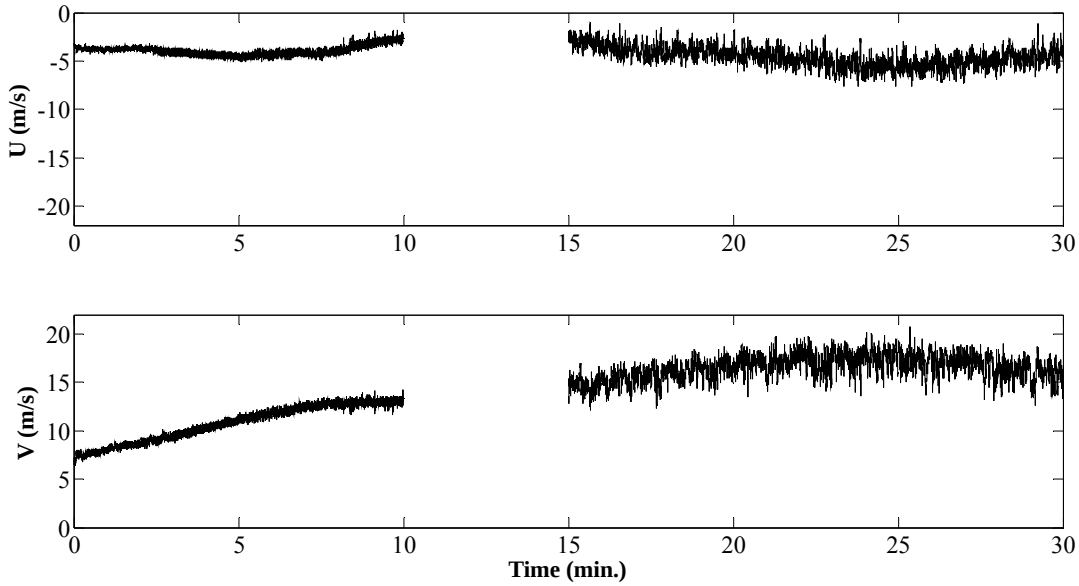

Figure 5.38 Wind components during a thirty-minute period

Figure 5.39 shows the vertical response (Disp-H) of the east deck recorded at the east edge at mid-span. The displacement time history is integrated from the acceleration recorded by a uniaxial accelerometer. In this case, the cut-off frequency of the sixth-order high-pass Butterworth filter is set at 0.2 Hz. The power spectral density functions were computed progressively along the time axis for segments of two minutes in length. Each segment overlaps the adjacent one(s) by half the length. Only the portions of the power spectra in the range of 0 to 2 Hz are presented in the figure because the major components of the response are in this range. It is evident that under the excitation of wind, the deck has developed vibration of moderate amplitude. In particular, the power spectra suggest that under the first ten minutes of smooth wind, the displacement is dominated primarily by the third vertical modes of the deck at 0.566 Hz and 0.586 Hz, respectively, and that under the more turbulent wind during the last fifteen minutes, the displacement is dominated by the first vertical mode at a much lower frequency of 0.293 Hz.

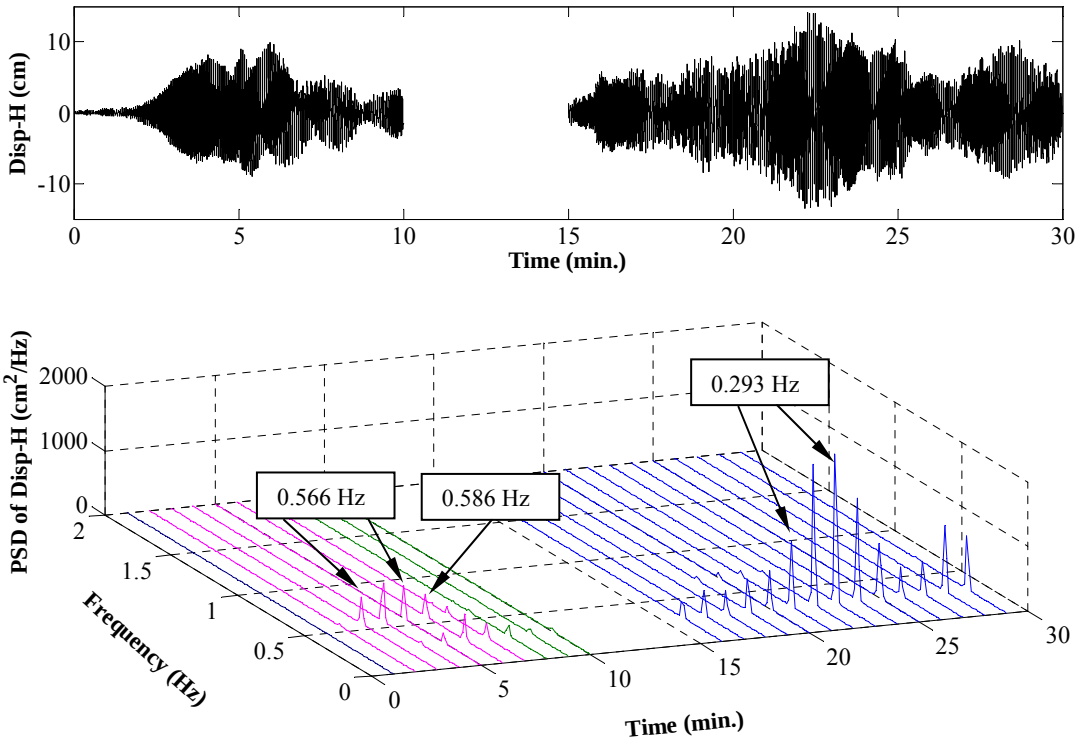

Figure 5.39 Response of the east deck at midspan

Figure 5.40 shows the evolution of the Strouhal frequency, N_S, of the deck associated with the component of wind normal to the bridge deck. According to the Strouhal relationship for Kármán vortex shedding,

$$N_S = \frac{VS}{D} \tag{5.3}$$

where D in this case is the height of the bridge deck (2.87 m). The Strouhal number (S) of the decks is estimated to be 0.15 according to wind tunnel tests (Mehedy Mashnad, University of Illinois, personal communication). By comparing Figure 5.40 with the power spectra of deck response at mid-span shown in Figure 5.39, it can be seen that for the first ten minutes of the event, the vibration frequency of the deck is very close to the Strouhal frequency associated with the normal component of wind. The only exception is that during the last three minutes of this ten-minute segment, the response of the deck at midspan does not show a frequency component close to the Strouhal frequency.

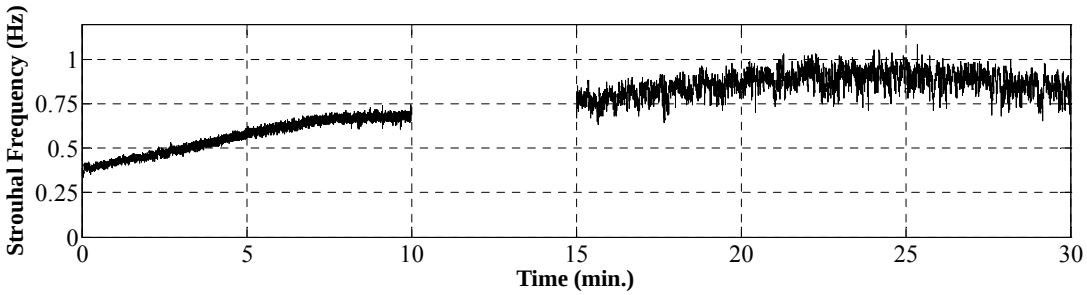

Figure 5.40 Evolution of Strouhal frequency associated with normal component of wind

Figure 5.41 shows the vertical response (Disp-H) of the east bridge deck recorded at a location near the anchorage of stay AS19. It is apparent again that during the first ten minutes of the event, the vibration frequency of the deck is very close to the Strouhal frequency associated with the component of the approaching wind that is perpendicular to the decks. In particular, the power spectra suggest that during the last three minutes of this ten-minute segment, the displacement at this location has strong frequency components near 0.761 Hz, which corresponds to the frequency of one of the sixth vertical modes of the deck. The

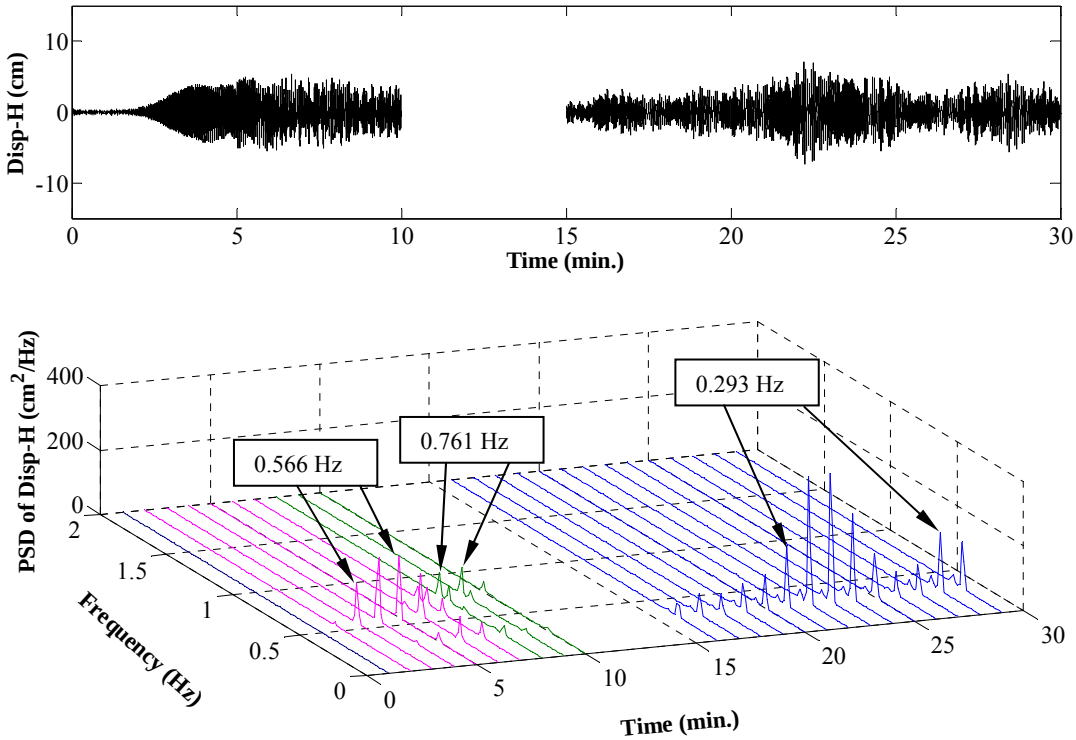

Figure 5.41 Response of the east deck at location near anchorage of stay AS19

reason why the vibration in the sixth vertical mode is present at the deck location near the anchorage of stay AS19 but not visible at mid-span is that the sixth mode is an asymmetric mode and that the mid-span point of the deck is located at one of the nodal points of this particular mode. This difference introduced by the locations of the measurements also manifests itself in the fact that according to Figure 5.39 and Figure 5.41, the amplitude of the vertical deck displacement in the first and third vertical modes are much larger at the mid-span point than at the location near the anchorage of stay AS19.

Due to the closeness between the theoretical Strouhal frequency and the observed frequency of deck vibration, the response of the bridge deck during the first ten minutes of this event is believed to have been induced by Kármán vortex shedding. The power spectra shown in Figure 5.41 also suggest that, during the last four minutes of this ten-minute segment, the displacement has a component at a frequency slightly lower than the frequency of the sixth vertical mode (0.761 Hz). This component of the displacement is suspected to represent the shedding frequency of the Kármán vortices at the corresponding wind speed. Because this frequency is not sufficiently close to the mechanical frequency of the sixth mode of the deck, however, the shedding of the Kármán vortices did not lock in with the

frequency of deck oscillation. The interaction between the Strouhal frequency and the mechanical frequency of the deck then created a wave-like beating structure that is apparent in the time history of the displacement during this period of time, as shown in Figure 5.42.

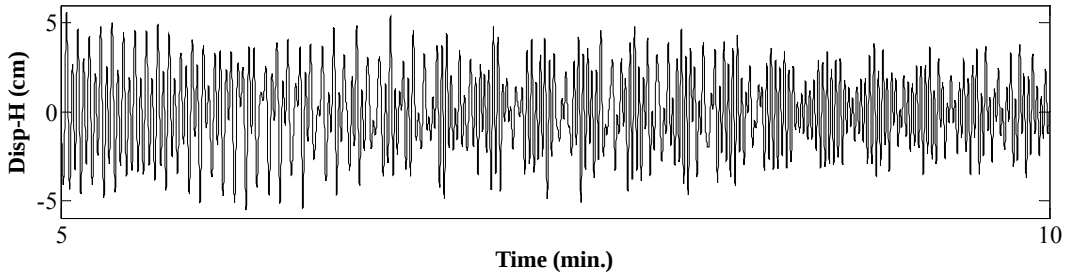

Figure 5.42 Beating type of vibration of bridge deck

Figure 5.39 to Figure 5.41 also indicate that during the last fifteen minutes of the event, the frequency of the dominant component of deck response is much lower than the nominal Strouhal frequency. This is believed to be due to the fact that during this period of time, the high level of turbulence in the wind prohibited the development of a regular Kármán vortex structure and that, as a result, the deck responded in the low-frequency first vertical mode to the low frequency turbulence in the wind instead of the mean component of the wind. The response of the deck during the last fifteen minute is then suspected to be due to buffeting.

The vibration of the bridge deck shown in Figure 5.39 and Figure 5.41 has resulted in two types of cable responses. Figure 5.43 shows the response of stay AS24, whose fundamental frequency (about 0.570 Hz) is very close to the third vertical modes of the bridge decks. By comparing the power spectra of the response of the stay AS24 shown in Figure 5.43 to the power spectra of deck vibration shown in Figure 5.39 and Figure 5.41, it is evident that during the entire duration of the thirty-minute event, stay AS24 essentially vibrated at the same frequency as did the bridge deck. The displacement time histories, however, suggest that the stay has been subjected to excitations of different mechanisms during different phases of the deck vibration. In particular, when the deck was vibrating in one of its third vertical modes, the resultant vibration of stay AS24 in its first mode reached a large amplitude due to the excitation from the deck oscillation; during the rest of the event, however, because the vibrating frequency of the deck is very different from the natural frequencies of the cable, stay AS24 did not vibrate at any of its local natural frequencies, but instead vibrated together with the deck in the global bridge modes at frequencies that are the same as those of the deck oscillation. In these segments of global vibration, the amplitude of the cable vibration in the in-plane direction is at a slightly smaller magnitude due to the inclination.

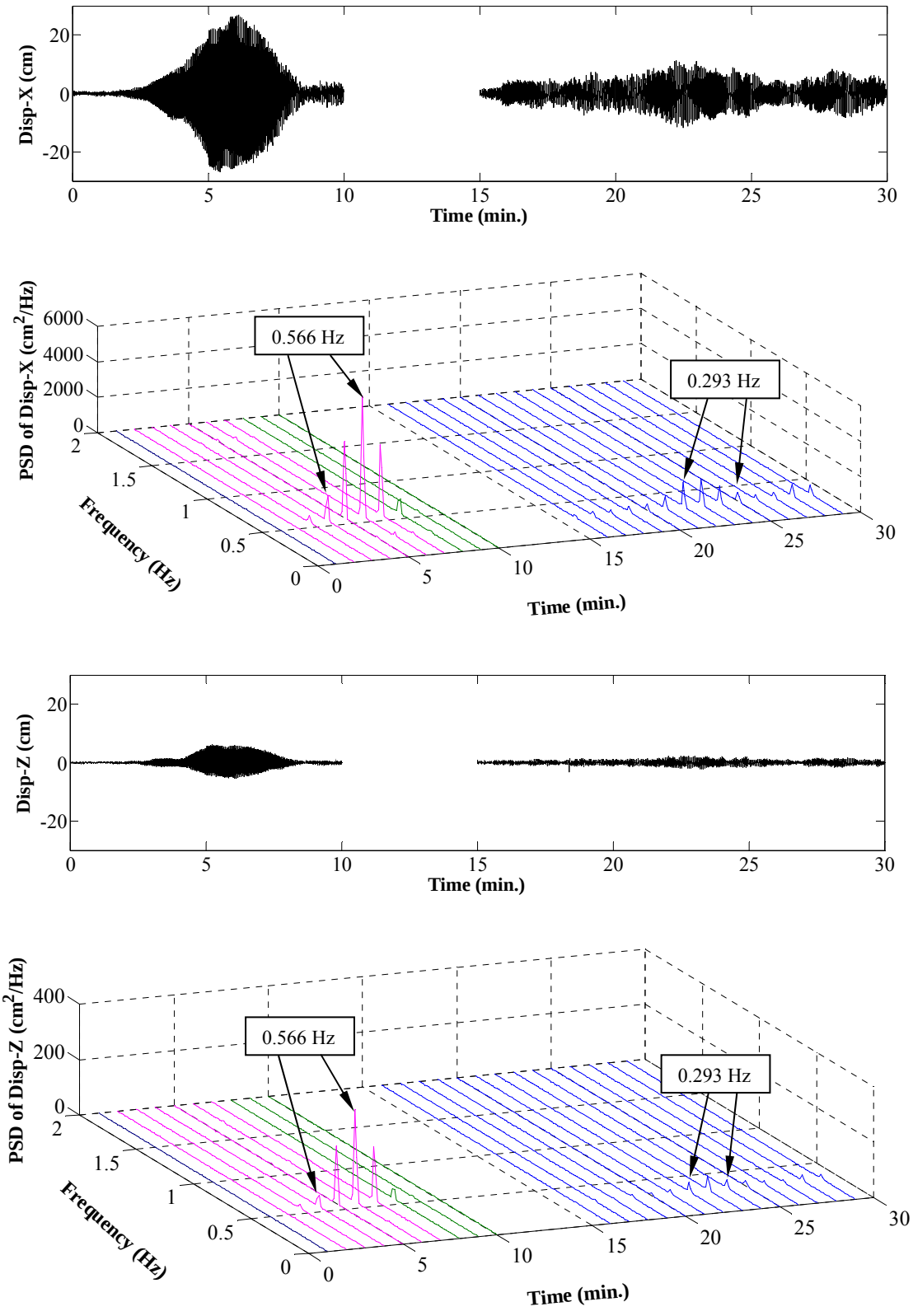

Figure 5.43 Response of stay AS24 to deck oscillation

It is important to note that under the excitation from the deck oscillation in the third vertical modes, stay AS24 also developed significant vibration in the lateral direction. This lateral component of the vibration is theoretically not expected because for a taut cable (such as stay AS24), the vibration components in the in-plane and lateral directions are uncoupled if the amplitude of the vibration is small (Takahashi and Konishi 1987). The exact cause for the lateral vibration has not been positively identified, but it is suspected that the lateral slope of the deck surface might have caused the cable anchorage to move in an inclined direction. This lateral vibration induced by deck oscillation has very important implications for the nature of deck-induced vibrations and the effectiveness of the mitigation devices designed to suppress such vibrations.

Figure 5.44 shows the response of stay BS24 to the excitation from wind-induced deck oscillation. The fundamental frequency of stay BS24 without attached mitigation devices is about 0.570 Hz in both the in-plane and lateral directions, which is also very close to the frequencies of the third vertical deck modes. During the occurrence of the event under discussion, however, this stay was in a cable network formed by the adjacent stays of BS17 to BS24. The fact that stay BS24 is interconnected with other stays through cross-ties changes the dynamic properties of the cable fundamentally. First, individual stays in cable networks can vibrate both in the global modes of the whole network and the local modes of the cable (Caracoglia and Jones 2005a). Second, the energy in the vibration of a cable can be redistributed among its local modes or be transferred into other stays (Ehsan and Scanlan 1989).

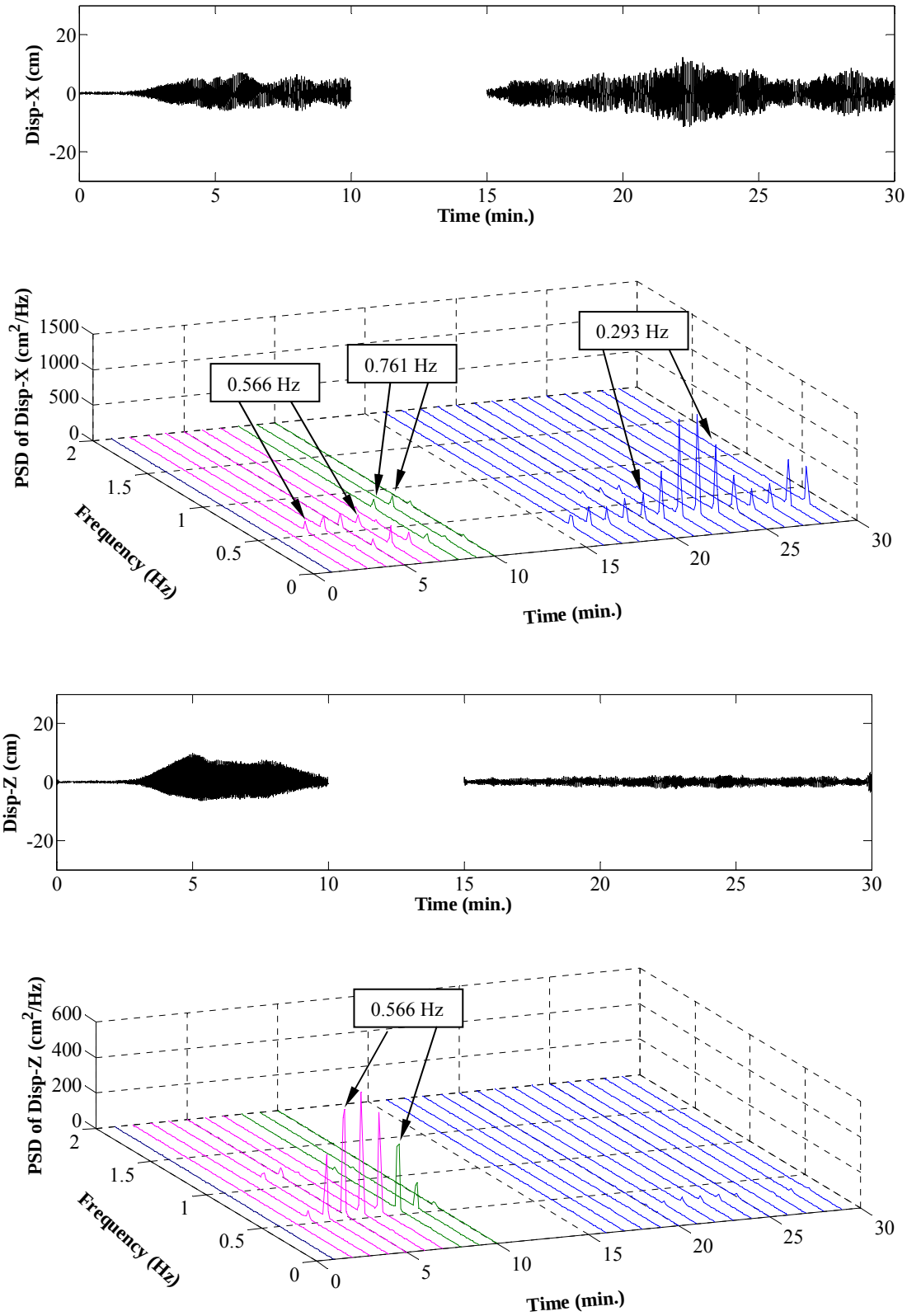

Figure 5.44 Response of stay BS24 to deck oscillation

By comparing the power spectra of the vibration of stay BS24 shown in Figure 5.44 with those of the deck vibration shown in Figure 5.39 and Figure 5.41, it is evident that, like stay AS24, stay BS24 also vibrated at the same frequency as did the bridge deck during the entire duration of the event. By comparing the displacement time histories of stay BS24 with those of stay AS24, however, it can be seen that the responses of the two stays were very different during the first ten minutes, when the deck was vibrating in its third vertical modes due to Kármán vortex shedding. Specifically, during this period of time, the displacement amplitude of stay BS24 in the in-plane direction was much smaller than the corresponding amplitude of stay AS24, while in the lateral direction, stay BS24 vibrated at a larger amplitude than did stay AS24. This different responses of the two stays is also evident in Figure 5.45 a) and Figure 5.45 b), which show the vibration locus of stay AS24 and stay BS24, respectively, for the fourteen-second segment of vibration immediately before the fifth minute, when the stays were subjected to the excitation of deck oscillation in the third mode. The reason why the displacement amplitude of stay BS24 was much smaller compared to that of stay AS24 is because stay BS24 was in a cable network and restrained in the in-plane direction, and that, as a result, the energy in its first mode vibration is redistributed within the network. Because stay BS24 was essentially not restrained in the lateral direction, however, its first mode in this direction can still respond to the excitation from the third modes of the bridge deck and develop large amplitude.

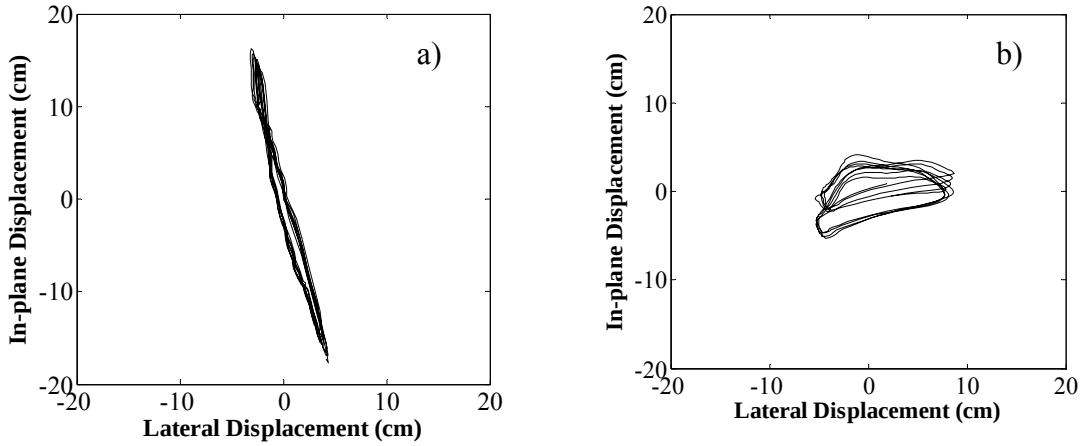

Figure 5.45 Vibration loci of stays a) AS24 and b) BS24 under the excitation of deck oscillation

Although the vibration amplitude of stay BS24 in the lateral direction is relatively small in this specific case because the vibration of the deck is primarily in a vertical mode, in the cases when the excitation is from a torsional deck mode due to mechanisms such as flutter, however, the stay cable can potentially develop vibration at much larger amplitude in the lateral direction. This ineffectiveness of the cross-ties in the lateral direction, therefore, needs to be taken into consideration in the design of mitigation devices for stay cable vibrations. Furthermore, the vibration of stay BS24 in the lateral direction also revealed a fundamental difference between deck-induced vibrations and other stay cable vibrations induced by aeroelastic mechanisms. For aeroelastic phenomena such as rain-wind-induced vibration, the change in the vibration will result in a change in the excitation force. Consequently, suppressing the vibration in one direction can potentially also suppress the

vibration in other directions. Deck-induced stay cable vibrations, however, are simply mechanically forced by the oscillation of the bridge deck. The vibration of the stay cable will have very little effect on the mechanism of wind-induced deck vibration due to the mass ratio between these two structural members. As a result, suppressing deck-induced vibration in one direction will not necessarily suppress the vibration in another direction.

It is important to point out that, deck-induced vibrations occur quite often at the Fred Hartman Bridge. This particular event is presented herein because it can reveal the essential aspects of deck-induced vibrations at one time. The amplitude of deck-induced stay cable vibrations in this event, although large, is not at an excessive level. In some other events of deck-induced stay cable vibration, however, the recorded peak to peak anti-nodal amplitude was estimated to reach as high as about 4 m, which is the largest among the amplitudes of all types of stay cable vibrations recorded. The problem of deck-induced vibrations, therefore, has to be carefully studied in the design of cable-stayed bridges.

5.5 Vibrations to be Categorized

In addition to the types of vibrations presented in the previous sections, the full-scale measurements have also recorded some vibrations that do not fall naturally into these categories or other classical categories of aeroelastic phenomena. In particular, some of these uncategorized vibrations can also reach very large amplitude and need to be a subject of further investigation.

A type of uncategorized vibrations is the particular responses of stays A14 and A12 on the Veterans Memorial Bridge in their respective fundamental modes under some specific wind conditions. As an example, Figure 5.46 shows the response of stay A14 to the wind shown in Figure 5.47 (record 1999032852). According to these figures, under the excitation from wind, stay A14 has developed large-amplitude vibration primarily in the first mode in the in-plane direction. This first mode vibration grows and decays intermittently, but the intermittent growing and decreasing of the amplitude of the vibration does not appear to match the changes in either wind speed or wind direction.

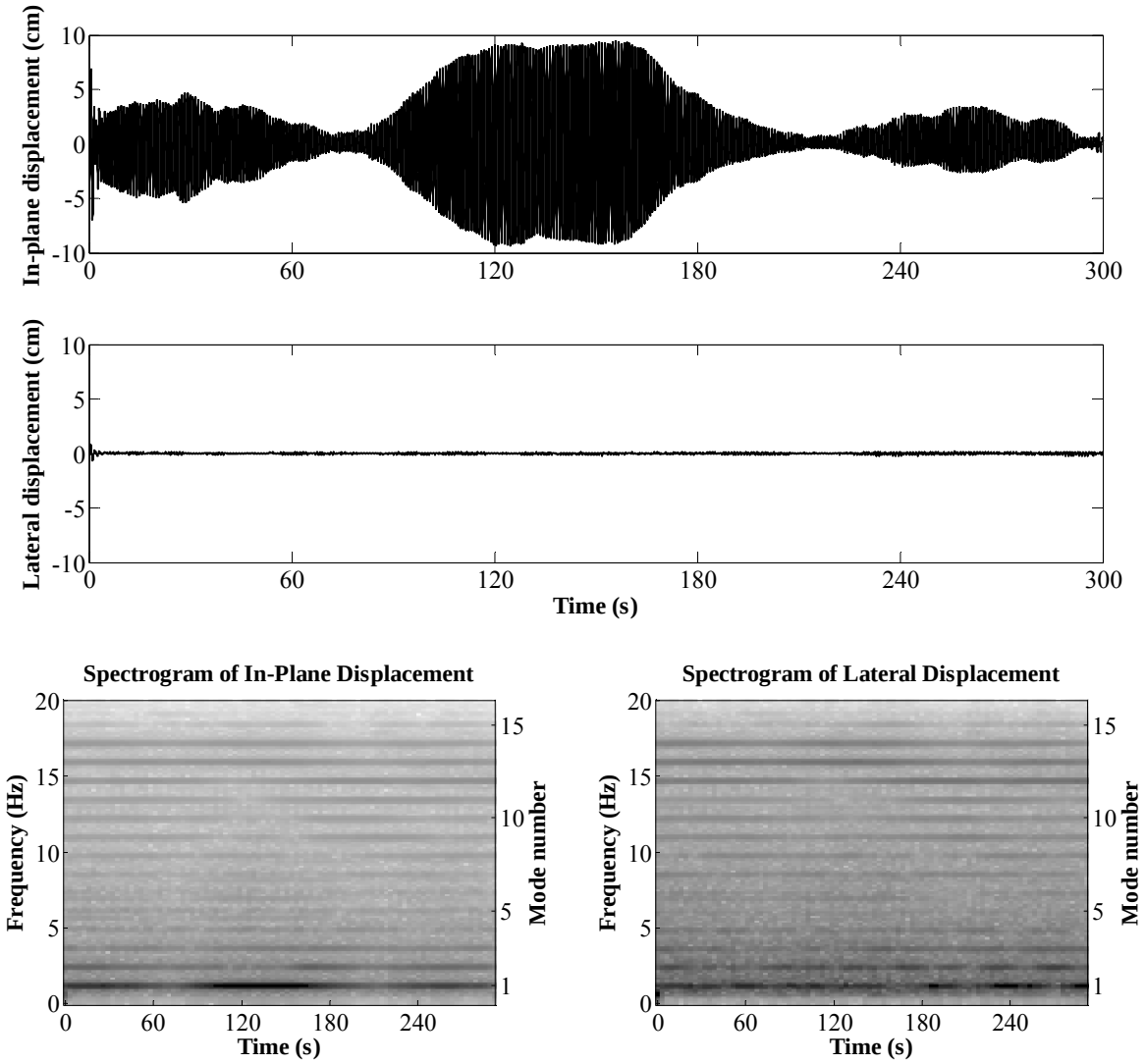

Figure 5.46 Typical example of an uncategorized type of stay cable vibration

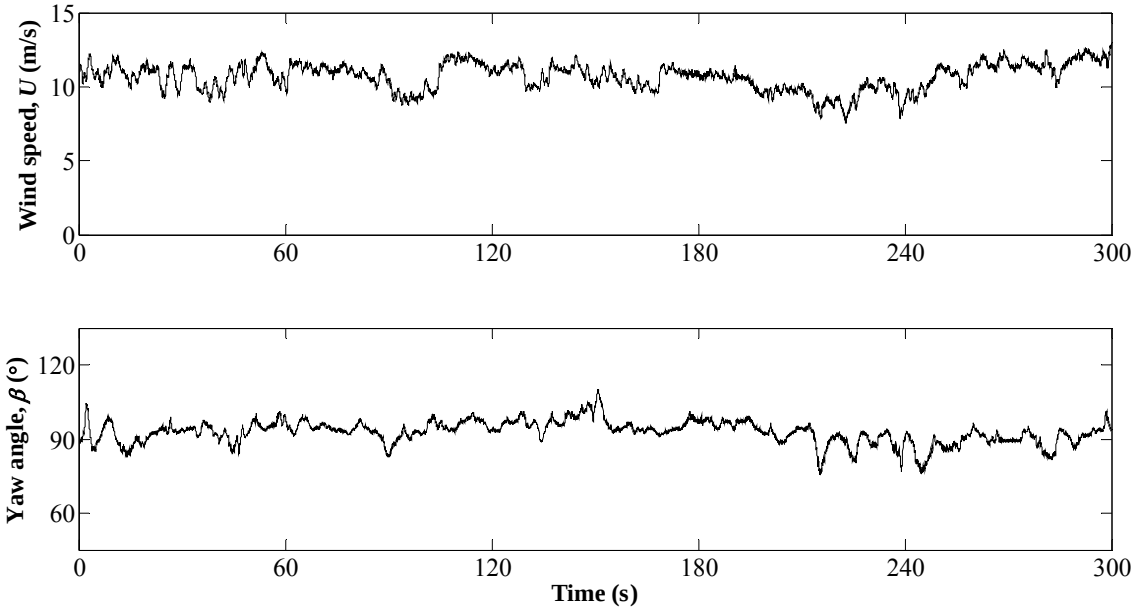

Figure 5.47 Wind speed and direction associated with a typical example of an uncategorized type of stay cable vibration

Figure 5.48 shows the ranges of wind speed and attack angle over which vibrations similar to the example record have occurred for stay A14, and Figure 5.49 shows the corresponding reduced velocity range associated with these vibrations in the first mode. These figures suggest that this particular type of uncategorized vibration occurred frequently to stay A14 over broad ranges of wind speed and direction, and that the reduced velocity associated with such vibrations can be much higher than the range over which rain-wind-induced vibrations occur. The secondary axis in terms of the Reynolds number in Figure 5.48 also suggests that this type of uncategorized vibration occurs in the sub-critical Reynolds number range and therefore does not belong to the divergent type of dry cable vibration observed by Cheng et al. (2003b).

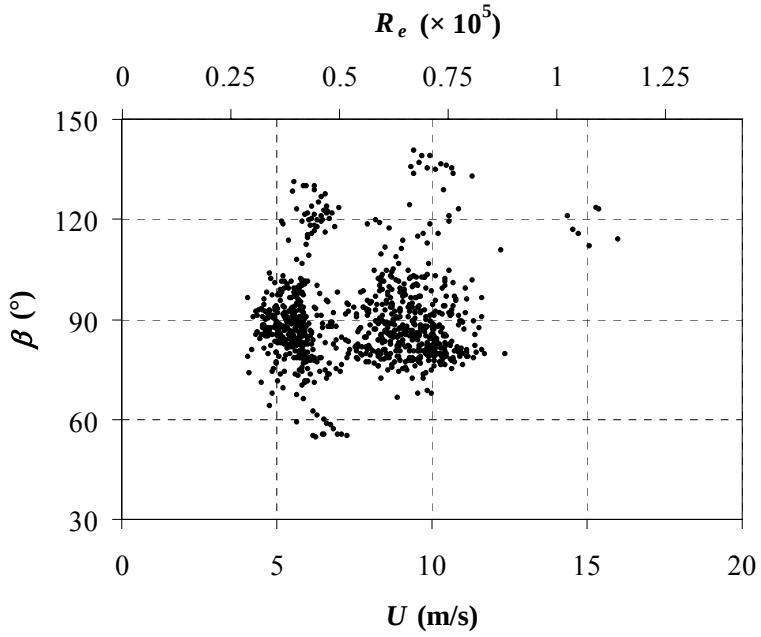

Figure 5.48 Ranges of wind speed and attack angle associated with an uncategorized type of stay cable vibration

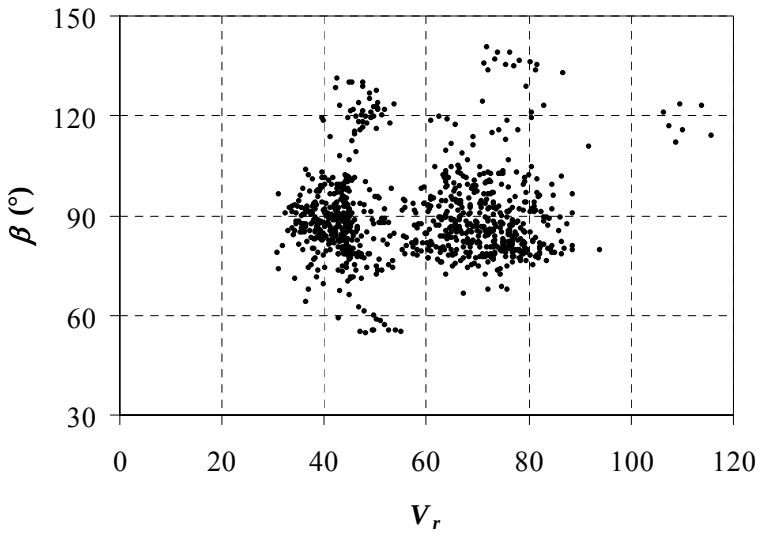

Figure 5.49 Ranges of reduced velocity and attack angle associated with an uncategorized type of stay cable vibration

Figure 5.50 shows the correlation between the major axis angle of such uncategorized vibrations of stay A14 and the attack angle with respect to wind. According to this figure, the vibrations always occur approximately in the in-plane direction regardless of the direction of the approaching wind. This feature of this type of vibration is also clearly different from the corresponding characteristics of rain-wind-induced vibrations and those of the type of dry cable vibration presented in Sections 5.2 and 5.3.

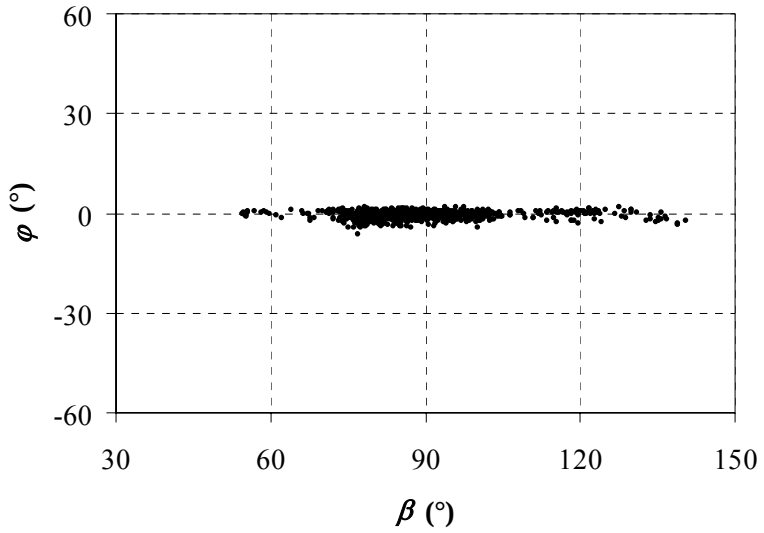

Figure 5.50 Correlation between major axis angle and attack angle for an uncategorized type of stay cable vibration

Vibrations with similar characteristics have also been observed for stay A12 on the Veterans Memorial Bridge, and such vibrations often occurred simultaneously for these two stays. For brevity, the vibration characteristics of stay A12 will not be presented herein. Due to these unusual characteristics, the mechanism of this type of vibration in the first mode of stays A14 and A12 has not been positively identified. These vibrations are not believed to be due to the oscillation of the deck or tower, however, since no significant deck oscillation was recorded simultaneously. In addition, during the occurrences of such vibrations, other stays did not simultaneously show signs of vibration at the same frequencies as those of the fundamental frequencies of stay A12 and A14, which is an evidence for excitation from the bridge deck or tower. Furthermore, this type of vibration is not believed to be a rain-wind-induced type either since it usually occurs without rainfall, although a limited number of occurrences of such vibrations have been observed during precipitation.

It is important to point out that stays A14 and A12 on the Veterans Bridge are the only ones that have exhibited this type of unidentified vibration. Whether or not some special dynamic properties of these two stays have rendered them susceptible to this type of excitation remains to be investigated. Nonetheless, the existence of these vibrations, as well as some other vibrations that cannot be easily categorized, does provide an important note for the study of wind- and rain-wind-induced stay cable vibrations. Due to their special aerodynamic and mechanical characteristics, stay cables are inherently susceptible to wind excitations of various types. These important characteristics of stay cables include

- that the cross-section of stay cables is circular in shape. This means that the flow can detach from any point on the cable surface and that even a slight change to the cable surface can significantly affect the flow.
- that stay cables are long, flexible structures with an infinite number of natural modes with low mechanical damping. This means that they can vibrate in a variety of modes under excitation with relatively small amount of energy.
- that stay cables are spatially inclined (with various inclination angles) and subjected to the excitation of three-dimensional, sheared wind flow in the atmospheric boundary layer. This means that the flow around a specific cross-

section of the cable can be very complex and that different segments of the cable can be subjected to different variants of the same excitation mechanism or different mechanisms.

Due to this inherent susceptibility to wind loading, stay cables can exhibit vibrations of different, very complex characteristics under the excitation of different mechanisms. It is therefore not appropriate to casually associate some observed stay cable vibrations with specifically known, or not so well-known, types of vibrations only based on some simple characteristics of the vibration, such as the magnitude of the vibration amplitude.

6 Assessment of Mitigation Devices

Three types of countermeasures have been utilized on the Fred Hartman Bridge and the Veterans Memorial Bridge to mitigate the wind- and rain-wind-induced stay cable vibrations: passive viscous dampers attached at the vicinity of the cable anchorages, cable restrainers (cross-ties) that tie the cables together to form cable networks and circular rings attached along the axis of the stay cables. Based on the full-scale measurement data, this chapter presents an assessment of the cross-ties and the dampers in mitigating wind and rain-wind stay cable vibrations. Evaluation of the performance of the circular rings is beyond the scope of the work performed by the group at JHU.

6.1 Performance of Passive Viscous Dampers

A total of four types of passive viscous dampers have been installed on selected strays of the Fred Hartman Bridge and the Veterans Memorial Bridge at different time during the field investigation project. The first type is a full-sized hydraulic damper designed by WDP (referred to as Type I WDP damper hereafter); the second type is a compact hydraulic damper designed by WDP (reffered to as compact WDP damper hereafter); the third type is a circumferential pressurized bladder damper designed by the Freyssinet Company (referred to as Freyssinet damper here after), and the fourth type is a full-sized hydraulic damper designed by WDP (referred to as Type II WDP damper hereafter) that is different from WDP damper I. This section presents an assessment of the performance of the dampers designed by WDP, as well as that of the Freyssinet damper in mitigating the stay cable vibrations.

6.1.1 Assessment of Inherent Damping in Stay Cables

In order to assist the evaluation of damper performance, manual forced vibration tests were performed on a number of stays B9, B11 and B13 on the Veterans Memorial Bridge to assess the inherent damping in stay cables. During these tests, the cables were forced to vibrate by periodically pulling the cables with a rope approximately at the frequency of the modes of interest. When the vibration of the cables attained sufficiently high amplitude, the pulling was stopped and the vibration was allowed to decay freely. The vibrations of the stay cables during these “pull-and-release” tests were recorded with the same type of accelerometers used in the long-term full-scale measurements, and the free-decaying portions of the vibrations were used to assess the damping in the stay cables.

Figure 6.1 shows the displacement time histories of stay B9 during two forced vibration tests and the corresponding spectrograms. Although the cable was pulled at approximately the frequency of its first mode during these tests, the spectrograms of the vibration suggest that, in addition to the strong response in the first mode, the cable also responded in the higher modes. These higher-mode responses are theoretically expected, however, since the manual periodic excitation is most probably not perfectly harmonic and as a result, the stay cable will respond to the super harmonics of the pulling frequency.

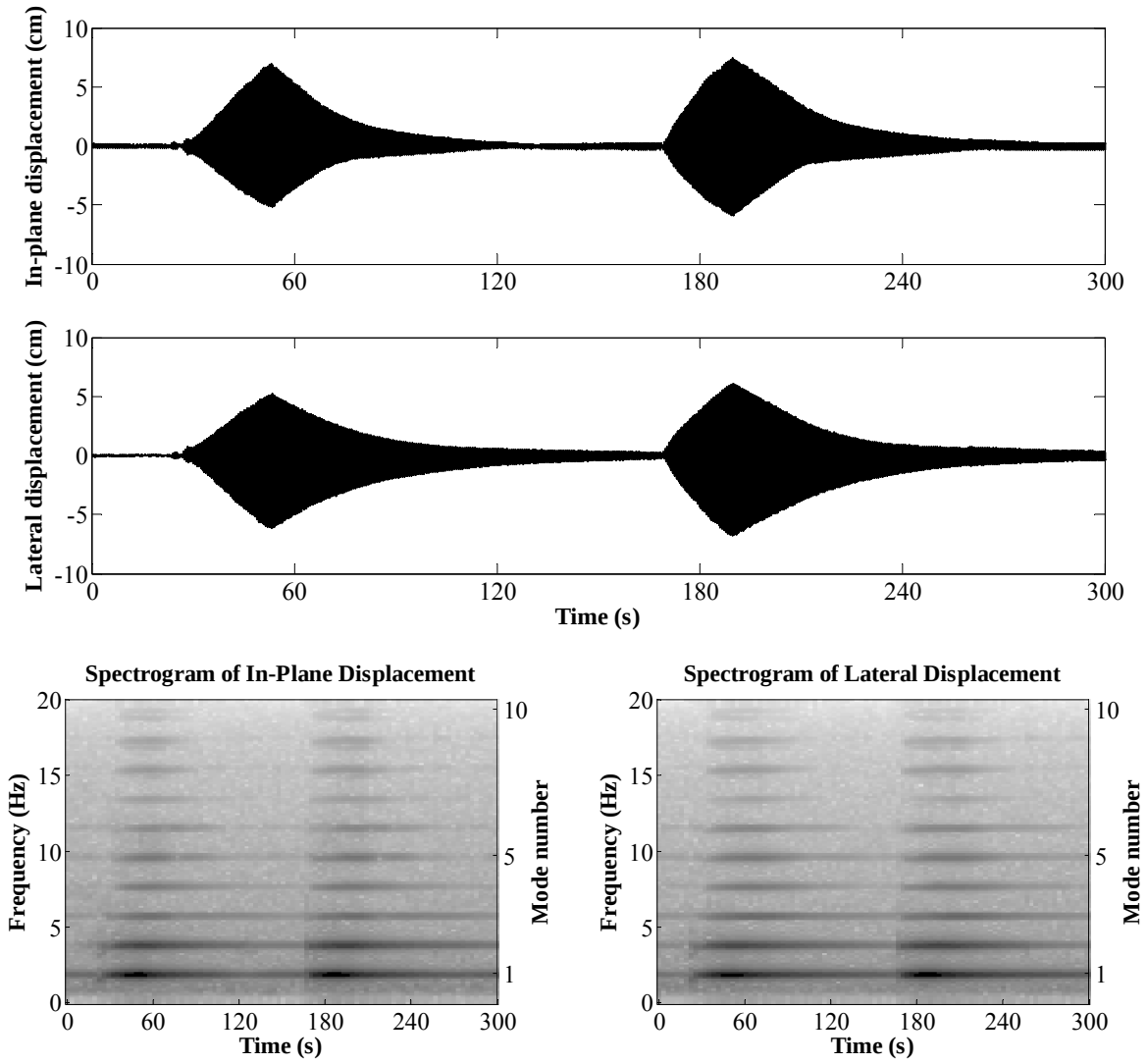

Figure 6.1 Displacement time histories and corresponding spectrograms of a manually forced vibration record

To assess the damping in the individual modes, the displacement time histories shown in Figure 6.1 are first decomposed into modal responses using the Butterworth filter. Figure 6.2 presents the response of the cable at the location of the accelerometer in the first two modes. In addition to showing the growing and decaying oscillation of the stay cable, this graph also reveals an important fact that the amplitudes of the vibrations in the two modes did not start decaying at the same time, after the pulling was stopped. This is especially true during the second test, wherein the amplitudes of the second mode vibration kept increasing long after the vibration in the first mode started decaying. This pattern of response is theoretically impossible for taut strings with perfectly clamped supports. The exact reasons for this pattern of response have not been positively identified, but the dynamic interaction among the stay cables, the deck and the towers of the bridge system is suspected to be an important factor. Since stay cables are interconnected with the bridge deck and the towers, the energy in the vibration of a structural element can be dynamically transmitted to others. In this particular case, the energy being input into stay B9 from the pulling test is also partly

transmitted into the deck and the tower, and through which into other stay cables. After the pulling is stopped, part of the energy in the vibration of the deck, the tower and other stays could have potentially been retransmitted back into stay B9 and contributed to the increase of the amplitude of the second mode after the pulling was stopped. The significant dynamic interactions between the stay cables and the bridge deck and tower in fact can be verified by an observation made during the manually forced vibration tests that, not only did the cable being pulled developed large amplitude vibration, the other cables with fundamental frequencies close to those of the stay being pulled also started vibrating noticeably.

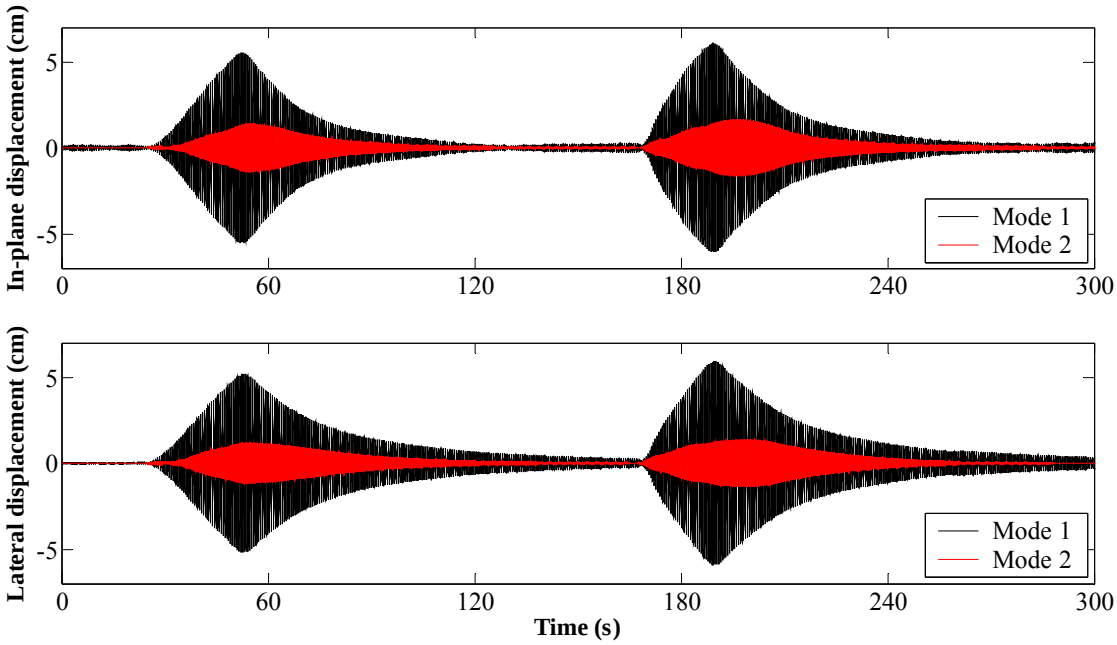

Figure 6.2 Modal responses of stay B9 to manual excitation

Figure 6.3 shows the response of stay B11 at the location of the accelerometer when it was subjected to a pull test and Figure 6.4 shows the simultaneous response of stay C11 at the location of the accelerometer on this stay. Stays B11 and C11 are practically two identical cables with the same natural frequencies, and are located symmetrically with respect to the center line of the bridge span. It is apparent that the responses of the two stay cables are quite well correlated, which indicates the dynamic energy transmision between the two through the bridge deck.

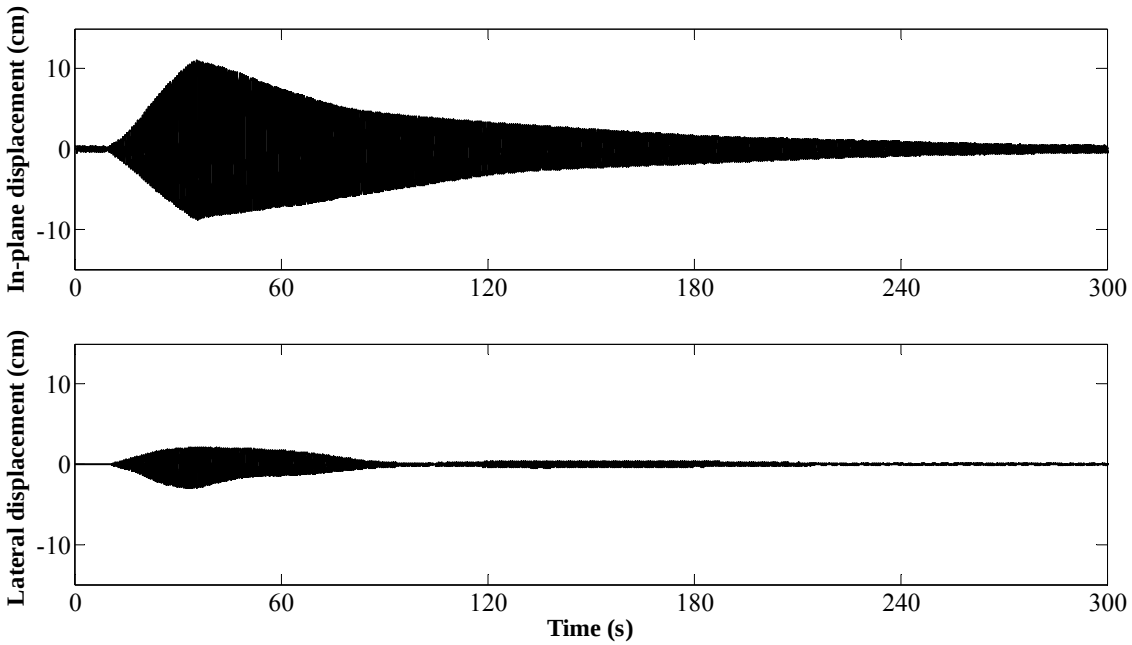

Figure 6.3 Response of stay B11 to a pull test

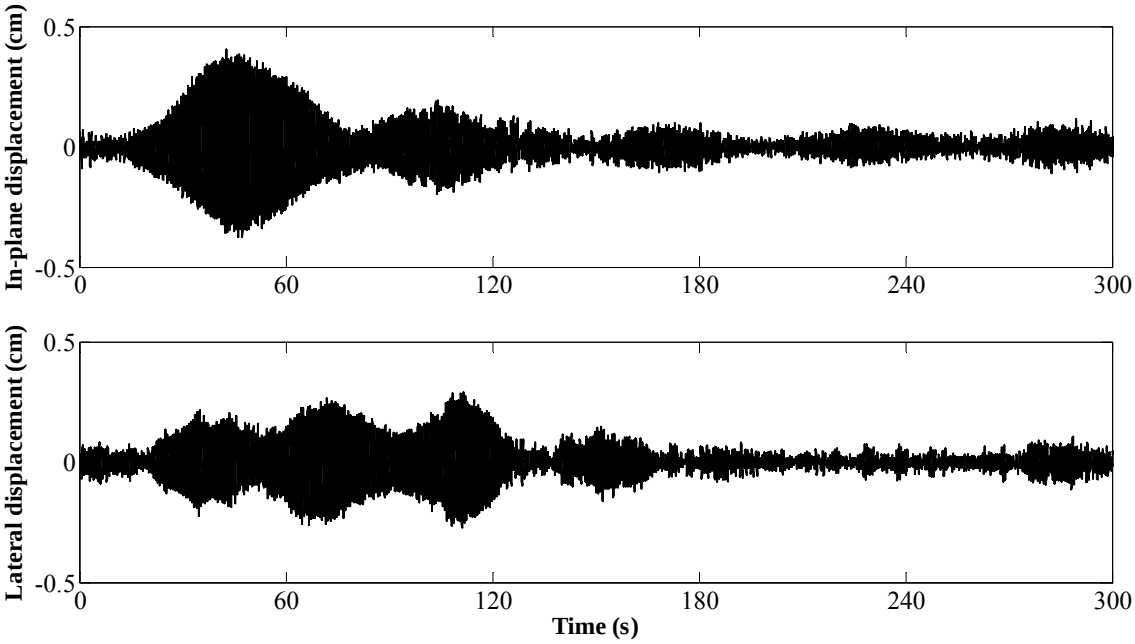

Figure 6.4 Response of stay C11 during pull test on stay B11

The dynamic energy exchange within the whole bridge system significantly complicates the dynamics of the stay cables. In particular, due to the energy exchange, the damping in the stays can potentially be significantly "non-viscous" that the damping estimation techniques based on the assumption of viscous damping can no longer be valid. Also, the damping may not be effectively assessed by treating the cables as isloated taut strings. Instead, the energy dissipation capability of the stay cables have to be investigated in the context of the whole bridge system. Nonetheless, in this section, the damping in the

individual modes of the stay cables is assumed to be close to viscous and the logarithmic decrement method (Chopra 2001) is used for the purpose of preliminary damping assessment. As an example, Figure 6.5 shows the damping estimation results for the first two modes of stay B9, based on the second pull test shown in Figure 6.2. Each data point in the figure represents the average value of the damping ratios estimated over nine successive cycles of free vibration and the corresponding average displacement amplitude. This graph reveals two distinct characteristics of the damping in stay B9. First, the modal damping ratios are not constant. Instead, they appear to depend in an irregular way on the modal amplitudes of the vibration. Second, the damping in a given in-plane mode can be significantly different from that in the corresponding lateral mode of the cable. These two characteristics of damping in stay cables can be due to the combination of a variety of reasons, but the dynamic energy exchange within the bridge system is believed to be a major contributing factor. Despite these complex characteristics of estimated damping, however, Figure 6.5 does provide a preliminary quantitative assessment of damping in stay B9. Due to these complex characteristics, however, it is not always appropriate to assign a single number of damping ratio to a specific mode. Rather, it is more rational to assess the damping ratio in a statistical manner. In the study herein, the mean value and the standard deviation of the damping estimated will be used to characterize the modal damping in stay cables.

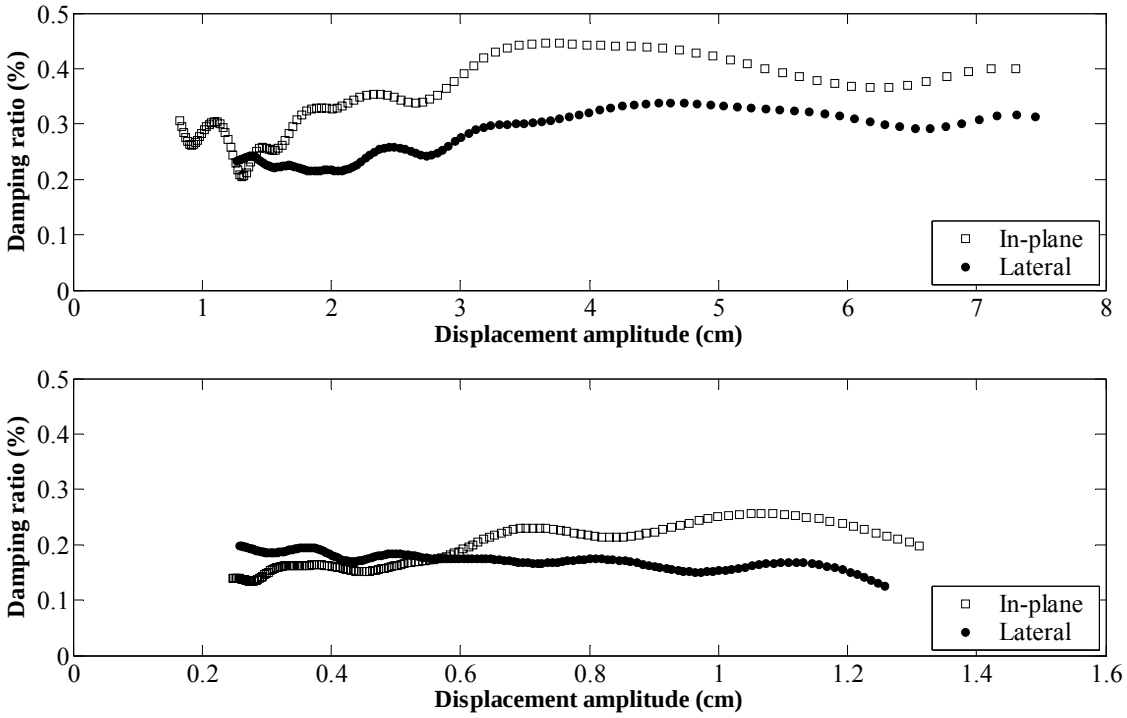

Figure 6.5 Modal damping values estimated from an example forced vibration test

Table 6.1 shows the results of damping estimation for the three stays on the Veterans Memorial Bridge that are subjected to manually forced vibration tests. For reference purposes, the coefficient of variation (CV) for the estimations is also listed. Although these results are based on a small number of forced vibration tests and may not completely reveal the damping characteristics in the cables tested, they do suggest that the damping in these

three cables are at a very low level and that the level of damping in a higher mode of a stay is usually lower than that in a lower mode. Similar forced vibration tests were also performed on some stay cables on the Veterans Memorial Bridge by other researchers (Whitlock Dalrymple Poston and Associates 1999). Some relevant damping estimation results from these tests are listed in Table 6.2. Stays C9 and A13 listed in this table are essentially identical to stays B9 and B13 listed in Table 6.1, but are at different locations on the bridge. By comparing the estimated damping ratios for the corresponding modes of the corresponding stays listed in the two tables, it is apparent that the damping estimation results based on the independently performed forced vibration tests are very consistent.

Table 6.1 Damping estimation results based on manually forced vibration tests

Stay Name	Mode Number*	ζ (%)	σ_ζ (%)	CV (%)
B9	1X	0.35	0.07	20
	1Z	0.27	0.06	22
	2X	0.18	0.03	17
	2Z	0.17	0.03	18
B11	1X	0.12	0.02	17
	1Z	0.16	0.06	38
	2X	0.09	0.03	33
	2Z	0.14	0.05	36
B13	1X	0.14	0.03	21
	2X	0.19	0.01	5

* X=In-plane; Z=Lateral

Table 6.2 Damping estimation results based on manually forced vibration tests by Whitlock Dalrymple Poston and Associates 1999)

Stay Name	Mode Number*	ζ (%)
C9	1X	0.41
B11	1X	0.13
A13	1X	0.15

6.1.2 Performance of Type I WDP Damper

Type I WDP dampers were used on stays AS16 and AS23 of the Fred Hartman Bridge and stay D14 of the Veterans Memorial Bridge. The dampers were optimized for vibration in the first mode of the individual stays based on the universal damping estimation curve for stay cables with attached viscous damper, which was developed by Pacheco et al. (1993). The Type I WDP damper installed on stay AS16 of the Fred Hartman Bridge is shown in Figure 6.6 as an example.

Figure 6.6 Type I WDP damper installed on stay AS16

Full-scale measurement data suggest that the Type I WDP dampers were generally effective in suppressing wind- and rain-wind-induced stay cable vibrations. Figure 6.7 a) and Figure 6.7 b) show the fourteen-second mean displacement amplitude of the most dominant mode against wind speed for the vibrations of stay AS16 on the Fred Hartman Bridge before and after the dampers are installed, respectively. Specifically, Figure 6.7 a) represents data recorded from October 3, 1997 to October 2, 1998, when stay AS16 was not restrained, and Figure 6.7 b) represents data recorded from March 6, 1999 to December 18, 2002, during which time stay AS16 was mitigated by a Type I WDP damper but was not cross-tied. The most dominant mode referred to herein is the mode with the largest displacement amplitude, and only segments with mean dominant-mode amplitude larger than five percent of the cable diameter are included. The word "dominant" is used herein only for convenience, since the significance of a specific mode in the vibration can be judged by other quantities, such as the acceleration and the energy of the vibration. Nonetheless, these figures do suggest that the damper was quite effective in keeping the vibration amplitude at a moderate level.

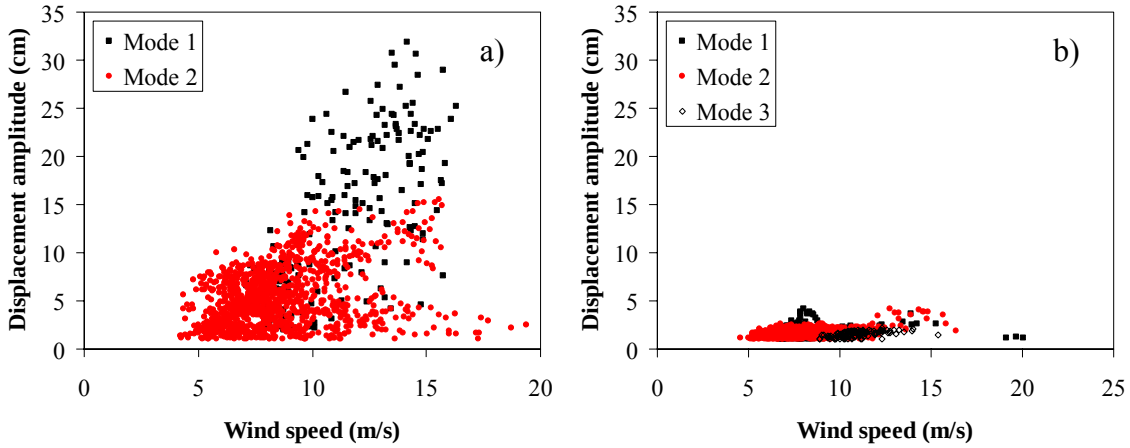

Figure 6.7 Amplitude vs. wind speed for stay AS16 a) before and b) after damper installation

Figure 6.8 a) and Figure 6.8 b) show the fourteen-second mean amplitude of the most dominant mode against wind speed for the vibrations of stay AS23 before and after the dampers are installed, respectively. Figure 6.8 a) represents vibrations recorded from October 3, 1997 to October 2, 1998, when stay As23 was not restrained, and Figure 6.8 b) represents data recorded from March 6, 1999 to June 6, 2001, when the was restrained by the type I WDP damper. It is evident that the damper was quite successful in suppressing the vibrations.

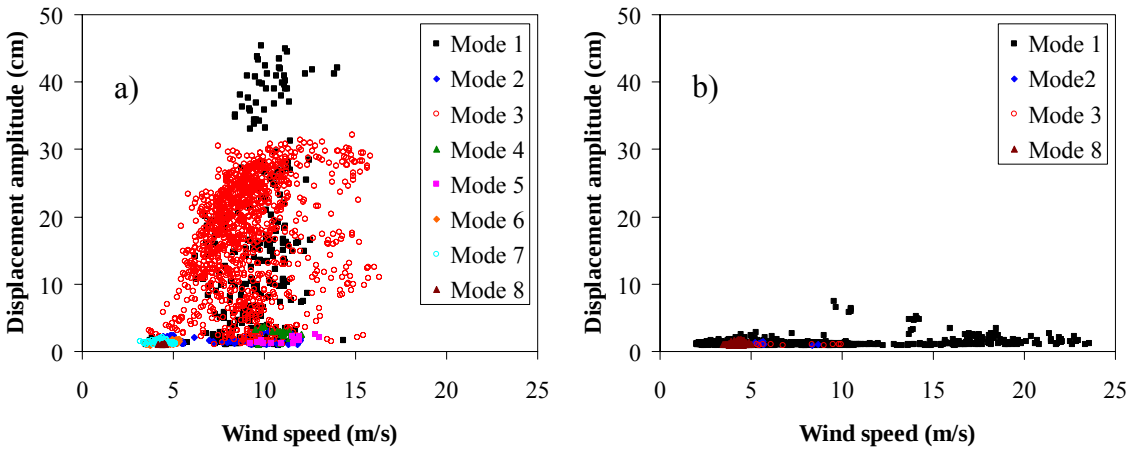

Figure 6.8 Amplitude vs. wind speed for stay AS23 a) before and b) after damper installation

Figure 6.9 a) and Figure 6.9 b) show the fourteen-second mean displacement amplitude of the most dominant mode against wind speed for the vibrations of stay D14 on the Veterans Memorial Bridge before and after the dampers are installed, respectively. Figure 6.9 a) represents vibrations recorded from January 22, 1999 to November 5, 1999, and Figure 6.9 b) represents data recorded from November 5, 1999 to June 9, 2001, when stay D14 was restrained by the type I WDP damper. It is apparent that the type I WDP damper was successful in suppressing the vibrations of D14.

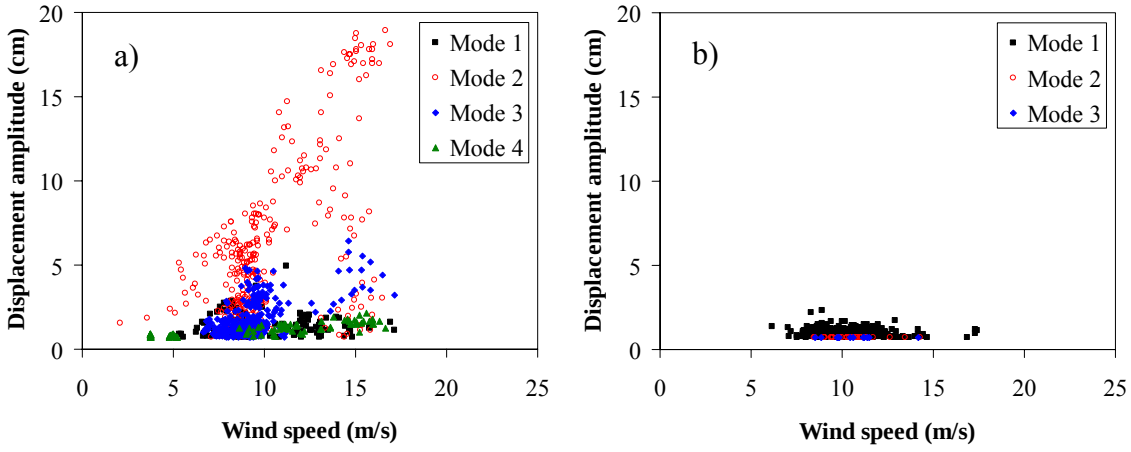

Figure 6.9 Amplitude vs. wind speed for stay D14 a) before and b) after damper installation

Full-scale measurement data also suggest, however, that although the Type I WDP dampers were effective in suppressing the vibrations, the performance of the dampers is

different from analytical predictions. The observed performance of the Type I WDP damper will be presented herein as an example.

The damper on stay AS16 is installed perpendicular to the cable axis in the in-plane direction at a distance of about 4 m from the cable anchorage; the design damping coefficient is 70 kN·s/m. According to Krenk (2000), for a viscous damper attached very close to the anchorage of the stay cable, the amount of supplemental damping that can be provided is

$$\zeta_n = \frac{(\eta n\pi a/L)}{1+(\eta n\pi a/L)^2}\frac{a}{L} \tag{6.1}$$

where n is the mode number; a/L is the clamping ratio of the damper in terms of a, which is the distance from the damper-cable connection to the anchorage of the cable, and L, which is the length of the cable, and

$$\eta = \frac{c}{\sqrt{Tm}} \tag{6.2}$$

is a non-dimensional parameter representing the damping coefficient of the damper (c) normalized by the square root of the cable tension (T) and cable mass per unit length (m). As an example, Figure 6.10 shows the damping ratio added to stay AS16 by dampers of various damping coefficients. It is apparent that, with the damping coefficient of 70 kN·s/m, the damper installed on stay AS16 is theoretically optimized for vibrations in the first mode. For the vibration in the higher modes, however, the damper only provides an amount of damping that is sub-optimal. Table 6.3 lists the amount of supplemental damping the damper on stay AS16 can provide to the first four modes of the cable based on Equation (6.1).

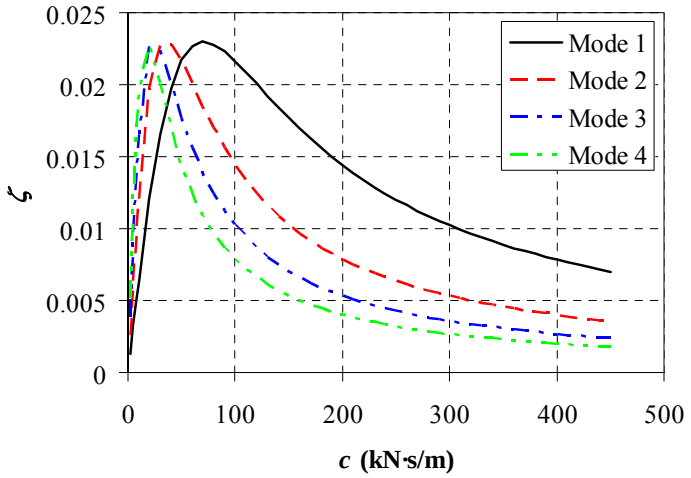

Figure 6.10 Damping supplemented to stay AS16 by dampers of different coefficient

Table 6.3 Damping provided to the first four modes of stay AS16 by attached damper

Mode number, n	1	2	3	4
Damping Ratio, ζ_n (%)	2.3	1.8	1.4	1.1

The damping modal supplemental damping ratios listed in Table 6.3 represents the expected values for the designed damper. Full-scale measurement data, however, have revealed that the actual supplemental damping is significantly different from the designed values due to particular performance features of the damper. Figure 6.11 a) and Figure 6.11 b) present, respectively, the modal damper force recorded by the load cell against the modal displacement amplitude in the in-plane direction of the cable at the anti-nodal points and the displacement amplitude recorded near the damper-cable connection by the string pot transducers, which can be considered the displacement amplitude of the damper piston. By comparing these two graphs, it is apparent that while the vibration of the cable has generated large forces in the damper, these large damper forces, however, are associated with only very

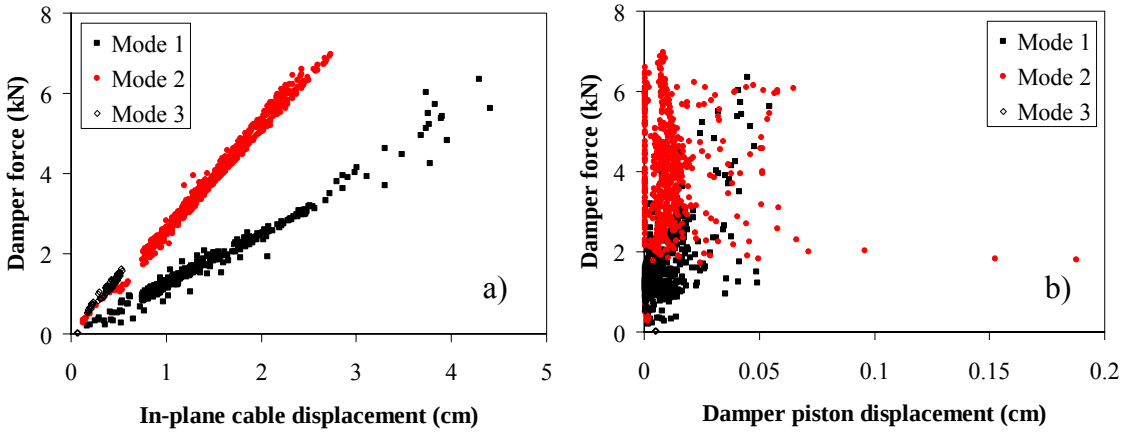

Figure 6.11 Damper force vs. a) anti-nodal cable displacement amplitude and b) damper piston displacement amplitude for stay AS16

small damper piston movements. In addition, while the amplitude of damper force in each mode has a clear linear relationship with corresponding mode of anti-nodal displacement amplitude according to Figure 6.11 a), such relationship does not exist between the damper force and the piston displacement according to Figure 6.11 b).

This pattern of damper behavior can also be illustrated by the relationship between the modal damper forces and the modal velocities of the cable at the anti-nodal point and modal velocities of damper piston movement: Figure 6.12 a) indicates a consistent relationship between the modal damper force and the modal anti-nodal velocity of cable vibration, but Figure 6.12 b) suggests that such a relationship does not exist between the damper force and the velocity of the piston. This performance of the damper suggests that there could be some mechanism that has been keeping the damper from working purely viscously as designed. Be examining a number of individual records, this mechanism is identified as the static friction in the damper device.

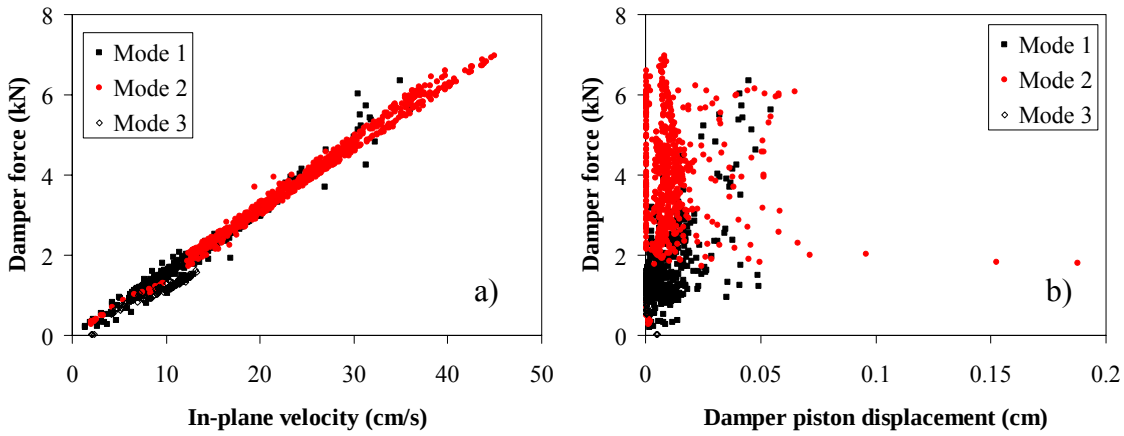

Figure 6.12 Damper force vs. a) anti-nodal cable velocity amplitude and b) damper piston velocity amplitude for stay AS16

To illustrate the effect of static friction on the performance of the damper attached to stay AS16, Figure 6.13 plots the time histories of the in-plane cable displacement (Disp-X) at the location of the accelerometer, which is about 12 m away from the cable anchorage, the displacement of the damper piston and the damper force, respectively, for a typical record in which large damper force is recorded. In this record, the vibration of the cable was dominated by its second mode at about 2.55 Hz. The time history of the piston displacement reveals that, instead of being engaged throughout the entire time duration, the damper worked only intermittently. Also, this intermittent engagement and disengagement of the damper appears to be well correlated with the intermittent increasing and decreasing of the amplitude of the damper force and the in-plane cable vibration, as suggested in Figure 6.13 a) and Figure 6.13 c). These facts collectively suggest that, in this particular record, the damper moved only when a threshold of damper force or cable displacement was exceeded, otherwise, it essentially remained locked up. This observation of damper performance can also be indirectly supported by the observed cable vibration in the lateral direction. Figure 6.14 a) and Figure 6.14 b) shows the lateral displacement of the cable at the location of the accelerometer and at the damper-cable connection, respectively. According to this figure, since the cable was not restricted in the lateral direction (Z), the portion of the cable near the damper-cable connection vibrated freely and this vibration is well correlated with the vibration at the location of the accelerometer.

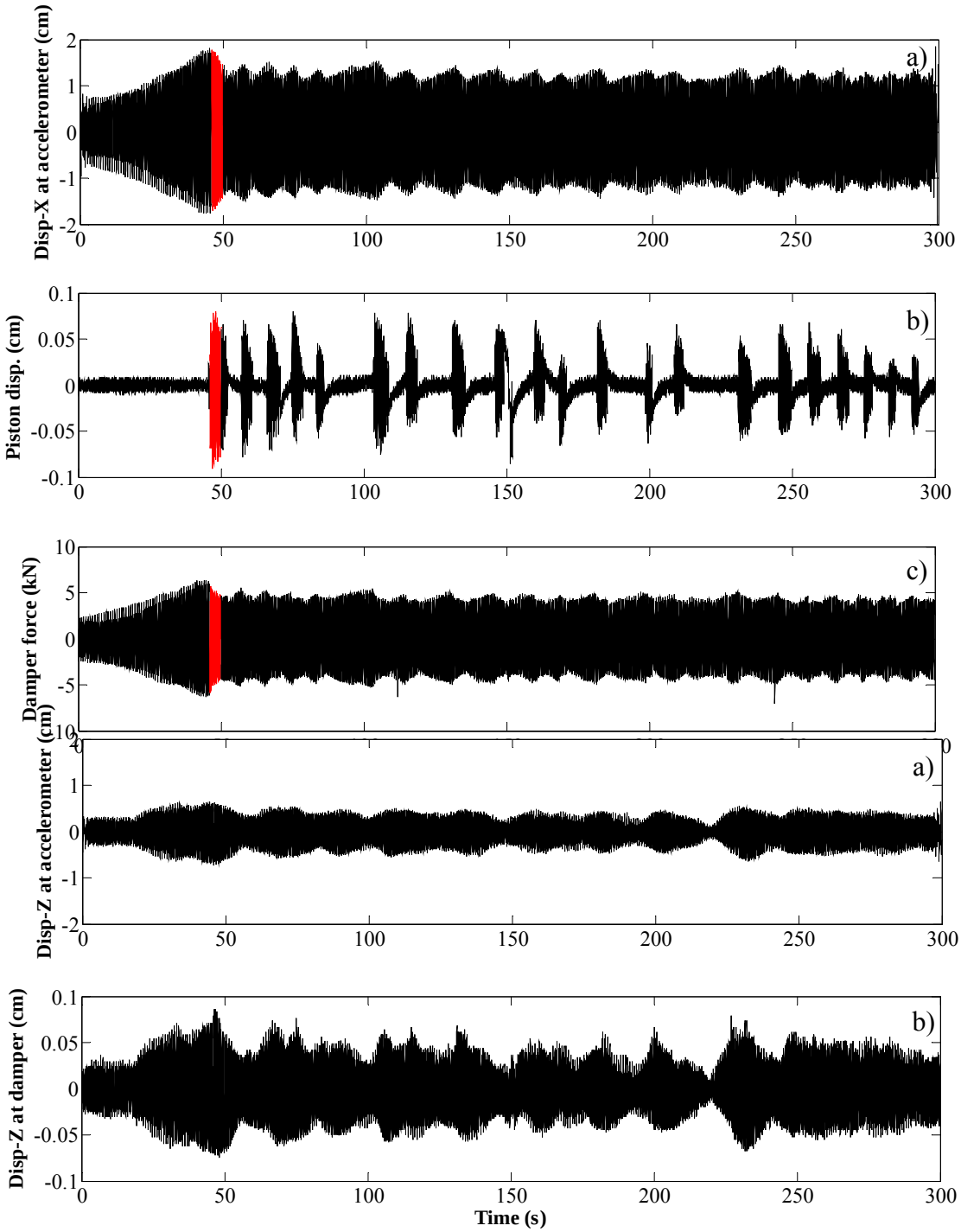

Figure 6.14 Lateral vibrations of stay AS16 in an example record

Figure 6.15 a) Figure 6.15 b) plot the damper force against the displacement and velocity of the damper, respectively, for the period of time between the 46th and the 50th second, during which the damper was engaged. The velocity of the damper piston is estimated by numerical differentiation of the measured displacement. For comparison purposes, the force-displacement and force-velocity relationships for the designed ideal viscous damper are also included in the figures. These figures confirmed the existence of the

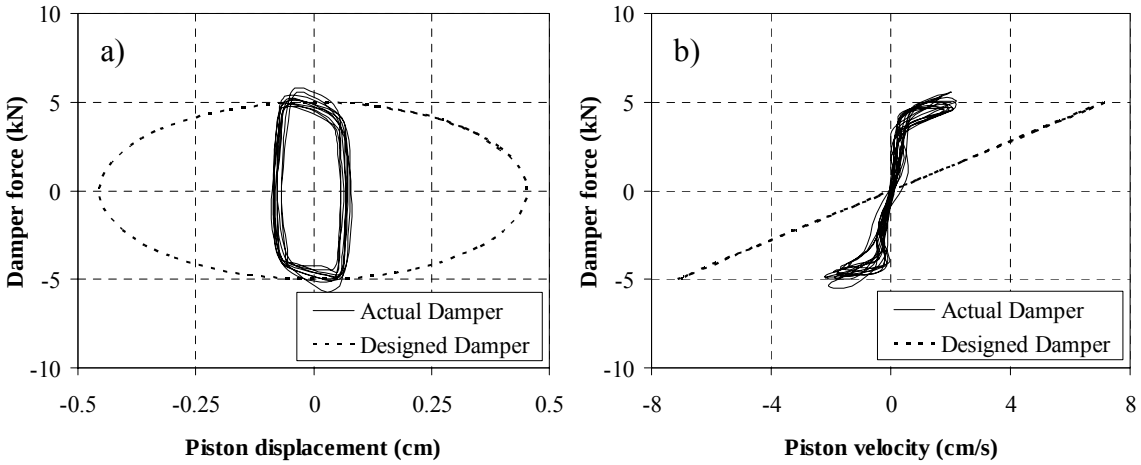

Figure 6.15 Damper force vs. a) piston displacement and b) piston velocity

static friction threshold of the damper at about 4 kN for the vibration at 2.55 Hz. Below this threshold, the damper essentially behaved like a friction damper. Figure 6.15 a) also suggested that, due to the static friction, the energy dissipation capacity of the damper, which is represented by the area enclosed by the force-displacement hysteresis loop, is significantly less than its designed capacity.

For an ideal viscous damper with coefficient c, the energy dissipated in one cycle of harmonic vibration driven by a force $f(t) = f_0 \sin(\omega t)$ can be expressed as

$$E_D = \int f_D du = \int_0^{2\pi/\omega} (c\dot{u})\dot{u}dt = \int_0^{2\pi/\omega} c\dot{u}^2 dt = c\int_0^{2\pi/\omega} (\frac{f_0 \sin \omega t}{c})^2 = \frac{\pi f_0^2}{c\omega} \qquad (6.3)$$

This expression suggests that, for the magnitude of damper force shown in Figure 6.15, the amount of energy the designed ideal viscous damper can dissipate in one cycle is about 0.072 kN·m. For the actual damper attached to stay AS16, however, the amount of energy dissipated in this same cycle of vibration is only about 0.014 kN·m. Using the energy-loss-per-cycle method, this amount of energy dissipated in one cycle of vibration is estimated to be an equivalent viscous damping ratio of 0.86 percent for the second mode of stay AS16, which is less than half of the value expected by design, as suggested in Table 6.3.

To verify the existence of static friction threshold in the Type I WDP damper, the damper installed on stay D14 on the Veterans Memorial Bridge has been brought in to the Johns Hopkins University and tested in the structures laboratory. During the tests, the damper was driven by a sinusoidal force and the displacement response of the piston was recorded. Figure 6.16 a) and Figure 6.16 b) show the damper force against the displacement and the velocity of the damper, respectively, for an example test. In this test, the damper is driven by a sinusoidal force at 2.5 Hz. It can be seen in Figure 6.16 that, at this particular frequency, the damper has a static friction threshold of about 4 kN.

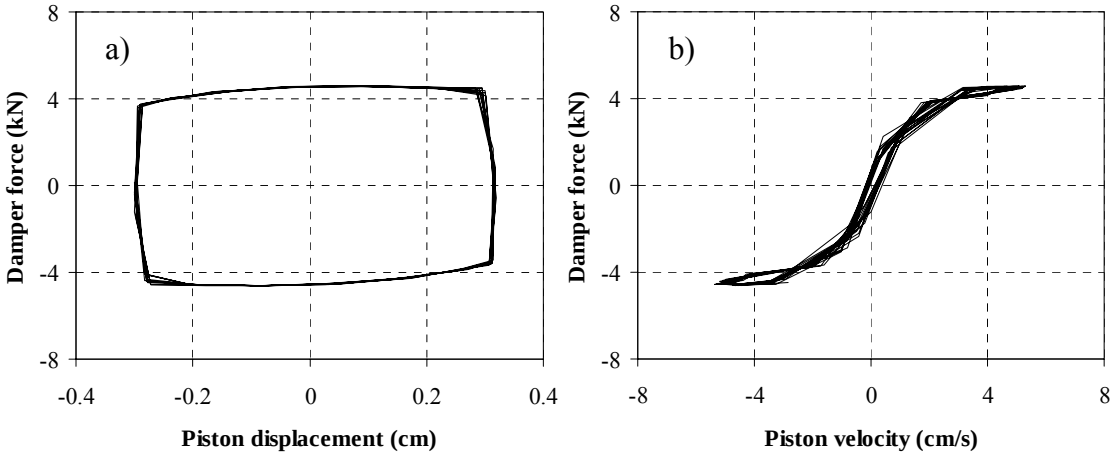

Figure 6.16 Damper force vs. a) piston displacement and b) piston velocity for an example experimental damper test

The discovery of the friction threshold in the Type I WDP dampers has inspired the analytical study of the vibration of stay cables with various types of dampers such as the damping effects of a linear viscous damper with static friction threshold and that of particular types of nonlinear dampers. Based on this analytical study, models for the design of these types of dampers have been proposed. The results of the analytical study have been presented in a number of publications (e.g., Main and Jones 2002a; Main and Jones 2002b), which are included in the literature package that accompanies this report.

In addition to revealing the static friction in the Type I WDP dampers, the full-scale measurement data also suggest that these dampers oriented in the in-plane direction of the stay cables have usually been able to suppress the wind- and rain-wind-induced vibrations that are highly two dimensional. Figure 6.17 shows the anti-nodal displacement amplitude in the in-plane direction against that in the lateral direction for vibrations of stay AS16 after the damper was installed. Again, only records with displacement amplitude greater than five percent of the cable diameter are included in this figure. This figure suggests that, with the damper attached in the in-plane direction, the amplitude of the vibration has in most cases been kept at a very low level in both planes of the cable. This special performance of the damper can also be interpreted by the fact that wind- and rain-wind-induced vibrations are aeroelastic in nature, and that suppressing the vibration component in one direction can usually disrupt the entire excitation mechanism and suppress the vibration in the other direction.

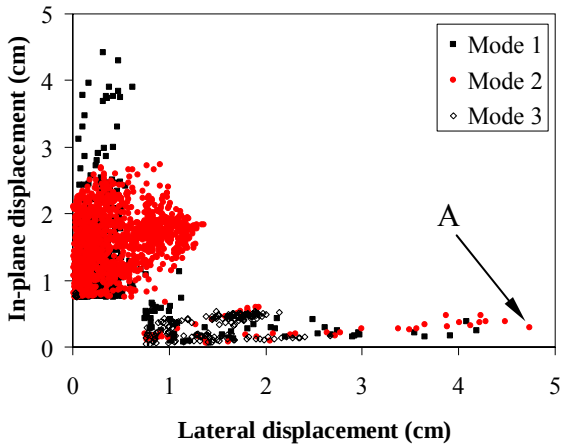

Figure 6.17 In-plane vs. lateral displacement amplitude for stay AS16 with damper

Special attention, however, has been devoted to record A and its adjacent ones in Figure 6.17, which have significant vibration component in the lateral direction but very small component in the in-plane direction. Measurement data suggest that such vibrations correspond to rain-wind-induced vibrations that occur when wind direction is almost parallel to the projection of the cable axis in the horizontal plane, i.e., when the attack angle β is close to 0° or 180°. This fact is apparent in Figure 6.18, which shows the ratio between the displacement amplitude in the in-plane direction and that in the lateral direction against the attack angle β for the vibrations shown in Figure 6.17. These observed significant-amplitude lateral vibrations suggest that the damper oriented in the in-plane direction is ineffective in mitigating vibrations induced by a mechanism primarily in the lateral direction. Such lateral stay cable vibrations did not occur often on the Fred Hartman Bridge or the Veterans Memorial Bridge, because the simultaneous occurrence of rain and wind approaching in directions close to the bridge axis were not observed often. For stay cables that are located in an environment where such wind and rain conditions occur frequently, however, lateral vibrations can potential occur often and the ineffectiveness of the damper in this direction can be a concern. In addition, as suggested in Chapter 6, the oscillation of the bridge deck can also induced large-amplitude stay cable vibrations with significant lateral component. In this case, a damper oriented in the in-plane direction will also be ineffective.

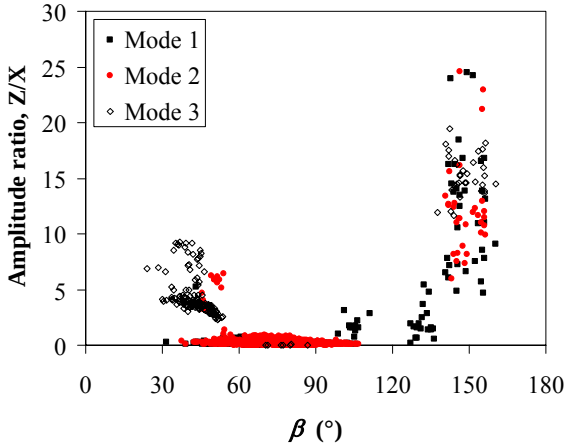

Figure 6.18 Ratio between in-plane and lateral amplitude vs. attack angle

6.1.3 Performance of Compact WDP Damper

A compact WDP damper has been attached to stay B13 on the Veterans memorial Bridge since August 1999. Full-scale measurement data suggest that this compact damper has been essentially ineffective in mitigating stay cable vibrations. This can be seen in Figure 6.19, which shows the timeline of the significant vibrations of stay B13 recorded from January 22, 1999 to October 25, 2003, except the periods of time when the accelerometer on this cable was not functioning (inactive). The data shown in the figure represent modal vibrations with anti-nodal amplitude greater than five percent of the cable diameter. The periods of time during which the accelerometer was inactive are indicated by the range marked with gray lines. It is evident that stay B13 frequently exhibited large amplitude vibrations even with the compact damper attached.

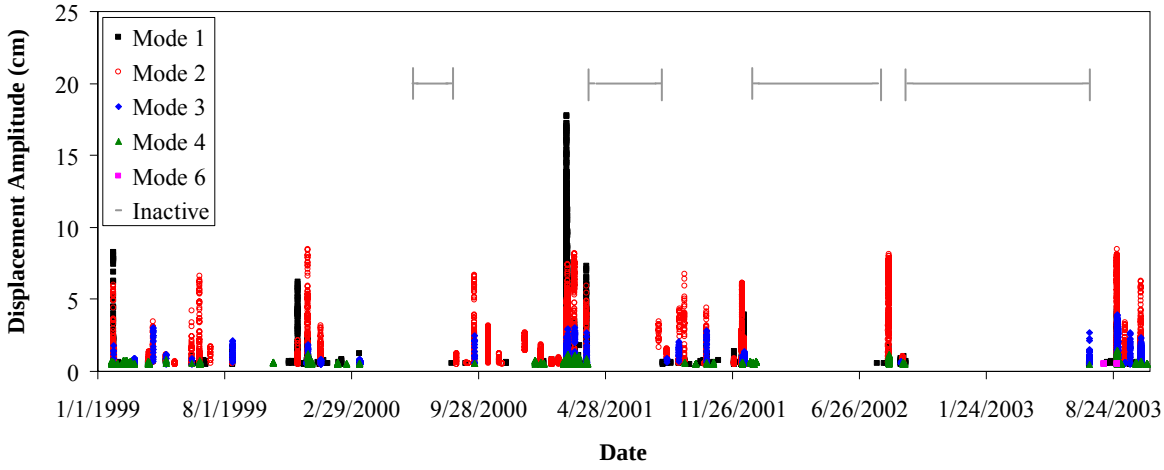

Figure 6.19 Modal vibration timeline of stay B13

6.1.4 Performance of Type II WDP Damper

During the later stage of the filed investigation project, Type II WDP dampers were installed on all the stays on the Veterans Memorial Bridge and all the stays except the first two of each stay plane on the side spans of Fred Hartman Bridge (i.e., the stays numbered one and two; for example, stays AS1, AS2, AN1, AN2, and so on). Installation of the Type II WDP dampers on the two bridges took place during the months of April to June of 2004, and all dampers were functional after the first week of June, 2004. Figure 6.20 shows the Type II WDP damper installed on stay AS24 on the Fred Hartman Bridge.

Figure 6.20 Type II WDP damper installed on stay AS24

While details of the Type II WDP dampers are not available to the authors at the present time, full-scale measurement data do suggest that these dampers have been mostly effective in suppressing wind and rain-wind-induced vibrations of the cables under monitoring. For example, no vibration with amplitude greater than five percent of the cable diameter has been recorded on stays B9, B11 and C13 on the Veterans memorial bridge during the period of time from June, 2004 to September 2005, when these stays were mitigated by Type II WDP dampers.

Full scale measurement data also suggest, however, that the Type II WDP dampers might not be able to suppress vibrations primarily in the lateral direction of the stay cables. As an example, Figure 6.21 displays the fourteen-second mean modal in-plane amplitude against the corresponding lateral amplitude of significant vibrations of stay AS22 recorded during the period between June, 2004 and September, 2005. During this time, stay AS22 was mitigated by both cross-ties and a Type II WDP damper. As a result, very few occurrences of significant-amplitude vibration, except those shown in Figure 6.21 have been observed. The data shown in Figure 6.21 represents vibrations recorded during three individual events. The vibrations in the first mode was likely due to the excitation from the oscillation of the bridge deck (records 2004112392 to 2004222393), as the other stays instrumented all had an oscillation component at frequencies close to that of the first mode of stay AS22, which is also close to the first torsional mode of the bridge deck, at the same time. This is a strong indication of deck-induced vibrations according to discussions in Chapter 5. The most direct evidence of deck-stay interaction, however, does not exist, since no accelerometer was available to record the oscillation of the decks during this event. If the vibration in the first mode of stay AS22 was indeed induced by deck oscillation, Figure 6.21 indicates that the combination of the Type II WDP damper and the cross-ties has been effective in suppressing such vibrations, as the amplitude of the vibrations were successfully kept at a moderate level.

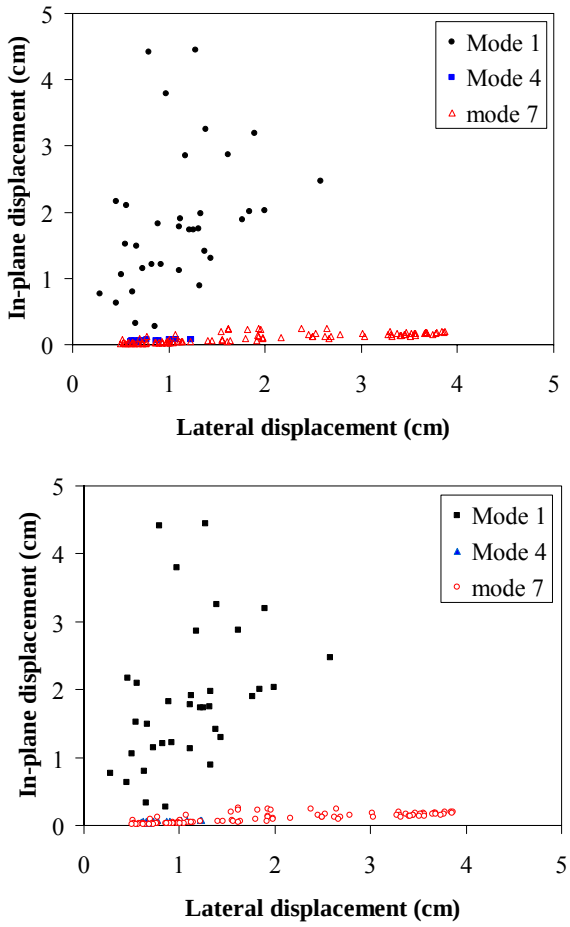

Figure 6.21 Amplitude of significant vibrations of stay AS22 with attached Type II WDP damper

On the other hand, the vibrations in the fourth and seventh modes shown in Figure 6.21 are recorded in two other separate events (records 2005011311-2005011312 and 2005022415-2004022416). The fact that the stay has exhibited significant lateral vibration amplitude in a higher local mode such as the seventh mode of stay AS22 suggests that neither the cross-ties, nor the Type II WDP dampers were able to suppress vibrations of the stay cable occurring primarily in the lateral direction. This observed performance of the Type II dampers confirms again the ineffectiveness of dampers installed in the in-plane direction of the stay cables in mitigating vibrations occurring in the out-of-plane direction.

6.1.5 Performance of Freyssinet Damper

Freyssinet dampers were installed on stays AS24 and BS16 on the Fred Hartman Bridge. This type of damper uses a pressurized bladder filled with viscous oil around the stay to limit vibratory motion. The bladder reacts against a collar attached to the guide pipe. The bladder pressure and other properties are adjusted to match individual stay characteristics. Figure 6.22 shows the Freyssinet damper installed on stay AS24.

Figure 6.22 Freyssinet damper installed on stay AS24

Full-scale measurement data reveal that the effectiveness of the Freyssinet dampers in mitigating stay cable vibrations was limited. Figure 6.23 a) and Figure 6.23 b) show the fourteen-second mean displacement amplitude of the most dominant mode against wind speed for the vibrations of stay AS24 before and after the Freyssinet was installed, respectively. Figure 6.23 a) represents vibrations recorded from October 3, 1997 to October 2, 1998, and Figure 6.23 b) represents data recorded from March 6, 1999 to December 18, 2001.

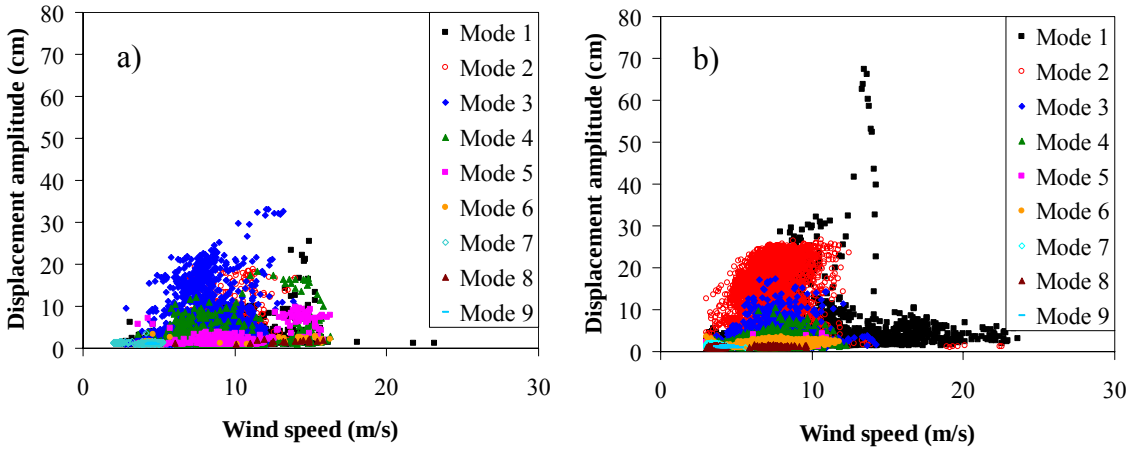

Figure 6.23 Displacement amplitude vs. wind speed for stay AS24 a) before and b) after damper installation

Similarly, Figure 6.24 a) and Figure 6.24 b) present the fourteen-second mean displacement amplitude of the dominant mode against wind speed for the vibrations of stay BS16 before and after the Freyssinet damper was installed, respectively. Figure 6.24 a)

represents vibrations recorded from October 3, 1997 to December 10, 1997, and Figure 6.23 b) represents data recorded during the time periods of November 18 to March 22, 2000 and from December 27, 2000 to June 5 2001, when the full-scale system was successfully monitoring the restrained vibrations of stay BS16. It can be seen that the Freyssinet damper was not effective in suppressing the vibration during the 10 months of observation.

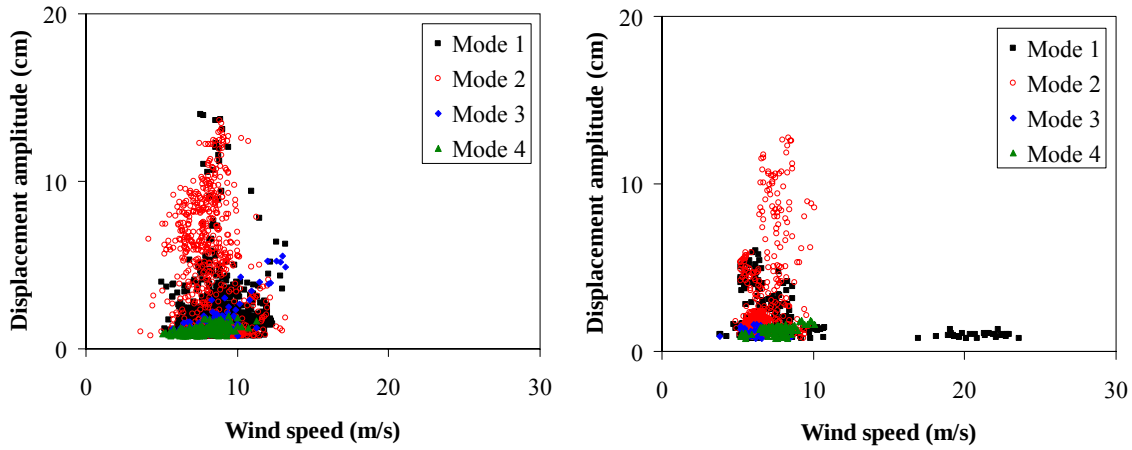

Figure 6.24 Displacement amplitude vs. wind speed for stay AS24 a) before and b) after damper installation

Full-scale measurement data also indicate that the effectiveness of the Freyssinet dampers might have deteriorated with time. As an example, Figure 6.25 shows the timeline of the large-amplitude vibrations recorded after the Freyssinet damper was installed on stay AS24. It appears that large-amplitude vibrations occurred much more frequently during the

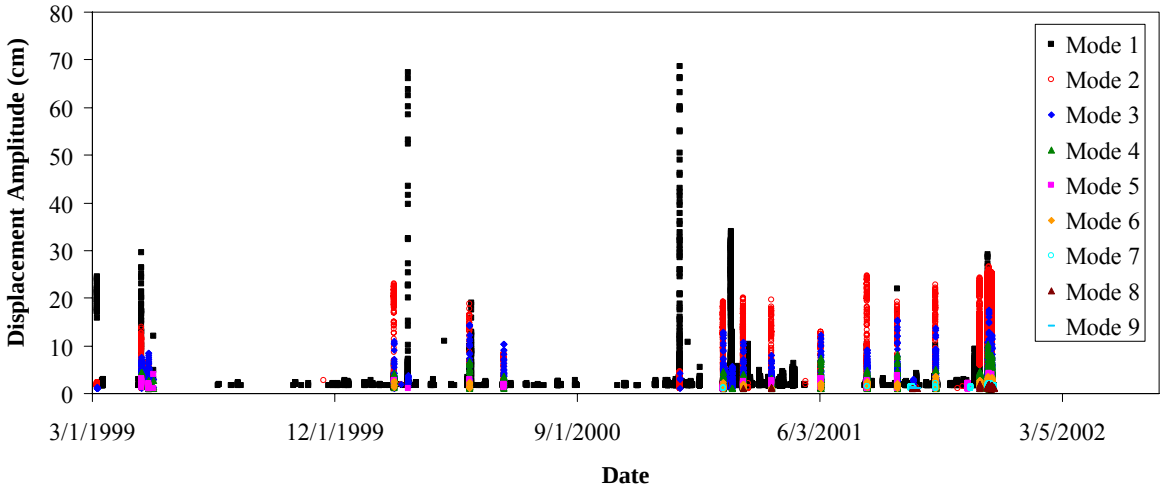

Figure 6.25 Performance timeline of Freyssinet damper on stay AS24

later phase of the monitoring period than during the earlier phase of the monitoring period. It has to be noted that more events of large-amplitude vibrations are included in Figure 6.25 than in Figure 6.24 (b). This is because that for some observed vibrations, there is no

corresponding wind measurement available and that, as a result, these vibrations cannot be included in Figure 6.24 (b), but they can be included in Figure 6.25.

6.2 Performance of Cross-ties

In addition to the viscous dampers, cross-ties are also used on the Fred Hartman Bridge to mitigate stay cable vibrations. Figure 6.26 displays a picture of several cable networks formed with cross-ties.

Figure 6.26 Cable networks formed with cross-ties

Full-scale measurement data suggest that these cross-ties have in most cases been effective in suppressing wind- and rain-wind-induced stay cable vibrations. Figure 6.27 a) and Figure 6.27 b) show the thirty-second root mean square (RMS) displacement amplitude in the in-plane direction vs. that in the lateral direction for the vibrations of stay AS5 before and after being mitigated by cross-ties, respectively. The data presented in Figure 6.27 a) were recorded during the time from October 3, 1997 to December 10, 1997, and the data presented in Figure 6.27 b) were recorded during two periods of time: one from April 23, 1999 to June 5, 2001 and the other from July 25, 2002 to December 12, 2002. The RMS amplitude referred to herein is computed based on the displacement of the cable at the location of the accelerometer and only records with RMS amplitude (either in the in-plane direction or in the lateral direction) larger than three percent of the cable diameter are included in the figures. The RMS amplitude is used herein instead of the anti-nodal modal amplitude because after being interconnected with adjacent stays, the vibration of a cable can be composed of both local cable modes and global modes of the cable network (Caracoglia and Jones 2005a). According to these graphs, when being mitigated with cross-ties, stay AS5 very seldom exhibited significant amplitude vibrations

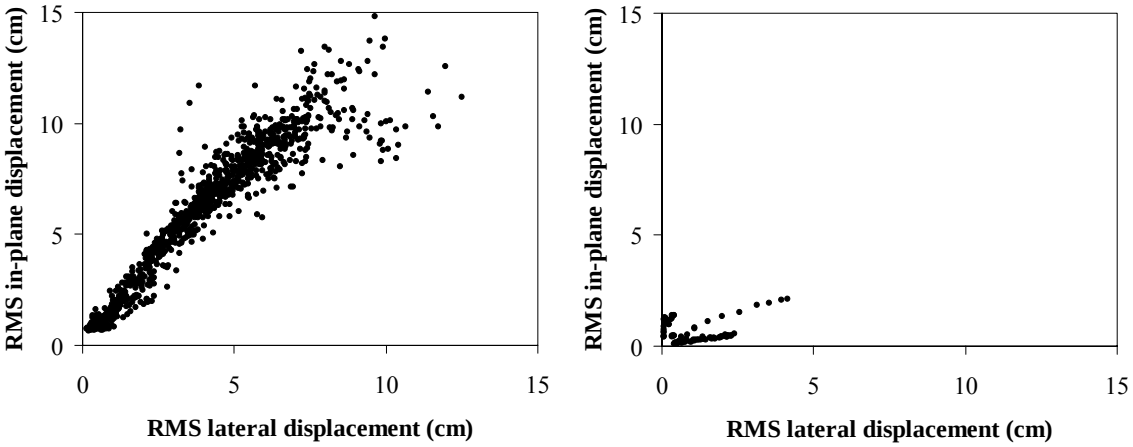

Figure 6.27 RMS displacement amplitude of stay AS5 a) before and b) after installation of cross-ties

Figure 6.27 b) also suggests, however, that although in-plane and highly two-dimensional large-amplitude vibrations did not occur after the installation of the cross-ties, stay AS5 did exhibit moderate-amplitude vibrations that are primarily in the lateral direction during this period of time. While the occasions of such lateral vibration are very few for stay AS5, for some other stays mitigated with cross-ties, this type of vibration occurred more frequently. Figure 6.28 shows the RMS displacement amplitude of the vibration in the in-plane direction against that in the lateral direction for stay AS20 after the cross-ties were installed (during the time from April 23, 1999 to December 12, 2002). Two clusters are present in this figure: cluster A which is primarily in the in-plane direction and cluster B that is mainly in the lateral direction. Analysis of individual records in these two clusters reveals that cluster A represents the vibrations of stay AS20 in the global modes of the bridge, which

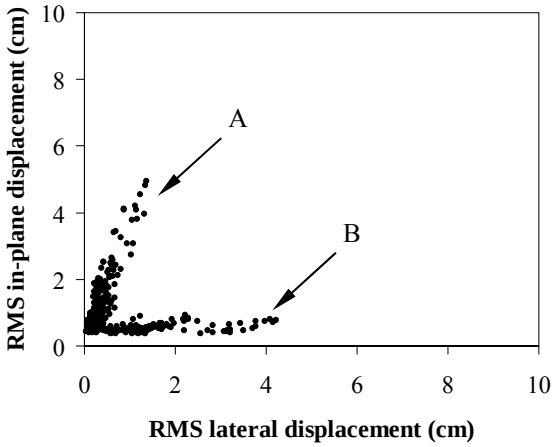

Figure 6.28 RMS displacement amplitude of stay AS20 after installation of cross-ties

are induced by oscillations of the deck in its lower vertical modes, and that cluster B represents rain-wind-induced vibrations associated with wind approaching in a direction very close to the projection of the cable axis in the horizontal plane. In fact, the vibrations in cluster B occurred at the same time when stay AS16 with attached damper exhibited

significant-amplitude lateral vibrations. The vibrations in cluster A is not a concern since in these cases the cable was simply moving with the deck and large stresses were not generated. The existence of the lateral vibrations in cluster B, however, suggests that the effectiveness of cross-ties in mitigating stay cable vibrations in the lateral direction is limited.

Figure 6.29 shows the displacement time histories and the corresponding spectrograms of an example record (2001100520) for stay AS20 after it was interconnected with adjacent stays. While the low-amplitude in-plane component of the vibration is very noisy due to the effect of the cross-ties, the lateral component has exhibited quite clear frequency characteristics of the cable without being restrained. This fact is evidence that the cross-ties are a mitigating mechanism only effective in the in-plane direction.

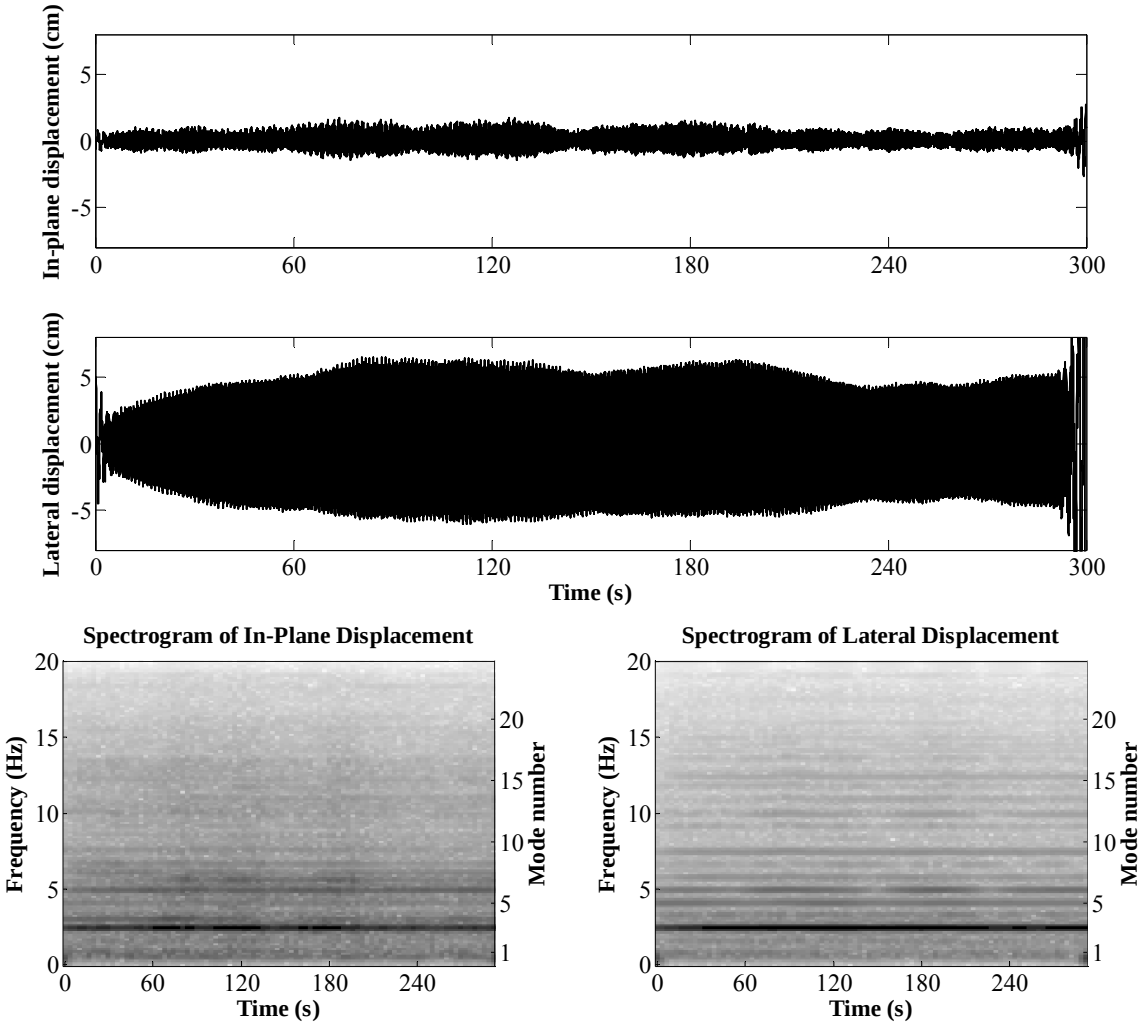

Figure 6.29 Response of stay AS20 in an example record after installation of cross-ties

In addition to revealing the inherent ineffectiveness of the cross-ties in the lateral direction, measurement data also suggests that the performance of cross-ties in the in-plane direction can also be significantly degenerated by imperfect design. In particular, stay AN24 on the Fred Hartman Bridge has frequently exhibited large-amplitude vibrations in several of its local modes after being interconnected with adjacent stays. Figure 6.30 shows the in-plane and lateral displacement amplitudes of stay AN24 in its fourth and eighth modes after the

cross-ties were installed (specifically, from April 23, 1999 to December 12 2002). For this stay, the cross-ties have been essentially ineffective in both directions in suppressing the vibrations in these two particular modes. This ineffectiveness of the cross-ties is believed to be due to the fact they are tied to the cable at locations very close to the nodal points of the fourth mode. While this particular problem with the crossties installed on stay AN24 can be fixed by relocating the connection points between the cables and crossties, it does demonstrate that the design of countermeasures should be based on good understanding of the vibrations themselves. Specifically, in the case of the design of cross-ties, the modes of the stay cables susceptible to large-amplitude vibrations should be identified and the cross-ties should be installed at locations adequately far away from the nodal points of these modes.

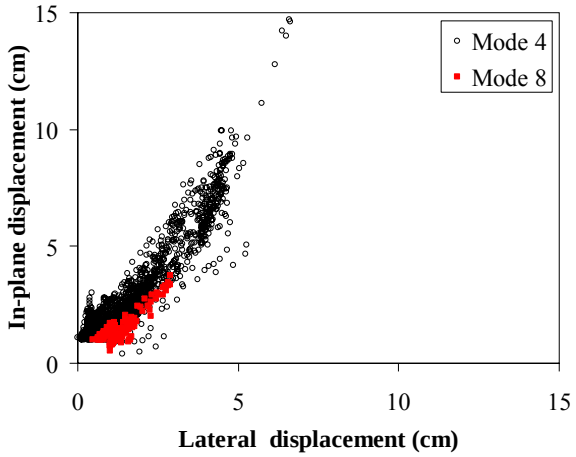

Figure 6.30 In-plane displacement amplitude vs. lateral displacement amplitude for stay AN24 after cross-tie installation

Furthermore, the observations in the field also revealed that the integrity of the cross-tie systems is very sensitive to the vibrations of stay cables. Figure 6.31 shows an example of a cross-tie being dislodged from its saddle due to the vibration of the stay cables. Incidents like this can significantly affect the performance of the crossties and potentially lead to damage to the secondary cables and the saddles.

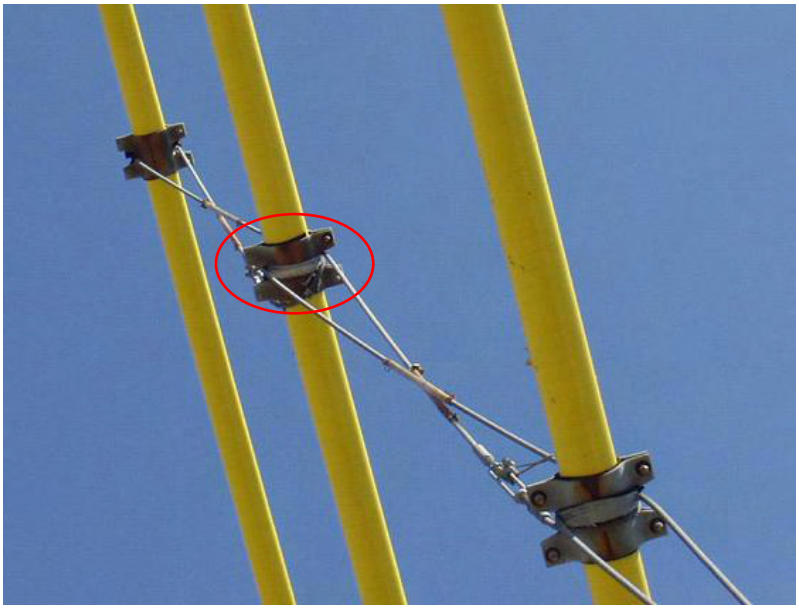

Figure 6.31 Dislocated cross-tie

Due to these problems with cross-ties, and the fact that they are considered by some people to be a distraction to the beauty of cable-stayed bridges, the usage of cross-ties alone do not appear to be an appealing solution for mitigating wind- and rain-wind-induced stay cable vibrations.

As in the case of dampers performance evaluation, the observations in the field have inspired the analytical study of the dynamic behavior of cable networks. The results of the study have been published in academic journals (e.g.,Caracoglia and Jones 2005a;Caracoglia and Jones 2005b) and have been included in the literature package that accompanies this report.

6.3 Insights Gained from Observed Performance of Mitigation Devices

A significant accomplishment of the field investigation project is the insights gained from evaluation of the mitigation devices. These insights can be philosophically summarized into two categories:

First, good understanding of the mechanisms of the physical phenomenon is essential for the rational design of mitigation countermeasures. This has been illustrated by the following example observations on the Fred Hartman Bridge and the Veterans Memorial Bridge:

- The WDP dampers were optimized for the vibrations in the first modes of the individual cables. Full-scale measurement data suggest, however, that most wind- and rain-wind-induced stay cable vibrations are reduced velocity dependent, and that for some stays, large-amplitude vibrations occur much more often in the modes other than the first. This fact suggests that, the design of the dampers could have been more effective if the prevalent modes of vibration had been identified in advance.
- Both the dampers and the cross-ties installed on the bridges are mechanisms that are effective only in the in-plane direction of the cables. Full-scale measurement

data suggest, however, that the major direction of wind- and rain-wind-induced stay cables is closely related to the direction of the approaching wind and that, under some wind conditions, the vibration can be primarily in the lateral direction. The designed of the mitigation devices, therefore, can be improved if the vibration in the lateral direction is considered.

Second, good understanding of the physical mechanics of the mitigation devices is also essential for rational design. This has been demonstrated in the observed performance of both the dampers and the cross-ties:

- The static friction of in the Type I WDP dampers was neglected in the design. Full-scale measurement data suggest, however, that this static friction is essential for the performance of the dampers and has to be considered in the design of such mechanical devices.
- On the Fred Hartman Bridge, the cross-ties on stay AN24 were installed at locations close enough to the nodal point of the fourth mode of the cable, which has resulted in the failure of the restrainers in suppressing the vibrations in the fourth and the eighth modes. This could have been avoided if the dynamics of cable networks had been better understood.

7 Summary and Conclusions

Through eight years of full-scale measurement on the Fred Hartman Bridge in Houston, Texas and the Veterans Memorial Bridge in Port Arthur, Texas, the goals and objectives of the field investigation project have been successfully achieved.

Robust full-scale measurement have been developed for the monitoring of both bridges and through effective maintenance, the systems have continued functioning and collected two baseline sets of data required for the study of the characteristics and mechanisms of wind- and rain-wind-induced vibrations, and for the evaluation of the mitigation devices in suppressing the vibrations.

One data set consists of the vibrations recorded with the stays unrestrained, and the corresponding conditions of wind and rain. Analysis of these vibrations has enabled successful classification and categorization of wind- and rain-wind-induced stay cable vibrations. The characteristics of Kármán-vortex-induced vibrations, rain-wind-induced vibrations, a type of large-amplitude dry cable vibration, deck-induced vibrations and an uncategorized type of vibration have been identified. Investigation of these characteristics and their correlation with wind and rain has shed light onto the mechanisms of these individual types of vibrations. In particular, it is revealed that the frequently occurring rain-wind-induced vibrations share similar characteristics with both Kármán-vortex-induced vibrations and the type of large-amplitude dry cable vibration. This suggests that the so-called rain-wind-induced vibrations might be an aeroelastic instability that exists inherently for yawed and inclined stay cables and that the role of rainfall is to promote or enhance this instability.

The other data set are composed of the vibrations recorded with the stay cables restrained. Comparison of this data set with the vibrations occurred before the restrainers were installed have enabled successful assessment of the mitigation devices. In particular, full-scale measurement data suggest that both the WDP dampers and the cross-ties have in general been effective in mitigating wind- and rain-wind-induced stay cable vibrations. At the same time, it has been revealed that the effectiveness of the Freyssinet dampers is limited in suppressing the vibrations. Furthermore, investigation of the performance of both the dampers and cross-ties suggest that good understanding of both the mechanism of the vibrations and the mechanics of the mitigation countermeasures is essential for rational design of such devices. The static friction is identified to be an important factor that affects the performance of viscous dampers. Also, it is suggested that the nature of the vibrations, such as the dominant modes and relationship between the direction of wind and the vibration direction has to be considered in the design of mitigation devices.

The understanding from the field investigation project can be of great value for future investigations. The characteristics of the vibrations observed in the field can be used both to assist the design of wind tunnel tests and to validate the results from these tests. The understanding of the mechanisms of the vibrations will be crucial for the development of analytical models. And, last but not least, the insights gained in the field will greatly benefit the design of mitigation strategies for wind- and rain-wind-induced stay cable vibrations.

Appendix A Major Publications

A.1 Ph. D. Dissertations

1. Main, J. A. (2002). "Modeling the vibrations of stay cable with attached damper," Ph. D. Dissertation, Johns Hopkins University, Baltimore, Maryland.
2. Ozkan, E. (2003). "Evaluation of response prediction methodology for long-span bridges using full-scale measurements," Ph. D. Dissertation, Johns Hopkins University, Baltimore, Maryland.
3. Zuo, D. (2005). "Understanding wind- and rain-wind-induced stay cable vibrations," Ph. D. Dissertation, Johns Hopkins University, Baltimore, Maryland.

A.2 Journal Papers

1. Caracoglia, L., and Jones, N. P. (2005a). "In-plane dynamic behavior of cable networks. Part 1: formulation and basic solutions." *Journal of Sound and Vibration*, 279(3-5), 969-991.
2. Caracoglia, L., and N.P.Jones. (2005b). "In-plane Dynamic behavior of cable networks. Part 2: Prototype prediction and validation." *Journal of Sound and Vibration*, 279(3-5), 993-1014.
3. Main, J.A., and Jones, N.P. (2002a). "Free vibrations of taut cable with attached damper. I. Linear viscous damper." *Journal of Engineering Mechanics*, 128(10), 1062-1071.
4. Main, J.A. and Jones, N.P. (2002b). "Free vibrations of taut cable with attached damper. II. Nonlinear damper." *Journal of Engineering Mechanics*, 128(10), 1072-1081.
5. Main, J.A. and Jones, N.P. (2001). "Evaluation of Viscous Dampers for Stay-Cable Vibration Mitigation." *Journal of Bridge Engineering*, 6(6), 385-397.
6. Jones, N. P., Raggett, J. D., and Ozkan, E. (2003). "Prediction of cable-supported bridge response to wind: coupled flutter assessment during retrofit." *Journal of Wind Engineering and Industrial Aerodynamics*, 91(12-15), 1445-1464.
7. Zuo, D., Jones, N. P., and Main, J. A. "Vortex- and rain-wind-induced stay cable vibrations in a three-dimensional environment." *Journal of Wind Engineering and Industrial Aerodynamics*, Accepted for Publication (2005).

A.3 Conference Proceedings

1. Caracoglia, L., and Jones, N.P. "Design of mitigation devices for stay-cable vibration", *6th International Symposium on Cable Dynamics*, Charleston, SC (USA.), 19-22 September 2005, AIM (Association of Engineers from the Montefiore Electrical Institute), Liège, Belgium
2. Caracoglia, L., and Jones, N.P. "Selection of an optimized cable network system configuration", *17th Engineering Mechanics Division Conference of the American Society of Civil Engineers*, University of Delaware, Newark, DE, June, 2004, CD-ROM.
3. Caracoglia, L., and Jones, N.P. "Dynamics of stay-cable systems and cross-tied networks", *5th International Symposium on Cable Dynamics*, Santa Margherita Ligure, Italy, September, 2003, AIM (Association of Engineers from the Montefiore Electrical Institute), Liège, Belgium, pp. 437-444.

4. Caracoglia, L., and Jones, N.P. "Dynamics of crossties with discrete dampers", *16th Engineering Mechanics Division Conference of the American Society of Civil Engineers*, Seattle, WA, July, 2003, CD-ROM.
5. Caracoglia, L., and Jones, N.P. "Understanding the mitigation of oscillation of stays through cross ties", *IMAC-XXI International Conference and Exposition on Structural Dynamics, Society for Experimental Mechanics (SEM)*, Kissimmee, FL, February, 2003, CD-ROM.
6. Caracoglia, L., and Jones, N.P. "Mitigation of wind-induced oscillation of stay cables with cross ties", *3rd US-Japan Workshop on Wind Engineering, UJNR Panel on Wind and Seismic Effects (Task Committee D)*, Seattle, WA, October, 2002, Department of Aerospace Engineering and Engineering Mechanics, Iowa State University, pp. 75-84.
7. Caracoglia, L., and Jones, N.P. "Analytical method for the dynamic analysis of complex cable structures", *15th Engineering Mechanics Division Conference of the American Society of Civil Engineers*, New York, NY, June, 2002, CD-ROM
8. Jones, N.P., Porterfield, M.L., and Main, J.A. (1997). "Measurements for mitigation of stay-cable vibration." Proc. 8th US National Conference on Wind Engineering, Baltimore, MD, June, 1997, CD-ROM.
9. Liu, M.Y., Zuo, D., and Jones, N.P. "Deck-induced stay cable vibrations: Field observations and analytical model." 6th International Symposium on Cable Dynamics, September, 2005, Charleston, South Carolina, USA.
10. Main, J.A. and Jones, N.P. (2004). "Combined effects of flexural stiffness and axial tension on damper effectiveness in slender structures." *Proc., 17th ASCE Eng. Mech. Conf.,* University of Delaware, Newark, DE, CD-ROM.
11. Main, J.A. and Jones, N.P. (2003). "Influence of rubber bushings on stay-cable damper effectiveness." *Proc., 5th Int. Symp. On Cable Dynamics*, 445-452.
12. Main, J.A. and Jones, N.P. (2002). "Analytical investigation of the performance of a damper with a friction threshold for stay-cable vibration suppression." *Proc., 15th ASCE Eng. Mech. Conf.,* Columbia University, New York, NY, CD-ROM.
13. Main, J.A. and Jones, N.P. (2001). "Analysis and design of linear and nonlinear dampers for stay cables." Proc., 4th Int. Symp. on Cable Dynamics, 309-316.
14. Main, J.A., Jones, N.P., and Yamaguchi, H. (2001). "Characterization of rain-wind-induced stay-cable vibrations from full-scale measurements." Proc., 4th Int. Symp. on Cable Dynamics, 235-242.
15. Main, J.A. and Jones, N.P. (2001). "Measurement and mitigation of stay-cable vibration." Proc. 5th Asia-Pacific Conf. on Wind Eng., Japan Assoc. for Wind Eng., JWE No. 89, Kyoto, Japan, 557-560.
16. Main, J.A. and Jones, N.P. (2000). "A comparison of full-scale measurements of stay cable vibration." Proc. 15th Structures Congress, ASCE, New York, CD-ROM.
17. Main, J.A. and Jones, N.P. (1999). "Full-scale measurements of stay cable vibration." Proc. 10th Int. Conf. on Wind Eng., Balkema, Rotterdam, The Netherlands, 963-970.
18. Main, J.A. and Jones, N.P. (1998). "Stay cable vibration measurements, mechanisms and mitigation." Proc. 12th ASCE Eng. Mech. Conf., La Jolla, CA, May, 1998.
19. Mashnad, M., Ozkan, E. and Jones N.P. "Observations of vortex-induced vibrations on a cable-stayed bridge", *10th Americas Con-ference on Wind Engineering*, June, 2005, Baton Rouge, Louisiana, USA, CD-ROM.

20. Ozkan, E. and Jones, N.P. “Evaluation of response prediction methodology for long-span bridges under full-scale measurements”, *11th International Conference on Wind Engineering*, June, 2003, Lubbock, Texas, USA
21. Ozkan, E. and Jones, N.P. “Multi-mode buffeting analysis of a twin-deck cable-stayed bridge”, *Response of Structures to Extreme Loading Conference*, 2003, Toronto, Canada.
22. Ozkan, E., Main, J.A., and Jones, N.P. (2001). “Long-term measurements on a cable-stayed bridge.”, Proc., IMAC-XIX Conf., Kissimmee, FL, CD-ROM.
23. Ozkan, E., Main, J.A., and Jones, N.P. (2001). “Full-scale measurements on a cable-stayed bridge”, Proc. 5th Asia-Pacific Conf. on Wind Eng., Japan Assoc. for Wind Eng., JWE No. 89, Kyoto, Japan, 553-556.
24. Ozkan, E., Main, J.A., and Jones, N.P. (2001) “Investigation of cable-deck interaction using full-scale measurements on a cable-stayed bridge”, Proc., 1st Americas Conf. on Wind Eng., Clemson SC, CD-ROM.
25. Ozkan,E. and Jones, N.P. “Predicted and measured response of a cable-stayed bridge”, *ASCE Structures Congress*, 2000, Denver CO., USA
26. Zuo, D., and Jones, N.P. "Large-amplitude dry cable vibrations and their implication on rain-wind-induced vibrations." *6th European Conference on Structural Dynamics*, September, 2005, Paris, France.
27. Zuo, D., and Jones, N.P. "The Mechanism of Rain-Wind-Induced Vibration: Vortex-shedding or Galloping." *10th Americas Conference on Wind Engineering*, June, 2005, Baton Rouge, Louisiana, USA, CD-ROM.
28. Zuo, D., Jones, N.P., and Main, J. A. "Vortex- and rain-wind-induced stay cable vibrations in a three-dimensional environment." 5th International Colloquium on Bluff Body Aerodynamics and Applications, July, 2004, Ottawa, Canada, 397-400.
29. Zuo, D., and Jones, N.P. "Interpretation of observed damper performance in mitigating wind and rain-wind induced stay-cable vibrations." *11th International Conference on Wind Engineering*, June, 2003, Lubbock, Texas, USA, 2133-2140.

Appendix B Measurement Channels

B.1 Fred Hartman Bridge System

Channel #*	Transducer	Measurement	Component	Location
1	Bi-Axial Accelerometer	Acceleration	X	AS1
2	Bi-Axial Accelerometer	Acceleration	Z	AS1
3	Bi-Axial Accelerometer	Acceleration	X	AS3
4	Bi-Axial Accelerometer	Acceleration	Z	AS3
5	Bi-Axial Accelerometer	Acceleration	X	AS5
6	Bi-Axial Accelerometer	Acceleration	Z	AS5
7	Bi-Axial Accelerometer	Acceleration	X	AS9
8	Bi-Axial Accelerometer	Acceleration	Z	AS9
9	Bi-Axial Accelerometer	Acceleration	X	AS16
10	Bi-Axial Accelerometer	Acceleration	Z	AS16
11	Bi-Axial Accelerometer	Acceleration	X	AS18
12	Bi-Axial Accelerometer	Acceleration	Z	AS18
13	Bi-Axial Accelerometer	Acceleration	X	AS20
14	Bi-Axial Accelerometer	Acceleration	Z	AS20
15	Bi-Axial Accelerometer	Acceleration	X	AS22
16	Bi-Axial Accelerometer	Acceleration	Z	AS22
17	Bi-Axial Accelerometer	Acceleration	X	AS23
18	Bi-Axial Accelerometer	Acceleration	Z	AS23
19	Bi-Axial Accelerometer	Acceleration	X	AS24
20	Bi-Axial Accelerometer	Acceleration	Z	AS24
21	Bi-Axial Accelerometer	Acceleration	X	AN24
22	Bi-Axial Accelerometer	Acceleration	Z	AN24
23	Bi-Axial Accelerometer	Acceleration	X	BS1
24	Bi-Axial Accelerometer	Acceleration	Z	BS1
25	Bi-Axial Accelerometer	Acceleration	X	BS8
26	Bi-Axial Accelerometer	Acceleration	Z	BS8
27	Bi-Axial Accelerometer	Acceleration	X	BS16
28	Bi-Axial Accelerometer	Acceleration	Z	BS16
29	Bi-Axial Accelerometer	Acceleration	X	BS18
30	Bi-Axial Accelerometer	Acceleration	Z	BS18
Channel #*	Transducer	Measurement	Component	Location

31	Bi-Axial Accelerometer	Acceleration	X	BS24
32	Bi-Axial Accelerometer	Acceleration	Z	BS24
33	Bi-Axial Accelerometer	Acceleration	X	CS16
34	Bi-Axial Accelerometer	Acceleration	Z	CS16
35	Bi-Axial Accelerometer	Acceleration	X	CS24
36	Bi-Axial Accelerometer	Acceleration	Z	CS24
37	Bi-Axial Accelerometer	Acceleration	X	DS1
38	Bi-Axial Accelerometer	Acceleration	Z	DS1
39	Bi-Axial Accelerometer	Acceleration	X	DS24
40	Bi-Axial Accelerometer	Acceleration	Z	DS24
41	Accelerometer**	Acceleration	X	Deck @ AS9
42	Bi-Axial Accelerometer	Acceleration	Z	Deck @ AS9
43	Accelerometer**	Acceleration	X	Deck @ AS16
44	Bi-Axial Accelerometer	Acceleration	Z	Deck @ AS16
45	Accelerometer**	Acceleration	X	Deck @ AS19
46	Bi-Axial Accelerometer	Acceleration	Z	Deck @ AS19
47	Accelerometer**	Acceleration	X	Deck @ MidA
48	Bi-Axial Accelerometer	Acceleration	Z	Deck @ MidA
49	Uni-Axial Accelerometer	Acceleration	X	Deck @ BS19
50	Accelerometer**	Acceleration	X	Deck @ CS19
51	Bi-Axial Accelerometer	Acceleration	Z	Deck @ CS19
52	String Pot	Displacement	X	AS9
53	String Pot	Displacement	X	AS16
54	String Pot	Displacement	Z	AS16
55	String Pot	Displacement	X	AS20
56	String Pot	Displacement	X	AS23
57	String Pot	Displacement	Z	AS23
58	String Pot	Displacement	X	AS24
59	String Pot	Displacement	Z	AS24
60	String Pot	Displacement	X	AN24
61	String Pot	Displacement	X	BS16
62	String Pot	Displacement	Z	BS16
63	String Pot	Displacement	X	BS24
Channel #*	Transducer	Measurement	Component	Location

64	Load Cell	Damper Force	X	AS16
65	Load Cell	Damper Force	X	AS23
66	String Gauge	Strain	Top	AS16
67	String Gauge	Strain	Bottom	AS16
68	String Gauge	Strain	Top	AS23
69	String Gauge	Strain	Bottom	AS23
70	String Gauge	Strain	Top	AS24
71	String Gauge	Strain	Bottom	AS24
72	String Gauge	Strain	Top	BS16
73	String Gauge	Strain	Bottom	BS16
74	Anemometer	Wind Speed	U	AS18
75	Anemometer	Wind Speed	V	AS18
76	Anemometer	Wind Speed	W	AS18
77	Anemometer	Wind Speed	U	MidA
78	Anemometer	Wind Speed	V	MidA
79	Anemometer	Wind Speed	W	MidA
80	Anemometer	Wind Speed		Tower Top
81	Anemometer	Wind Direction		Tower Top
82	Rain Gauge	Rainfall		AS18
83	Rain Gauge	Rainfall		Tower Top
84	Thermometer	Temperature		AS18
85	Barometer	Air Pressure		AS18
86	Power Meter	Power Supply		Tower Room

* The channel numbers listed herein do not correspond to the physical channel numbers in the data acquisition system. The physical numbers of the data acquisition system are listed in the configuration files included in the data package that accompanies this report.

** Bi-axial accelerometers were used during the earlier stage (Before November 1999)of the measurement project. Uni-axial accelerometers with better resolution were used during the later stage (After November 1999) of the measurement project.

B.2 Veterans Memorial Bridge System

Channel #*	Transducer	Measurement	Component	Location
1	Bi-Axial Accelerometer	Acceleration	X	A10
2	Bi-Axial Accelerometer	Acceleration	Z	A10
3	Bi-Axial Accelerometer	Acceleration	X	A12
4	Bi-Axial Accelerometer	Acceleration	Z	A12
5	Bi-Axial Accelerometer	Acceleration	X	A14
6	Bi-Axial Accelerometer	Acceleration	Z	A14
7	Bi-Axial Accelerometer	Acceleration	X	B9
8	Bi-Axial Accelerometer	Acceleration	Z	B9
9	Bi-Axial Accelerometer	Acceleration	X	B11
10	Bi-Axial Accelerometer	Acceleration	Z	B11
11	Bi-Axial Accelerometer	Acceleration	X	B13
12	Bi-Axial Accelerometer	Acceleration	Z	B13
13	Bi-Axial Accelerometer	Acceleration	X	C11
14	Bi-Axial Accelerometer	Acceleration	Z	C11
15	Bi-Axial Accelerometer	Acceleration	X	C13
16	Bi-Axial Accelerometer	Acceleration	Z	C13
17	Bi-Axial Accelerometer	Acceleration	X	D12
18	Bi-Axial Accelerometer	Acceleration	Z	D12
19	Bi-Axial Accelerometer	Acceleration	X	D14
20	Bi-Axial Accelerometer	Acceleration	Z	D14
21	Bi-Axial Accelerometer	Acceleration	X	Deck @ Mid-Span
22	Bi-Axial Accelerometer	Acceleration	Z	Deck @ Mid-Span
23	Load Cell	Damper Force	X	D14
24	Anemometer	Wind Speed	U	Mid-Span
25	Anemometer	Wind Speed	V	Mid-Span
26	Anemometer	Wind Speed	W	Mid-Span
27	Anemometer	Wind Speed		S. Tower Top
28	Anemometer	Wind Direction		S. Tower Top
29	Rain Gauge	Rainfall		Mid-Span
30	Rain Gauge	Rainfall		S. Tower Top
31	Thermometer	Temperature		Mid-Span
32	Thermometer	Temperature		Control Room

Channel #*	Transducer	Measurement	Component	Location
33	Power Meter	Power Supply		BS16

* The channel numbers listed herein do not correspond to the physical channel numbers in the data acquisition system. The physical numbers of the data acquisition system are listed in configuration files included in the data package that accompanies this report.

Appendix C Correlation between wind measurements at the Fred Hartman Bridge

C.1 Correlations between Wind Measurements at Deck Level

As shown in Figure C.1, the wind measurements at the deck level by the UVW anemometers at mid-span and at the anchorage of stay AS18 are quite consistent. The data points in the figures represent fourteen-second mean values broken from five-minute records collected from May 1998 to May 1999, excluding the periods of time during which at least one set of the anemometers was known to be malfunctioning. Only data points representing wind approaching from the east side of the decks (i.e., wind direction in the range of 0° to 180°) are included in the figures, because the UVW anemometers are directly in the wake of the bridge decks when wind approaches from the west side. The reason why the records are broken into fourteen-second segments is to achieve better resolution when cable vibrations are investigated in association with wind speed and direction. As indicated by the linear regression results shown in the graphs, the wind measurements by the two sets of UVW anemometers are usually in quite good agreement. Also, the relatively large R-squared values suggest that, for both wind speed and direction, most of the data can be accounted for by the linear regression equations shown. The R-squared value, also known as the coefficient of determination, is a measure of the percent of the variation that can be explained by the regression equation. For linear regression, the R-squared value is simply the square of the correlation coefficient. That is,

$$R^2 = \left(\frac{\sum(x-\bar{x})(y-\bar{y})}{\sqrt{\sum(x-\bar{x})^2 \sum(y-\bar{y})^2}}\right)^2 \qquad \text{(C.1)}$$

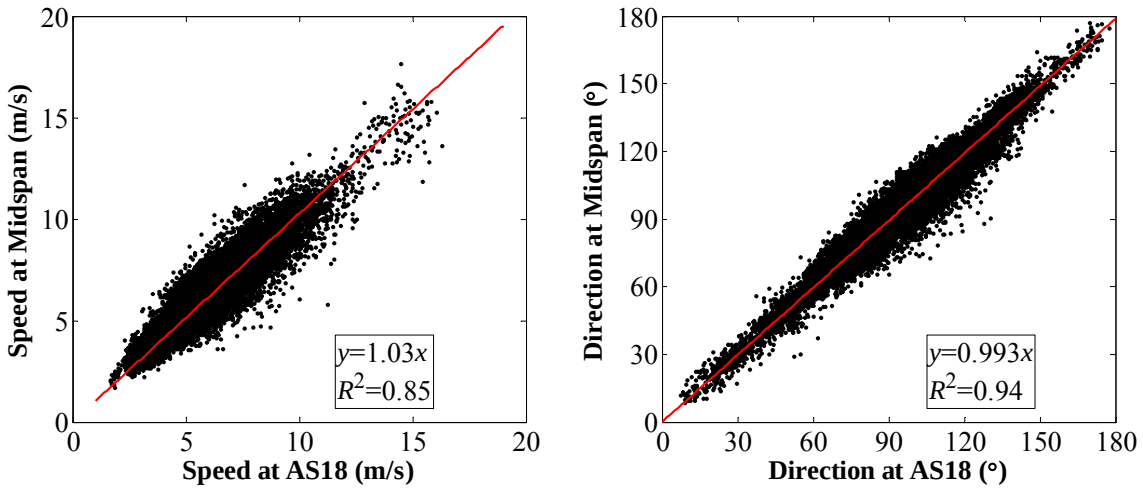

Figure C.1 Correlation between wind measurement at midspan and at AS18 of the Fred Hartman Bridge

C.2 Correlation between Wind Measurements at Deck Level and at Tower Top

While the wind measurements by the two sets of UVW anemometers are reasonably consistent with each other, discrepancies have been found between these measurements at the deck level and the measurements taken by the propeller-vane anemometer at the tower top. Figure C.2 a) shows the fourteen-second mean wind direction measured at the tower top against that measured at the deck level for wind measurement taken from May 1998 to May 1999. Again, only data points with measured deck level wind direction in the range of 0° to 180° are presented. This graph suggests a reasonably clear relationship between wind direction measurements at these two locations, but this relationship is apparently nonlinear. In particular, the relationship appears to be different for three ranges of wind directions measured at the deck level, that is, from 0° to approximately 65°, from approximately 65° to approximately 115°, and from approximately 115° to 180°. To exclude the possible dependence of direction measurement on wind speed, the wind measurement data are divided into three groups based on the wind speed measured at the deck level. The first group represents wind of relatively low speed and includes data with mean deck-level wind speed in the range of 0 m/s to 4 m/s; the second group represents wind of intermediate speed and includes data with mean deck-level wind speed in the range of 4 m/s to 8 m/s; the third group represents wind of relatively high speed and includes data with mean deck-level wind speed greater than 8 m/s. Figures 4.10 b), c) and d) show the fourteen-second mean wind direction measured at the tower top against that measured at the deck level for these three groups of data, respectively. Comparison of these figures suggest that when wind speed is low (Figure C.2 b)), the relationship between the wind direction measured at the tower top and that measured at the deck level is not as clear as in the cases when wind speed is higher (Figures C.2 c) and d)). This suggests that, for at least one type of anemometer, the measurement for wind of low speed is not as consistent as for wind of higher speed.

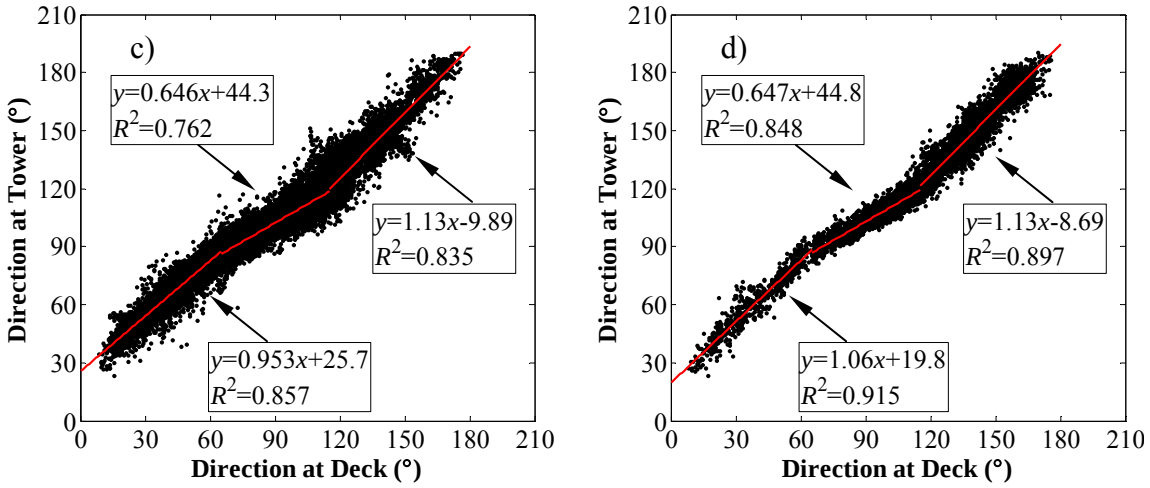

Figure C.2 Correlation between wind directions measured at tower top and at deck level of Fred Hartman Bridge for deck-level wind speed in the range of a) all data, b) 0 to 4 m/s, c) 4 to 8 m/s and d) greater than 8 m/s

Although the relationship between the wind direction measured at the tower top and that measured at the deck level is clearly nonlinear, it does appear to be approximately piece-wise linear. This is especially true when wind speed is adequately high, as suggested by the linear regression results shown in Figures C.2 c) and d). While the possible imperfect calibration during the installation of the anemometers might have been one of the factors responsible for the nonlinear relationship between the wind measurements at the two elevations, the different slopes of the linear regression lines for the three groups of wind directions suggest that there could be other factors involved, such as the inherent distortion of the wind profile at the vicinity of the anemometers by the bridge structure. The fact that the correlation between the wind directions measured at the two elevations changes abruptly at the deck-level wind directions of approximately 65° and 115°, instead of smoothly over the whole direction range of 0° to 180°, however, implies that the distortion to the flow at the tower top is likely to be more significant and, as a result, more responsible for the nonlinear correlation shown in Figure C.2. This conclusion is drawn since the decks of the Fred Hartman Bridge are long, line-like structure members that have no significant abrupt changes along their axes that could result in a sudden change of wind flow structure when the wind direction is approximately 65° or 115°. On the other hand, due to the sharp corners of the tower, the flow at the tower top can change abruptly at specific directions and this change is suspected to be responsible for the abrupt change of the correlation between the direction measurements at the two elevations.

The fact that the wind measurements have been affected by the presence of the bridge structure has also manifested in the correlation between the wind speed measurements at the tower top and at the deck level. Figure C.3 a) shows the correlation between the wind speed measured at the tower top and that measured at the deck level. Although there appears to be a linear relationship between the speeds measured at these two elevations, the scatter of the data points, represented by the relatively small R^2 value, suggests that this relationship is not always consistent. To investigate whether the complex relationship between the wind

direction measurements has contributed to this scatter, the correlation between the wind speeds measured at the two locations are shown in Figures C.3 b), c) and d), respectively, for three groups of wind data. The three groups consist of data with measured deck-level direction in the range of 0° to 65°, 65° to 115°, and 115° to 180°, respectively. Results of linear regression analysis for these groups of data are shown in the respective figures. In this case, the interceptions of the linear regression line at the axes are set at the origin point, since for all three groups of data, the offset between the wind speed measured at the tower top and that measured at the deck level is insignificant. These linear regression results suggest that

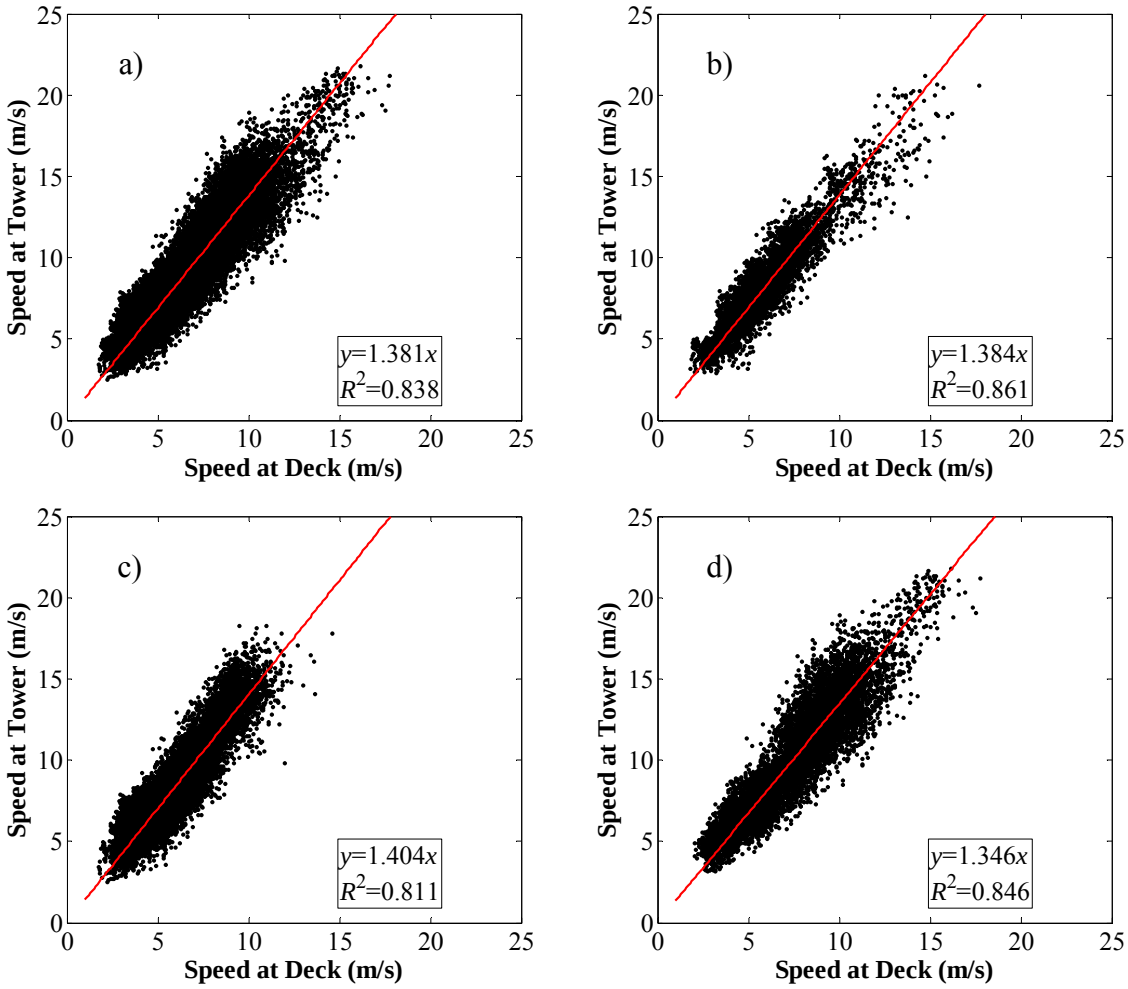

Figure C.3 Correlation between wind speeds measured at tower top and at deck level of Fred Hartman Bridge for deck-level wind direction in the range of a) all data, b) 0° to 65°, c) 65° to 115° and d) 115° to 180°

the wind speed measured at the tower top is approximately 1.35 to 1.40 times of that measured at the deck level, and that the direction dependence of wind speed measurements is relatively insignificant.

This correlation between the wind speeds measured at the tower top and at the deck level, however, is significantly different from what predicted by the so called logarithmic law, which is considered the best representation of strong wind profiles in the lower atmosphere

(Simiu and Scanlan 1996). According to the logarithmic law, the mean wind speed (U) at the altitude z can be expressed as (Tennekes 1973):

$$U(z) = \frac{1}{k} u_* \ln \frac{z}{z_0} \tag{C.2}$$

where $k \approx 0.4$ is the von Kármán's constant; u_* is the shear velocity; z_0 is the roughness length. The ratio between the wind speeds at altitudes z_1 and z_2 therefore can be expressed as

$$r = \frac{U(z_1)}{U(z_2)} = \frac{\ln(z_1 / z_0)}{\ln(z_2 / z_0)} \tag{C.3}$$

For the Fred Hartman Bridge, the decks are about 53 m above the water level and the height of the towers is about 134 m. Figure C.4 shows the theoretical ratio between the free-stream speed at the tower top and that at the deck level for z_0 values ranging from 0.0001 m (for sand surface) to 1 m (for densely built-up suburbs). It is apparent that over this whole range of z_0 values, the theoretical ratio is smaller than the ratios obtained by the linear regression analysis of the full-scale measurement data, as shown in Figures C.3 a), b), c) and d). This is another fact which suggests that the measurements taken by the anemometers represent the flow distorted by the bridge structure, instead of the free-stream wind.

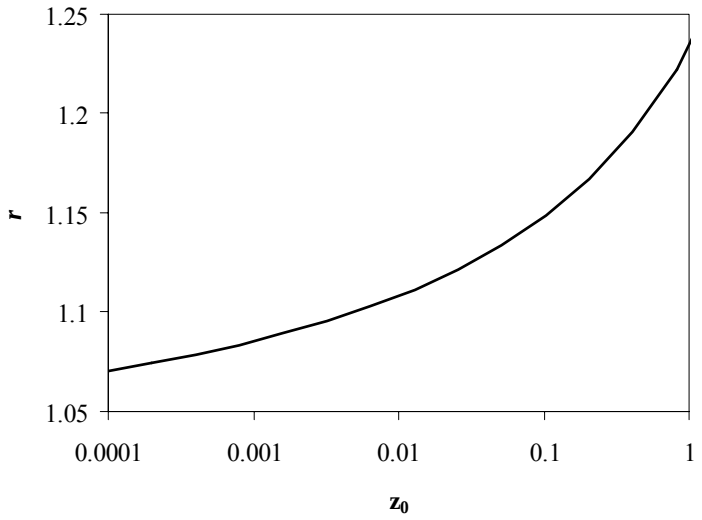

Figure C.4 Theoretical ratios between wind speeds at tower top and at deck level of the Fred Hartman Bridge for different values of z_0

Appendix D Correlation between wind measurements at the Veterans Memorial Bridge

Unlike in the case of the wind measurements at the Fred Hartman Bridge, the wind measurements at the tower top and at the deck level of the Veterans Memorial Bridge are much more consistent. Figures D.1 a) and b) shows the wind direction measured at the tower top of the Veterans Memorial Bridge by a propeller-vane anemometer against that measured at the mid-span of the bridge at deck level by a set of UVW anemometer. The anemometers are the same type as those used on the Fred Hartman Bridge. The data presented herein are from the measurement taken from January to June of 1999 and only data with deck level wind direction in the range of 0° to 180° are included. Figure D.1 a) represents the group of data with measured deck-level wind speed in the range of 4 m/s to 8 m/s; Figure D.1 b) represents the group of data with measured deck-level wind speed faster than 8 m/s. In this case, the average correlation between the wind direction measurements at the two elevations appears to be consistently linear throughout the whole range of 0° to 180°. This different pattern of wind measurement is suspected to be due to the fact that the upper part of the towers of the Veterans Memorial Bridge is smaller than that of the Fred Hartman Bridge and, more importantly, that the towers of the Veterans Memorial Bridge are a straight column, which is geometrically much simpler than the diamond-shaped towers of the Fred Hartman Bridge and therefore less capable of creating complex three-dimensional flow structure in their vicinities.

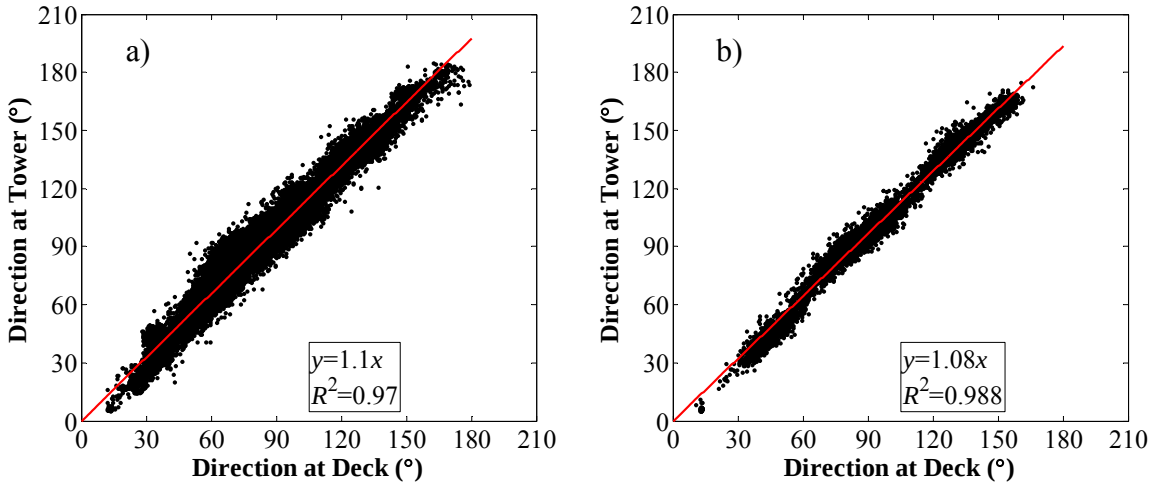

Figure D.1 Correlation between wind directions measured at tower top and at deck level of Veterans Memorial Bridge for deck-level wind speed in the range of a) 4 to 8 m/s and b) greater than 8 m/s

Appendix E Data Packages

The data packages that accompany the present report contain all the raw data recorded by the full-scale measurement systems and four databases that store the summary statistics of the measurement. The following two sections provide some basic information that is essential for processing and interpretation of the data included in the packages.

E.1 Raw Data

The raw data package contains five-minute binary files recorded by the full-scale measurement systems. The files are named according to the measurement system that recorded them and the date and sequence when they are recorded. Specifically, each file name begins with a letter specifying the recording system and the stage of the monitoring project. The names of all the files recorded on the Veterans Memorial Bridge are prefixed with the letter "v". For the files recorded on the Fred Hartman Bridge, different prefixes are used for files recorded at different stages of the measurement program. Table E.1 lists the prefix letters for the files recorded on the Fred Hartman Bridge. For files recorded on both bridges, the prefix of the file names is followed immediately by a four-digit number specifying the date and then letters indicating the sequence (which starts at "0") of the recording. All the files are stored in individual folders according to the year in which they are recorded and the specific configuration of the full-scale measurement systems at the time of recording. For example, the file "v01220" stored in folder "veterans\veterans99\vetproc32_99a\" is the first file recorded on the Veterans Memorial Bridge on January 22, 1999, and during the time of recording, the full-scale measurement system had 32 active channels. Similarly, the file "h091421" stored in folder "hartman\hartman05\hartproc35_05\" is the 22nd file recorded on the Fred Hartman Bridge on September 14, 2005, and the full-scale measurement system on this bridge had 35 active channels during the time of recording.

Table E.1 Prefix for files recorded on the Fred Hartman Bridge

Time of Recording	Prefix Letter	Comments
10/03/1997-10/02/1998	x	Unrestrained vibration
10/03/1998-02/21/1999	h	Some stays restrained by cross-ties
03/06/1999-03/26/1999	d	Only stays with damper monitored
03/27/1999-Present	h	N/A

Each raw data file consists of voltage recordings sampled by the active channels during a period of five minutes at a frequency of 40 Hz. As stated before, the number of active channels during a specific period of time can be inferred by the name of the folder in which the record files are stored. This information, as well as the specific number of the individual channels, can also be found in the Matlab configuration files accompanying the raw data. The configuration files for the measurement systems on the Fred Hartman Bridge are stored in the folder of "Hartman\Matlab_Files\", and those for the measurement system on the Veterans Memorial Bridge are stored in the folder of "Veterans\Matlab_Files\". Because the data stored in each file represents the voltages recorded by the transducers, they

have to be converted to the corresponding measurements of interest by applying specific scale factors. These scale factors can be found in Matlab files "hartman_calibrations.m" and "transducer_id" for the transducers installed on the Fred Hartman Bridge and files "veterans_calibrations.m" and "transducer_id" for the transducers installed on the Veteras Memorial Bridge. These files are also stored in the respect folders for Matlab files for the two bridges. To illustrate typical processes used to extract measurement data from the record files, a Matlab file named "data_process_demo.m" has been created and stored in the folder of "Hartman\Matlab_Files\". Other data-processing procedures can be developed by following this example. In the case that Matlab is not the environment of choice for data processing, all the information stored in the Matlab files can be accessed by open the files in generic text editors.

E.2 Databases

A total of four Microsoft Access databases, two for the Fred Hartman Bridge and two for the Veterans Memorial Bridge, have been included in the database package that accompanies the present report. These databases are:

1. Hartman_Disp_Stats.mdb. This database stores statistics of displacement response of stay cables on the Fred Hartman Bridge and the corresponding mean meteorological conditions. The processes used for generation of the statistics have been described in Chapter 4 of the report. The database consists of the following components:
   - Table "File_Date" stores the date and time at which each record was collected. This table contains the following fields:
     - Segment_id: Index of the fourteen-second segments. The format for the index is "four-digit year + two digit month + two digit day + three-digit record number + . + segment number". For example, the segment with the index of 2005091421.06 is the 6th segment of the 22nd record collected on September 14, 2005. The field of "Segment_id" is also included in all the other tables in this database and serves as the link among the tables.
     - Date: The date on which the record was collected;
     - Time: The time at which the record was collected;
   - Table "Dominant_Mode" stores the characteristics of the mode of vibration that has the largest mean anti-nodal major-axis amplitude over the four-second segments. This table contains the following fields:
     - Segment_id;
     - Stay: Name of the stay;
     - Mode: Mode number;
     - f_maj: Mean frequency of the vibration in the major-axis direction;
     - f_min: Mean frequency of the vibration in the minor-axis direction;
     - A_maj: Mean anti-nodal amplitude of the vibration in the major-axis direction;
     - A_min: Mean anti-nodal amplitude of the vibration in the minor-axis direction;
     - Angle: Mean major-axis angle of the vibration.
   - Table "Secondary_Modes" stores the characteristics of the modes of vibration whose major-axis amplitudes are smaller than the largest. This table contains all the fields in table "Dominant_Mode" and the field "Rank", which indicates the index of a specific mode of vibration ordered by the magnitude of the anti-nodal major-axis amplitude. For example, if a mode has the rank of 2 in a fourteen-second

segment, this means that the anti-nodal major-axis amplitude of this specific mode is the second largest among the modal components.

- Table "RMS_Disp" stores the root-mean-square (RMS) amplitude of the vibration of the stay cables during the fourteen-second segments. This table contains the following fields:
  - Segment_id;
  - Stay: Name of the stay;
  - RMS_Disp_x: RMS displacement amplitude in the in-plane direction;
  - RMS_Disp_Z: RMS displacement amplitude in the lateral direction.
- Table "AS18_Wind" stores the fourteen-second mean value of the wind information recorded by the UVW anemometers located near the anchorage of stay AS18 at the deck level. This table contains the following fields:
  - Segment_id;
  - Mean_Speed: Mean speed of the wind;
  - Mean_ Azimuth: Mean direction of the wind in the horizontal plane;
  - Mean_Elevation: Mean direction of the wind in the vertical plane;
  - Turb_Intensity: Turbulence intensity computed based on seventy-second segments (five fourteen-segments; the same value is assigned to all five fourteen-second segments.).
  - Replaced_Comment: Indicates if a certain component (U, V or W) of the measurement has been replaced by the corresponding component record by the UVW anemometers at midspan of the deck.
- Table "Ave_Wind" stores the average values of the wind measurements by the two sets of UVW anemometers at the deck level. This table contains the same fields as the ones in tables AS18_Wind and Midspan_Wind except that it does not have the field "Replaced_Comment".
- Table "Tower_Wind" stores the fourteen-second mean value of the wind information recorded by the propeller-vane anemometer installed on the top of the southeast tower. This table contains the following fields:
  - Segment_id;
  - Mean_Speed: Mean speed of the wind;
  - Mean_ Azimuth: Mean direction of the wind in the horizontal plane;
  - Turb_Intensity: Turbulence intensity computed based on seventy-second segments (five fourteen-segments; the same value is assigned to all five fourteen-second segments.).
- Table "Rain" stores the fourteen-second mean rainfall rate recorded at the bridge site. This table contains the following fields:
  - Segment_id;
  - AS18_Rain_Rate: Rainfall rate computed based on the amount of rainfall recorded by the rain gauge located near the anchorage of stay AS18 at the deck level;
  - Tower_Rain_Rate: Rainfall rate computed based on the amount of rainfall recorded by the rain gauge located at the tower of the southeast tower;
  - Max_Rain_Rate: Maximum of the rainfall rates computed based on the amount of rainfall recorded by the two rain gauges.

2. Hartman_database.mdb: This database stores one-minute statistics of the major measurements by the system on the Fred Hartman Bridge. The database consists of the following components:
   - Table "File_Date" stores the recording date of the records and the sequence of the each one-minute record;
   - Table "Std" stores the one-minute RMS values of the measurements;
   - Table "Max" stores the maximum values of the one-minute measurements;
   - Table "Min" stores the minimum values of the one-minute measurements;
   - Table "Mean" stores the one-minute mean values of the measurements;
   - Table "Kurt" stores the kurtosis values of the one-minute measurements;
   - Table "Skew" stores the skewness values of the one-minute measurements;
   - Table "Wind_Means" stores the one-minute mean values of the wind information recorded by the anemometers.
   - Table "Climate" stores the climatic information, including the amount of rainfall, the average temperature and the average barometric pressure of the air recorded at the bridge site during one-minute time segments.

Many tables in this databases share the same fields. The names of these fields are usually the combination of a number of symbols. Table E.2 lists the symbols commonly used to construct the filed names. The meaning of the field names can be inferred from the descriptions listed in the table.

Table E.2 Commonly used symbols in the field names of database "Hartman_Database.mdb"

Symbol	Description
St	Stay
Dk	Deck
acc	Acceleration measured by accelerometers
LVDT	Displacement measured by string pots
Load	Damper force measured by load cells
U	U component of wind measured by UVW anemometers
V	V component of wind measured by UVW anemometers
W	W component of wind measured by UVW anemometers
Str	Strain measured by strain gauges
Spd	Speed (of wind)
Dir	Direction (of wind)
x	In-plane direction of stay cables, horizontal direction of decks
z	Lateral direction of stay cables, vertical direction of decks
top	Top component of the strain measured by strain gauges
btm	bottom component of the strain measured by strain gauges
1	(Used with "LVDT") In-plane direction of stay cables

	Unless otherwise noted in the configuration files
2	(Used with “LVDT”) Lateral direction of stay cables
	Unless otherwise noted in the configuration files

3. Veterans_Disp_Stats.mdb. The counterpart of “Hartman_Disp_Stats.mdb” for the measurement on the Veterans Memorial Bridge. The structure of this database is similar to that of “Hartman_Disp_Stats.mdb”.
4. Veterans_database.mdb. The counterpart of “Hartman_database.mdb”. The structure of this database is similar to that of “Veterans_Database.mdb”.

References

Bendat, J. S., and Piersol, A. G. (1986). *Random Data*, Wiley Interscience.

Bosdogianni, A., and Olivari, D. (1996). "Wind- and rain-induced oscillation of cables of cable-stayed bridges." *Journal of Wind Engineering and Industrial Aerodynamics*, 64, 171-185.

Caracoglia, L., and Jones, N. P. (2005a). "In-plane dynamic behavior of cable networks. Part 1: formulation and basic solutions." *Journal of Sound and Vibration*, 279(3-5), 969-991.

Caracoglia, L., and Jones, N. P. (2005b). "In-plane Dynamic behavior of cable networks. Part 2: Prototype prediction and validation." *Journal of Sound and Vibration*, 279(3-5), 993-1014.

Cheng, S., Irwin, P. A., J.B., J., J., L., Larose, G. L., Savage, M. G., Tanaka, H., and C., Z. "Divergent motion of cables exposed to skewed wind." *5th International Symposium on Cable Dynamics*, September, 2003a, Santa Margherita Ligure, Italy, 271-278.

Cheng, S., Larose, G. L., Savage, M. G., and Tanaka, H. (2003b). "Aerodynamic Behaviour of an Inclined Circular Cylinder." *Wind and Structures*, 6(3), 197-208.

Chopra, A. K. (2001). *Dynamics of structures*, Prentice Hall.

Cosentino, N., Flamand, O., and Ceccoli, C. (2003). "Rain-wind induced vibration of inclined stay cables. Part I: Experimental investigation and physical explanation." *Wind and Structures*, 6(6), 471-484.

Ehsan, F., and Scanlan, R. H. "Damping stay cables with ties." *5th U.S. Japan Workshop on Bridge Engineering*1989, 203-217.

Fitzgibbon, A., Pilu, M., and Fisher, R. B. (1999). "Direct least square fitting of ellipses." IEEE Transactions on Pattern Analysis and Machine Intelligence, 21(5), 476-480.Flamand, O. (1995). "Rain-wind induced vibrations of cables." *Journal of Wind Engineering and Industrial Aerodynamics*, 57, 353-362.

Fujino, Y. (2002). "Vibration, control and monitoring of long-span bridges--recent research, developments and practice in Japan." *Journal of Constructional Steel Research*, 58(1), 71-97.

Fuzier, J. P., and Stubler, J. "The Normandie Bridge stays." *Conference oon Cable-Stayed and Suspension Bridges*, 12-15, Oct., 1994, Deauville, France, 699-706.

Gu, M., Liu, C. J., and Lou, G. Q. (1998). "Rain-wind induced vibration of cables on cable-stayed bridges and its control." *Shanghai Journal of Mechanics (in Chinese)*, 21(1), 281-288.

Hikami, Y., and Shiraishi, N. (1988). "Rain-wind induced vibrations of cables of cable-stayed bridges." *Journal of Wind Engineering and Industrial Aerodynamics*, 29, 409-418.

Johnson, E. A., Christenson, R. E., and Spencer Jr, B. F. (2003). "Semiactive damping of cables with sag." *Computer-Aided Civil and Infrastructure Engineering*, 18(2), 132-146.

Krenk, S. (2000). "Vibrations of a taut cable with an external damper." *Journal of Applied Mechanics*, 67(4), 772-776.

Kristensen, L. (1993). "The cup anemometer and other exciting instruments." *R-615*, Risø National Laboratory, denmark.

Larose, G. L., and Smitt, L. W. "Rrain/wind induced vibrations of the parallel stay cables for the Oresund High Bridge." *IABSE Conference*, June, 1999, Malmo, 1-12.

Main, J. A., and Jones, N. P. (2002a). "Free vibrations of taut cable with attached damper. I: Linear viscous damper." *Journal of Engineering Mechanics*, 128(10), 1062-1071.

Main, J. A., and Jones, N. P. (2002b). "Free vibrations of taut cable with attached damper. II: Nonlinear damper." *Journal of Engineering Mechanics*, 128(10), 1072-1081.

Matsumoto, M., Daito, Y., Kanamura, T., Shigemura, Y., Sakuma, S., and Ishizaki, H. (1998). "Wind-induced vibration of cables of cable-stayed bridges." *Journal of Wind Engineering and Industrial Aerodynamics*, 74-76, 1015-1027.

Matsumoto, M., Saitoh, T., Kitazawa, M., Shirato, H., and Nishizaki, T. (1995). "Response characteristics of rain-wind induced vibration of stay-cables of cable-stayed bridges." *Journal of Wind Engineering and Industrial Aerodynamics*, 57(2-3), 323-333.

Matsumoto, M., Shiraishi, N., Kitazawa, M., Knisely, C., Shirato, H., Kim, Y., and Tsujii, M. (1990). "Aerodynamic behavior of inclined circular cylinders-cable aerodynamics." *Journal of Wind Engineering and Industrial Aerodynamics*, 33(1-2), 63-72.

Matsumoto, M., Shiraishi, N., and Shirato, H. (1992). "Rain-wind induced vibration of cables of cable-stayed bridges." *Journal of Wind Engineering and Industrial Aerodynamics*, 43(1-3), 2011-2022.

Matsumoto, M., Yagi, T., Shigemura, Y., and Tsushima, D. (2001). "Vortex-induced cable vibration of cable-stayed bridges at high reduced wind velocity." *Journal of Wind Engineering and Industrial Aerodynamics*, 89(7-8), 633-647.

Matsumoto, M., Yagi, T., and Tsushima, D. "Vortex-induced vibration of inclined cables at high wind velocity." *10th International Confference on Wind Engineering*1999, Copenhagen, Denmark, 979-986.

Mitra, S. K. (2001). *Digital signal processing*, Thomas Casson.

Ohya, Y. (2004). "Drag of circular cylinders in the atmospheric turbulence." *Fluid Dynamics Research*, 34, 135-144.

Ozkan, E. (2003). "Evaluation of response prediction methodology for long-span bridges using full-scale measurements," Johns Hopkins University, Baltimore, MD, USA.

Pacheco, B. M., Fujino, Y., and Sulekh, A. (1993). "Estimation curve for modal damping in stay cables with viscous damper." *Journal of Structural Engineering*, 119(6), 1961-1979.

Peil, U., and Nahrath, N. (2003). "Modeling of rain-wind induced vibrations." *Wind and Structures*, 6(1), 41-52.

Perkins, N. C. (1992). "Modal interactions in the non-linear response of elastic cables under parametric/external excitation." *International Journal of Non-Linear Mechanics*, 27(2), 233-250.

Pinto da Costa, A., Martins, J. A. C., Branco, F., and Lilien, J. L. (1996). "Oscillations of bridge stay cables induced by periodic motions of deck and/or towers." *Journal of Engineering Mechanics*, 122, 613-622.

Raoof, M. (1992). "Free-bending fatigue life estimation of cables at points of fixity." *Journal of Engineering Mechanics*, 118(9), 1747-1764.

Ruscheweyh, H. "The mechanism of rain-wind-induced vibration." *10th International Conference on Wind Engineering*1999, Copenhagen, Denmark, 1041-1047.

Shirakashi, M., Hasegawa, A., and Wakiya, S. (1986). "Effects of Secondary Flow on Karman Vortex Shedding from a Yawed Cylinder." *Bulletin of JSME*, 29, 1124-1128.

Simiu, E., and Scanlan, R. H. (1996). *Wind Effects on Structures*, John Wiley and Sons.

Takahashi, K., and Konishi, Y. (1987). "Non-linear vibrations of cables in three dimensions, part II: Out-of-plane vibrations under in-plane sinusoidally time-varying load." *Journal of Sound and Vibration*, 118(1), 85-97.

Tennekes, H. (1973). "The logarithmic wind profile." *Journal of Atmospheric Sciences*, 30, 234-238.

Virlogeux, M. "Cable vibrations in cable-stayed bridges." *International Symposium on Advances in Bridge Aerodynamics*, May, 1998, Copenhagen, Denmark, 213-233.

Virlogeux, M. (1999). "Recent evolution of cable-stayed bridges." *Engineering Structures*, 21, 737–755.

Wang, L., and Xu, Y. L. (2003). "Wind–rain-induced vibration of cable: an analytical model (1)." *International Journal of Solids and Structures*, 40, 1265–1280.

Warnitchai, P., Fujino, Y., and Susumpow, T. (1995). "A non-linear dynamic model for cables and its application to a cable-structure system." *Journal of Sound and Vibration*, 187(4), 584 601.

Whitlock Dalrymple Poston and Associates, I. (1999). "Evaluation and repair of stay-cable vibrations: Fred hartman Bridge and Veterans Memorial Bridge. Progress report number 2."

Wianecki, J. "Cables wind excited vibrations of cable-stayed bridge." *5th International Conference of Wind Engineering*1979, 1381-1393.

Yamaguchi, H. (1990). "Analytical study on growth mechanism of rain vibration of cables." *Journal of Wind Engineering and Industrial Aerodynamics*, 33(1-2), 73-80.

Yamaguchi, H., and Fujino, Y. "Stayed cable dynamics and Its vibration control." *Int. Symp. on Advances in Bridge Aerodynamics*1998, Balkema, Rotterdam, Netherlands, 235-253.